THE UNIVERSITY OF CHICAGO

THE EFFECT OF POLYELECTROLYTE ARCHITECTURE ON POLYELECTROLYTE COMPLEXATION

A DISSERTATION SUBMITTED TO

THE FACULTY OF THE PRITZKER SCHOOL OF MOLECULAR ENGINEERING

IN CANDIDACY FOR THE DEGREE OF

DOCTOR OF PHILOSOPHY

BY

KADEN COLE STEVENS

CHICAGO, ILLINOIS

AUGUST 2023

To Hannele, Wilson and Mae Stevens.

TABLE OF CONTENTS

Lists of Figures

Lists of Tables

Acknowledgements

Writing this document is surreal. My friends and family have helped me achieve more than I ever dreamed was possible for this lanky Mississippi kid, and I am truly thankful. Before I get to them, I would like to formally thank Professor Matthew V. Tirrell for welcoming me into his group, trusting me to pursue my curiosity and supporting me throughout my time in his lab. I have learned a great deal from observing the way Matt treats those around him, the types of questions he asks and the way he asks them. Matt showed me how one can simultaneously be funny while also serious, forthright while remaining tactful and influential but not overbearing. Telling stories about Matt is a quick way to make fellow grad students jealous, and I consider myself lucky to have been in his group. I would also like to thank my other thesis committee members, Stuart Rowan and Paul Nealy. Stuart welcomed me into his lab for a short research experience before I officially started graduate school in 2018, and he and his group have been my adopted lab family ever since. Watching him ask his group members incisive questions has taught me how to think critically at a high level. He has always welcomed me into group events and made time for spontaneous conversations, supporting me long after I joined another group, and I am deeply grateful. Paul was one of the first professors I spoke to at UChicago, and I still remember him telling me precisely what he thought a graduate student must do to earn a PhD. His said “a student earns a PhD when they are the worlds expert in their very narrow topic of study”. His clear vision for what a PhD means has given me a goal to strive for throughout grad school. Each of these scientists has contributed to my personal and professional growth and I consider myself lucky to have received their mentorship.

My fellow Tirrell Group members have helped keep me sane through this arduous process. Within this star-studded cast of excellent scientists, I feel the need to give extra special thanks to

Jeffrey Ting, Alexander Marras and Siqi Meng. Jeff has endured a barrage of inane questions with grace, always going above and beyond to help, even after he left the group and I was not technically his problem anymore. He also was the first person in the group to encourage me to pursue my own interests and to make me feel like my ideas were valuable. Jeff is consistently selflessness, persistently curious and constantly thoughtful. I consider myself lucky to call him a friend and I look forward to many more years of talking science in a hot tub with this gentleman. Ironically enough, I have probably done more work with Alex despite our dramatically different backgrounds. I know that when I am done talking with Alex my ideas will be more focused and useful than they were before we spoke. Nerding out with him over music, family and fantasy football kept me sane throughout some of the worst times, and I am very grateful he is my friend. I owe Siqi a great deal both as a friend and a mentor. Our weekly lunches during my time at PPG were always filled with the best advice. My only complaint about Siqi is that she graduated before I was done asking her questions. In no particular order, I would also like to thank Dean, Yan, Carlos, Shinya and Ed for being great lab mates, always being willing to talk and making me laugh.

As I said before, the Rowan group has adopted me as one of their own. As such, it would be disrespectful to daddy not to mention a few of them (they'll get that reference). Charlie Lindberg has been my best good buddy throughout my time in the PME. Whether it be shooting the breeze about raw displays of flour, introducing each other to new music or discussing the details of confusing data, I always know she'll be a joy to waste time with. My time at UChicago would not have been half as enjoyable without her. I guess I should mention Adarsh Suresh. I can't think of anyone I'd rather have 2AM panic attacks with than Adarsh Suresh, and I can't wait to see what you decide to apply that big, scatterbrain of yours towards. For fear of making this list into its own chapter, I will have to thank the rest of the Rowan members briefly. Here goes. Thank

you to Marissa Tranquilli for teaching me to write good, Jerry Hertzog for letting me loan all those solvents, Elina Ghmire for proving once and for all USM students are the best, Nick Macke for teaching me what butyl acrylate tastes like, Ben Rawe for introducing me to Muse, polycatenanes and existential dread, Neil Dolinski for being a benevolently curmudgeonly sage, Samir for curing cancer or whatever and Nick Boyton for getting us to Mars. You guys are the best.

A few people that deserve thanks do not fit neatly into a broader category. So here are the unsorted, but deserved acknowledgements. First, Phillip Griffin deserves a huge thank you for teaching me how to use and interpret data and how to breathe deep when things get overwhelming. To Sam, John, Guru, all the other wonderful people I met while working at PPG, I am deeply grateful for the way you treated me and made me feel at home during my time in Pittsburg. Samuel Esarey deserves more thanks than I can possibly give for being an incredible, endlessly patient mentor and great friend. Finally, thank you to Mike Sims (Solvay). I would be making much more money for much less work in the future if you hadn't pushed me out of my comfort zone and convinced me to pursue a dream. In all seriousness, you've always looked out for me more than I deserve and I am truly grateful. For anyone else that I forgot, I didn't mean to I promise. I'm sure you're great.

Finally, I would like to thank my family. I could not have done this without them. First and foremost, my wife Hannele Heusser has been my best friend, my biggest supporter and the love of my life for as long as I've known her. She has always seen more in me and expected more from me than I do, and there is no way I'll ever be able to thank her enough. Calling her my wife makes me smile every time. My son, Wilson Stevens, and my daughter Mae Stevens have been the source of endless joy through stressful times. Many people have said some iteration of "I don't see how you do grad school with kids" and I always reply "I don't understand how you stay motivated

without them". Being their father is by far my proudest accomplishment. I would also like to thank my father, Rusty Stevens, for his constant support. I always know who to call for a quick pep talk. To my mother, Regina Lott, thank you for picking up the phone when I'm anxious. Your voice has always been able to calm me down. To my little sister, Rachel, thanks for not smacking me into next week (yet). To my grandmother and grandaddy (Betty and Delton Raybourn), thank you for always caring about what's going on in my life and having the bandwidth to keep my story separate from the other few dozen grandkids. To the rest of the Raybourn extended family, I love and miss you very much. To Keith Lott, I am deeply grateful for the way you welcomed my family into yours without a second thought. To Melaine Bryan, thank you for welcoming me into your family and loving me and my children so much. To the rest of the Heussers, thanks for accepting me into the group. Everyone in my family has been incredible and supportive throughout this whole process and I love you all.

Abstract

Polyelectrolyte complexes (PECs) form spontaneously upon mixing aqueous solutions of oppositely charged polymers, forming a polymer rich complex phase and polymer poor supernatant phase. PECs are promising material platforms for various industrial applications due to their biocompatibility, low surface tension and stimuli-responsiveness. Molecular design also allows us to design core-shell micelle systems with polyelectrolyte complex cores and hydrophilic coronas, named polyelectrolyte complex micelles (PCMs). However, there are currently few predictive design principles that allow for rational PEC design, limiting the adoption of PEC technologies. Here, we aim to investigate molecular architecture to develop chemically agnostic design principles that work consistently across various chemistries. In Chapter 1 of this dissertation, we discuss the relevant background information and highlight influential work in foundational PEC concepts, the use of non-linear architectures and the structure-property relationships of polyelectrolye complex micelles (PCMs).

In Chapter 2, we first focus on blocky polyelectrolyte architectures, specifically with the intention of creating double-diblock PCMs (D-PCMs) with unmatched charged block lengths for the first time. Using salt annealing, we were able to overcome barriers to D-PCM formation from blocky polyelectrolytes with charged block lengths up to 10x different. Using a combination of characterization techniques, we show that the cores grow via a unique interdependent mechanism where the block length of one diblock influences the ability of the other diblocks charged block to contribute to core size, aggregation number and density. This study provides a straightforward path to ordered PEC materials with unmatched charged block lengths and demonstrates the unique interdependent growth they undergo.

For Chapter 3, we examined the role of lightly branched star polyelectrolytes in PECs. Charge density has been shown to directly influence the stability and mechanics of PECs and branched polyelectrolytes have higher charge density than linear counterparts. To understand if charge density could be modulated through lightly branched polymer architectures, we synthesize pairs of homologous polyelectrolytes to create model PEC systems of various architectures. We find that branched architectures influence the salt stability of PECs while leaving the mechanical properties and internal structure unchanged, suggesting that changing charge density via architecture alters PEC properties precisely, paving the way for more intentional PEC design.

Chapter 4 focuses on the structure-property relationships of bottlebrush polyelectrolytes. We synthesize densely charged bottlebrush polyelectrolytes which form gel-like solids when complexes. To understand their gel-like rheological behavior, we delve into structural characterization using Cryo-TEM and SAXS. Together, they allow us to understand the structural development of bottlebrush PECs (BPECs) from the network level to the sidechain conformations as a function of salt. Our results in this chapter lay the groundwork for future studies into incorporating highly branched polyelectrolytes into PECs.

In Chapter 5, we summarize our results and make the case for utilizing architecturally advanced polyelectrolytes to achieve otherwise unattainable structures in PEC materials. Combined, the results contained here broaden the PEC design space considerably, provide insight into molecular-level structure property relationships for PECs and pave the way for further study of advanced polyelectrolyte architectures within ordered PCMs and bulk PECs.

Chapter 1. Introduction to Polyelectrolyte Complexation

1.1 Polyelectrolyte Complexation

1.1.1 Foundations of Polyelectrolyte Complexation

Polyelectrolytes are polymers with ionic moieties along some or all the repeat units.[1] In solution, small molecule counterions and water molecules condense along the polyelectrolyte backbone to reduce the effective charge density and minimize electrostatic repulsion along the chain. When solutions of oppositely charged polyelectrolytes are mixed, the oppositely charged polymers condense around each other, freeing the aforementioned small molecules and restoring their translational entropy.[2, 3] Counterion release drives polyelectrolyte complexation, the spontaneous association of oppositely charged polyelectrolytes.[4] Polyelectrolyte complexation drives phase separation into a polymer rich phase known as the polyelectrolyte complex (PEC) which exists in equilibrium with the polymer poor supernatant phase.[5, 6]

PECs are an interesting materials platform because they can exhibit a wide range of properties, display unique stimuli-responsivity and easily interface with biological materials.[7-11] To explain these properties, we must discuss the molecular organization of a polyelectrolyte complex. PECs are composite materials composed of at least two oppositely charged polymers, water and counterions. Within the complex, charged groups can either be complexed with oppositely charged groups on another polymer or a small molecule counterion.[2, 12, 13] Polymer-polymer ion pairs are referred to as intrinsic ion pairs, whereas polymer-counterion pairs are referred to as extrinsic ion pairs.[12] Extrinsic pairs, in addition to adding a counter-ion, also draw water into the PEC.[14] Adding salt to a PEC shifts the proportion of intrinsic to extrinsic ion pairs, favoring extrinsic ion pair formation and swelling the material.[12]

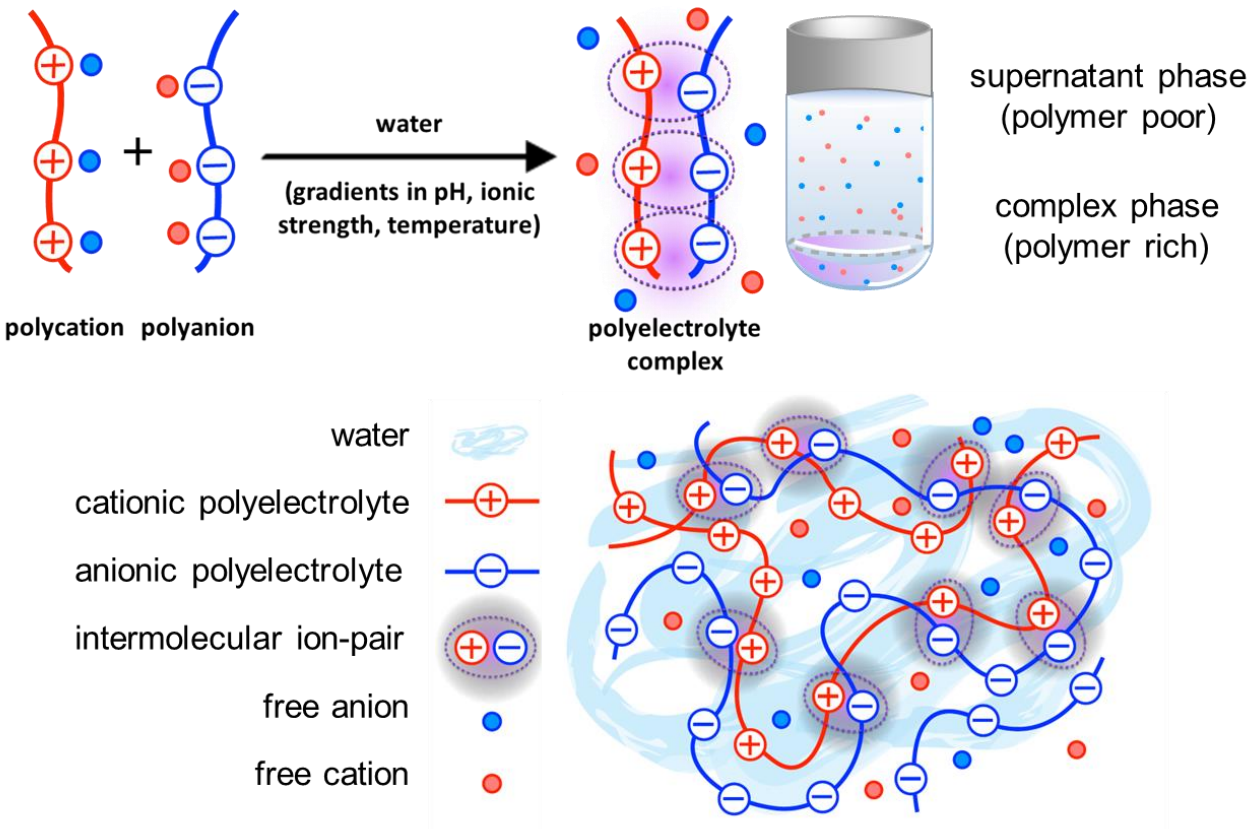

Figure 1.1 Schematic illustrating polyelectrolyte complexation and the internal structure of polyelectrolyte complexes with polyanions shown in blue and polycations shown in red. Illustrations show (top left) oppositely charged polyelectrolytes condensing and releasing small molecule counterions, (top right) cartoon representation of phase separation into complex and supernatant and (bottom) the internal structure of polyelectrolyte complexes.

The formation and maintenance of intrinsic ion pairs between oppositely charged polymers is central to many behaviors of polyelectrolyte complexes. The entropic gain upon forming intrinsic pairs is directly related to the thermodynamic driving force for complexation, which in turn determines the critical salt resistance of a PEC.[2, 15] Separately, the electrostatic interactions between intrinsic ion pairs play a crucial role in determining the mechanical properties of PECs.[14, 16] Molecular features of the constituent polyelectrolytes determine the degree of extrinsic pair formation as a function of added salt, the amount of water in the complex at equilibrium and the ratio of intrinsic to extrinsic sites at no added salt.[12] Unfortunately, predicting the relationship between polyelectrolyte design and PEC properties remains challenging.

1.1.2 Physical Characteristics of Polyelectrolyte Complexes

The properties of polyelectrolyte complexes can be divided into a few fundamental areas, which interact with each other to generate the unique material profile characteristic of polyelectrolyte complexes. The most fundamental characteristics of PECs are the phase behavior, mechanical properties and internal structure. Together, these attributes generate most ofe the emergent properties of PECs.

The complex and supernatant phase exist in equilibrium with salt and polymer exchanged between phases at a constant rate.[5, 17] The proportion of polymer in the complex and supernatant depends on the salt content the complex was prepared at, with higher salt concentrations favoring more polymer in the supernatant. The salt concentration where phase separation ceases is defined as the critical salt concentration (CSC), or the maximum amount of salt that a PEC can withstand before dissolution. The length of a polymer is directly related to the CSC, with a dramatic dependence on degree of polymerization (DP) at low DP that plateaus at moderate DP. Li et al. measured the phase diagram for a PEC for the first time, showing the increase of CSC as a function of salt and the partitioning of salt and polymer into the complex and supernatant phase as a function of salt at various environmental salt concentrations.[5] The salt partitioning, denoted with dashed lines in Figure 1.2 A, deserves further consideration. When this line has a positive slope, salt preferentially partitions in the supernatant phase, meaning the complex is more salophilic than the supernatant under those conditions. A complete understanding of what makes a complex salophilic or salophobic relative to the supernatant remains elusive, but would be a powerful tool in tailoring and predicting the degree of intrinsic and extrinsic ion pairing between a complex. In recent years, precise measurement of PEC phase separation through thermogravimetric measurements have provided more precise measurements, informing more physically accurate predictive theories.[18, 19]

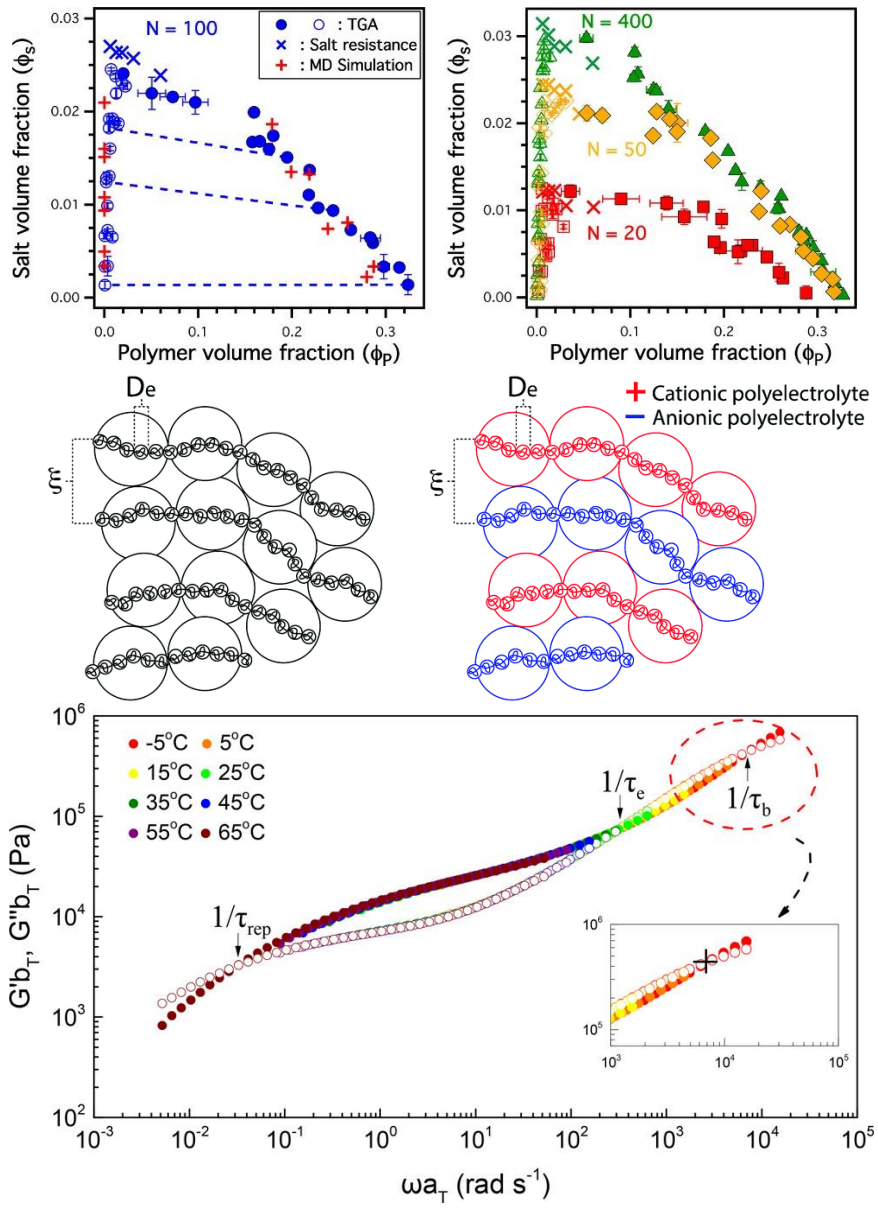

Figure 1.2 Figures illustrating primary features of polyelectrolyte complexes. (A) salt and polymer partitioning at complexes prepared at different salt concentrations and using different polymer lengths. (B) schematic illustrating semidilute polyelectrolyte conformation (left) and PEC internal structure (right). (C) TTS of an entangled polyelectrolyte complex showing the characteristic reptation, entanglement and ion-pairing times.

The internal structure of complexes has only recently been investigated, and there is still little known about how the configurations of PECs change as a function of molecular weight and charge density, for example. However, based on the limited study done so far, polyelectrolyte complexes tend to adopt a random, overlapping network structure with akin to semidilute solutions

(Fig. 1.2 B).[20, 21] This fundamental structure can be altered by secondary interactions like hydrogen bonding, pi-pi stacking etc., but these are generally considered to be deviations from the standard network architecture of interpenetrating oppositely charged sidechains.[18, 20] Elucidating the driving forces for unique PEC structural development would be a key step towards developing predictive design in PECs. Blocky and non-linear polyelectrolyte architectures can be used to direct the formation of ordered PEC gels and micelles, which will be covered in more detail in Sections 1.2 and 1.3.

The mechanical properties of PECs are highly variable and connected to the polymer, salt and water content and chemistry as well as the internal structure.[22-25] In general, polyelectrolyte complexes behave as viscous "sticky" associating polymers softened by solvent. The presence of solvent in a PEC both softens the material and increases the entanglement molecular weight relative to uncharged materials, which leads to many PEC systems displaying soft, unentangled viscoelastic behavior. Small angle oscillatory shear (SAOS) measurements have been used extensively to measure the mechanical properties of PECs with great success. In general, PECs can successfully undergo time-temperature superposition (TTS), which allows a dramatic widening of the frequency regime available for study (Fig. 1.2 C). Interestingly, salt and temperature have analogous effects on the rheology of PECs in many systems, allowing for time-salt superposition (TSS) as well. More exotic superpositions like time-pH and time-hydration superposition have been discovered in certain PEC systems, but only in rare cases.[26, 27] The ability of any superposition technique to work suggests that the primary influence of salt, temperature pH etc. on PEC mechanics is primarily through altering hopping dynamics between intrinsic ion pairs, not through larger structural changes.[25] It is still unclear what sort of chemical changes correspond to different changes in mechanical properties, as altering hydrogen bonding, pi-pi stacking,

hydrophobic interactions and other molecular details do not consistently alter the rheology of PECs. The interconnectivity of PEC properties is what leads to their vast potential as well as the difficulty in fully understanding their properties. Chemical methods to simplify the study of PEC have recently emerged and show great promise in developing foundational understanding.

1.1.3 Reactive Polymers for Polyelectrolyte Complexes

There are numerous synthetic considerations that must be considered when designing a PEC (Fig. 1.3). The length, The complexity is compounded by the fact that PECs are combinatorial materials by nature. As a result, it is common for PECs to have disparate molecular features, making it difficult to precisely attribute PEC properties to molecular features. While this issue has delayed the development of straightforward chemical design principles in PECs, clever chemistry has provided a pathway to more straightforward PEC systems with reduced intermolecular variables.

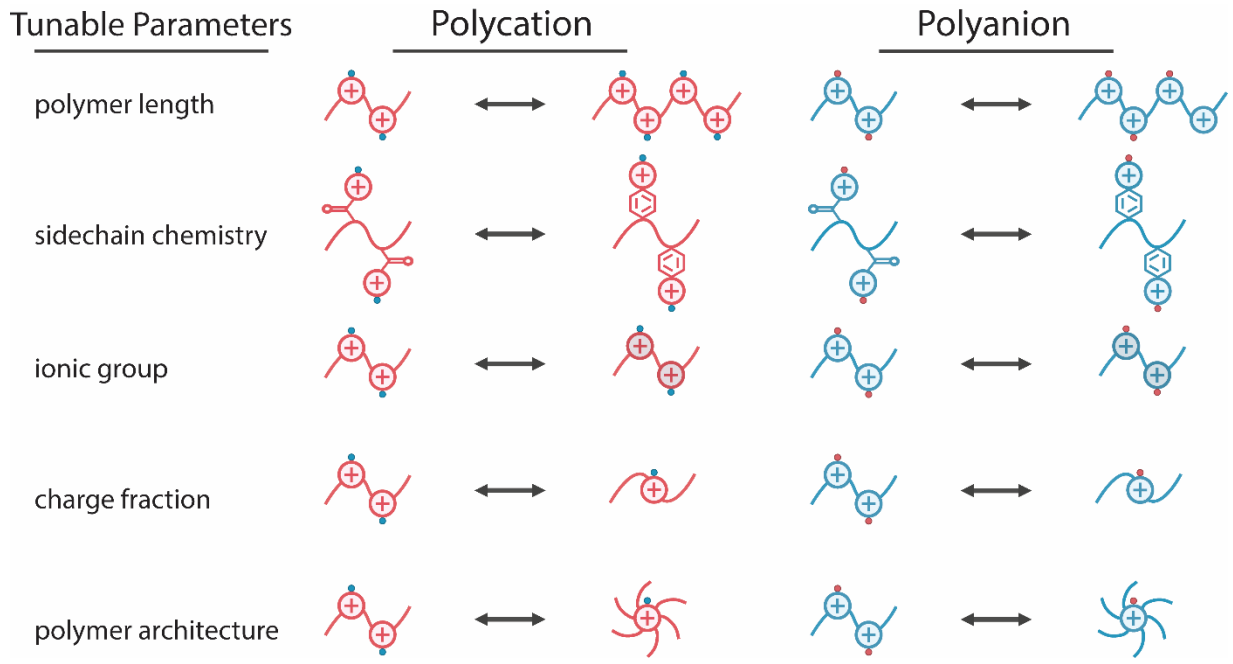

Figure 1.3 Schematic illustrating the tunable molecular parameters within PEC design.

To address the complexity that emerges from the combinatorial nature of PEC design, some researchers harness reactive polymers and click chemistry to create homologous polyelectrolyte pairs. Reactive polymers have reactive moieties on some or all the monomers that compose the polymer. These reactive groups allow for post polymerization modification (PPM) reactions, which can attach a variety of functional groups pendant to a polymer.[25–28] Previous research demonstrates how using these polymers can give structurally identical but oppositely charged polyelectrolytes that can be used as model systems to uncover otherwise unattainable structure-property relationships in PECs. The first reported application of reactive precursors in PECs made a library of ABA triblock polymers based on an ethylene oxide (EO) mid-block and allyl glycidyl ether (AGE) outer-blocks, and then used the pendant alkenes of the AGE blocks to attach oppositely charged groups via thiol-ene PPM reactions (Fig. 1.4).[29] Within this series of reactive polymers, Hunt *et al*. varied neutral and charged block length, which enabled the researchers to understand w ha t effect charged block length and ionic moiety have on the hydrogels that were formed by mixing the oppositely charged triblocks.

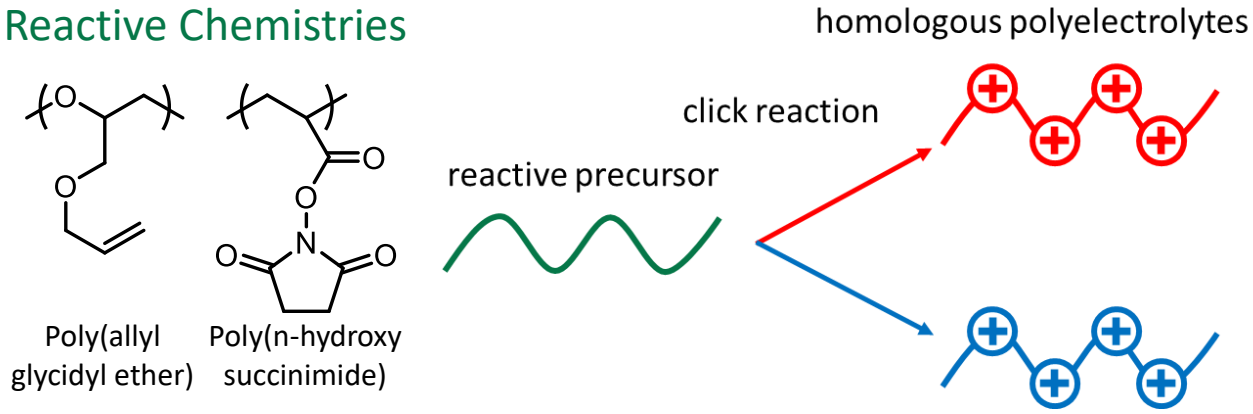

Figure 1.4 Schematic illustrating common reactive chemistries used in PECs (left) and the general approach of combining reactive polymer precursors and click chemistry to achieve homologous polyelectrolyte pairs (right).

The reactive monomer N-acryloxy succinimide (NAS) presents another synthetic approach to homologous polyelectrolytes. NAS has a labile N-hydroxysuccinimide group susceptible to nucleophilic attack by a variety of nucleophilic amine containing molecules and has been employed to create pairs of polyelectrolytes in two ways. The first method is via direct attachment of the polyelectrolyte moitey onto the reactive backbone. In one example, Huang *et al*. reacted one poly(NAS) precursor with hydrophobic and hydrophilic uncharged amines as well as amines that contain carboxylate and tertiary amines to create a library of oppositely charged statistical copolyelectrolytes with identical amounts of hydrophobic and hydrophilic neutral comonomers.[35] Their synthetic design allowed them to demonstrate that their statistical PECs were sensitive to the fraction of charged units, but relatively insensitive to whether the comonomer was hydrophibicity/hydrophilicity.

Inspired by the AGE system, *Lou et al*. have modified poly(NAS) with allyl amine to convert poly(NAS) into poly(allyl acrylamide), which has reactive pendant alkenes that can undergo thiol-ene PPM reactions.[36] In addition, they oxidized the thioether bond formed from the thiol-ene PPM reaction to evaluate the effect of changing the polarity close to the charged groups on PEC stability. From this study, they were able to develop a thermodynamic model that accurately described the phase diagram of their PECs as a function of polyelectrolyte length and local polarity of the charged groups. Unfortunately, poly(NAS) has solubility issues, its modifications are prone to side reactions and it is unstable in the presence of water.[37] These studies demonstrate the power of reactive polymers for elucidating structure-property relationships of PECs and highlight the need for the optimization of reactive chemistry towards use in PEC studies.

1.2 Architecturally Complex Polyelectrolytes

1.2.1 PEC Self-Assembly Mediated by Polyelectrolyte Architecture

Among the landmark achievements in polymer science over the past 100 years, polymeric self-assembly stands apart for its versatility, ubiquity, and potential. [28-32] Evolving through a century of biology inspired and curiosity driven research, polymer science developed and harnessed a wealth of synthetic capabilities to create numerous classes of ordered polymer systems with diverse chemical functionality and unique physical properties. Currently, most macromolecular self-assembly studies employ driving forces based on incompatibility, often quantified by the material-specific Flory-Huggins interaction parameter (χ), which serves as a measure of solvent-polymer or polymer-polymer interactions.[33] In contrast, polyelectrolyte complexation occurs through the association of oppositely charged polyelectrolytes and the resulting entropy gain due to small counterion release. As such, polyelectrolyte complexation represents a new and unique mode of self-assembly promising to drive polymer science beyond χ driven assembly and aid the polymer community as it continues to push the boundaries of soft matter structuring to meet and exceed that of biological systems.

Polyelectrolyte complexation occurs when aqueous solutions of oppositely charged polymers are mixed, and results in a polymer-rich coacervate phase and a polymer-poor supernatant phase.[5] While polyelectrolyte complexes (PECs) have been studied for almost a century, they have received a surge in interest in the past decade. As aqueous polymerization techniques have become more robust, PEC systems have featured polyelectrolyte pairings with richer chemical and structural variety, which has led to a deepening of our understanding of fundamental thermodynamic features of polyelectrolyte complexation. While foundational aspects of the of the polymer-rich PEC phase have been the subject of numerous research directions,[1]

block polyelectrolytes have provided vast opportunities to exploit microphase separation and form an array of morphologies across length scales and discrete ordered domains.[34, 35] For example, through polyelectrolyte complexation, diblock polyelectrolytes can form completely hydrophilic polyelectrolyte complex micelles (PCMs), a promising strategy to address existing challenges of encapsulating and delivering hydrophilic biological molecules such as DNA or RNA that hold incredible potential for applications in nanomedicine.[36-38] Simple architectural considerations, such as the length of each block, can control size or manifest the formation of different shapes in designer nanoscale delivery vehicles, tailored specifically toward overcoming biological barriers.[10, 39-42] However, beyond double hydrophilic diblock polyelectrolytes lie a bevy of existing and prospective polymer architectures – each with the potential to direct PEC assembly along unique pathways towards novel morphologies, properties, and functions.

Expanding polymer architecture from strictly linear to branched structures provides a direct method to manipulate the sequence, size, connectivity, and spatial distribution of the constituent chemical and ionic attributes of polymers within self-assembled materials, making it an attractive parameter to explore in pursuit of new PEC morphologies.[43] Polymer processing,[44, 45] characterization,[35] and synthesis[43, 46] have devoted substantial efforts in developing strategies to access existing morphologies more effectively and uncover new structures more efficiently. To this end, recent developments in advanced polymer synthesis have provided direct routes to increasingly complex blocky and branched macromolecular architectures[33, 47-49] and multiblock polymers,[50, 51] which have expanded our understanding of the structure-property relationships within structured polymeric materials. Despite the increased availability of advanced architectures, some of the largest classes of PECs such as homopolymer/homopolymer bulk complexes, layer-by-layer assemblies, and PEC micelle nanocarriers employ linear homopolyelectrolytes or diblock

systems, almost exclusively. These classes of PEC materials, as well as the thermodynamic and theoretical treatments of PECs have been exhaustively reviewed elsewhere[3, 9, 52-54] and will not be elaborated on in this section. Here, we demonstrate the nascent potential of harnessing controlled macromolecular architecture in conjunction with polyelectrolyte complexation to achieve novel PEC properties (Fig. 1.5).

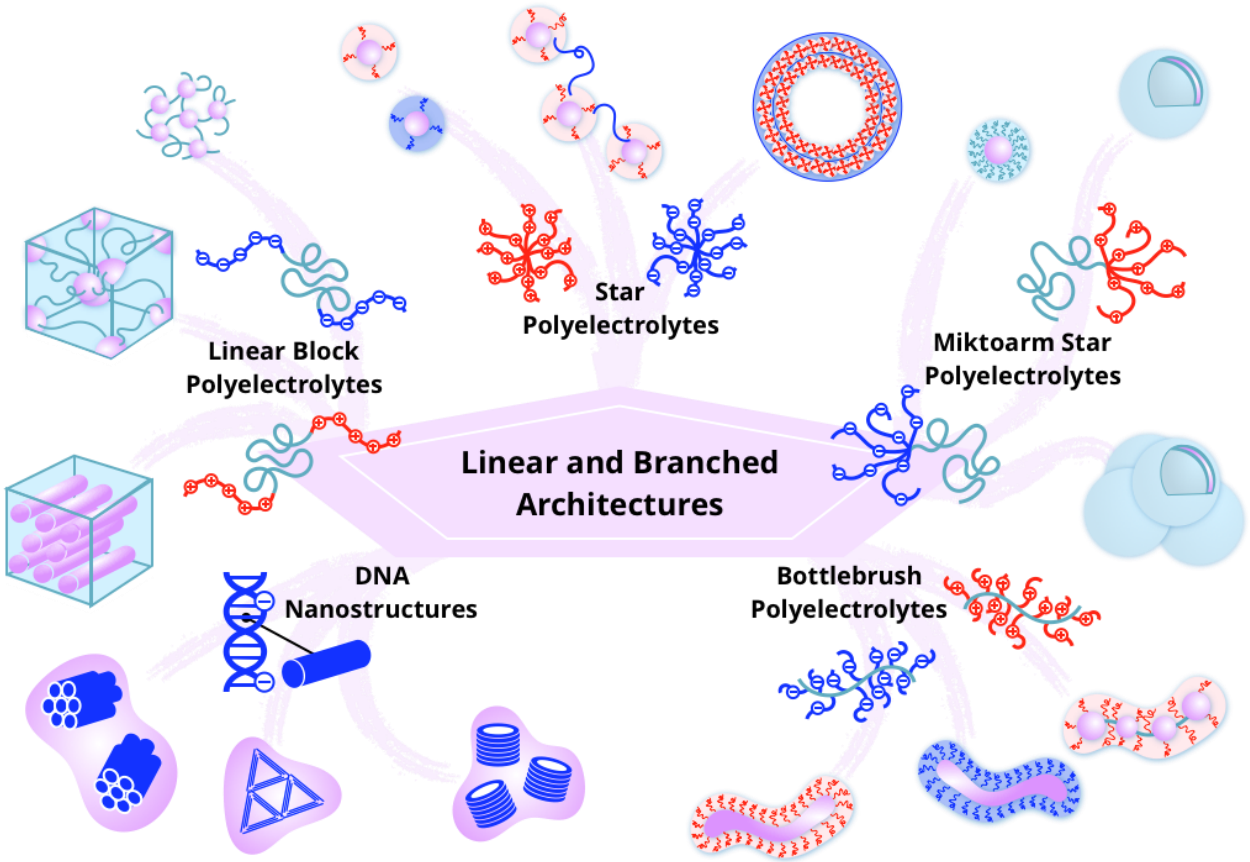

Figure 1.5 Illustration of the diverse array of linear and branched charged polymer architectures. Hierarchical assemblies highlighted in this section include linear block polyelectrolytes, star polyelectrolytes, miktoarm star polyelectrolytes, bottlebrush polyelectrolytes, and DNA nanostructures. For simplicity in these cartoons, counterions are not shown, and structures are not drawn to scale. Charged blocks are colored red (polycation) and dark blue (polyanion), while neutral blocks are shown as light blue to represent hydrophilic polymers.

1.2.2 Structured PEC Gels and Networks

By controlling polymer concentration and polyelectrolyte architecture, polyelectrolyte complexation can be harnessed to provide hierarchically structured bulk materials, with opportunities to form physical PEC gels that can be stimuli-responsive in water and potentially useful as multifunctional biomaterials.[8, 55, 56] Mixing oppositely charged ABA triblock has led to a rich variety of periodic structures, demonstrating body-centered-cubic (BCC) spheres[57], hexagonally packed cylinders (HPCs), bicontinuous gyroids and lamellae.[58] Hunt et al. synthesized a series of poly(allyl glycidyl ether)$_x$-*b*-poly(ethylene oxide)$_y$-*b*-poly(allyl glycidyl ether)$_x$ (PAGE$_x$-*b*-PEO$_y$-*b*-PAGE$_x$) of varying block lengths and functionalized the pendant alkene groups of the PAGE blocks via thiol-ene click to attach sulfonate, carboxylate, ammonium, and guanidinium ionic species.[57] This use of reactive polymers in conjunction with click chemistry provides a facile route to oppositely charged, but structurally identical polyelectrolytes (Fig. 1.6 A) that have been subsequently used to systematically evaluate structure-property relationships and internal structure of PEC materials.

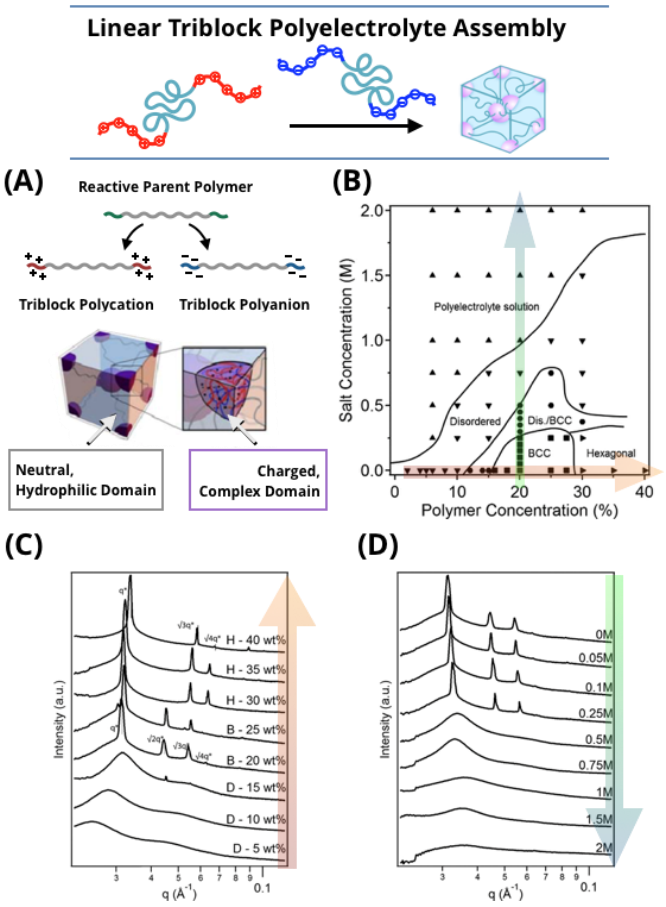

Figure 1.6 Complex phase behavior of triblock polymer coacervate gels. (A) Scheme of preparing triblock polycations and polyanions via post-polymerization functionalization to form ordered charged, complex domains within a neutral, hydrophilic matrix. (B) Phase diagram depicting the gel structure as a function of polymer and salt concentration, using small-angle X-ray scattering (SAXS) and dynamic mechanical data. Solid black lines were drawn to guide the eye; orange and green arrow correspond to polymer concentration studies at salt-free conditions and salt concentration studies at constant polymer concentration conditions, respectively. (C) SAXS patterns of salt-free samples at varying polymer concentration, ranging from a disordered array of spherical domains (D: 5, 10, and 15 wt %), spherical domains on a BCC lattice (B: 20 and 25 wt %), and hexagonally packed cylinders (H: 30, 35, and 40 wt %). SAXS patterns were shifted vertically for clarity. (D) SAXS patterns of 20 wt % samples at varying salt concentration, ranging from a BCC structure (0, 0.05, 0.1, and 0.25 M) to disordered domains (0.5 and 0.75 M) to a polyelectrolyte solution (1, 1.5, and 2 M). SAXS patterns were shifted vertically for clarity. Adapted from Krogstad et al. Copyright 2013 American Chemical Society.

1.2.3 Block Length and Salt Effects.

In a series of papers, Krogstad et al. focused on networks formed by guanidinium and sulfonate functionalized derivatives of PAGE-*b*-PEO-*b*-PAGE to quantify the effect of polymer concentration, pH, and salt concentration on the internal structuring of PEC networks.[58, 59] Figure 1.2(B)-(D) shows the breadth of ordered morphologies documented in these works. By SAXS, increasing polymer concentration corresponded to an increase in the materials storage modulus until the transition from BCC spheres at 25 wt. % to HPCs at 30 wt. %, which resulted in a 25% decrease in the storage modulus due to the difference in stress relaxation modes available to the differently ordered phases. Importantly, this report demonstrated that a variety of internal structures and mechanical properties can be easily achieved and altered by changing the polymer and salt concentration. Comparisons of the triblock and a diblock copolymer (PEO_{216}-*b*-$PAGE_{30}$) at the same polymer and salt concentration demonstrated similar structural trends, but distinct dynamic behavior, with the triblocks showing dramatically slower rearrangement compared to the diblocks.[60] This difference was hypothesized to be due to the different connectivity and mobility allowed by diblock and triblock polyelectrolytes, highlighting the consequences of higher order block polymers on PEC gel properties.

In a recent effort, Srivastava et al. synthesized a series of PAGE-*b*-PEO-*b*-PAGE polymers with two PEO lengths to understand the effect of charged and neutral block length on network structure and bulk rheology.[61] They observed previously unreported gyroidal and lamellar ordering in samples with high end group fraction and polymer concentration, demonstrating a trend reminiscent of traditional χ driven block copolymer assembly despite the different assembly mechanism (Figure 1.7). Interestingly, they report how the slow dynamics of triblocks are exacerbated in samples with long charged blocks. Samples with high charged group fraction were

more likely to exhibit coexistence of multiple ordered phases, suggesting that the combination of triblock architecture and increased electrostatic associations in the PEC domains prevented homogenous network formation as shown in the upper right-corner of Figure 1.7 A. Importantly, the structural trends were similar for both midblock molecular weights, suggesting that the structural relationships shown in Figure 1.7 could serve as a general guide for PEC gel design in biomaterial applications.

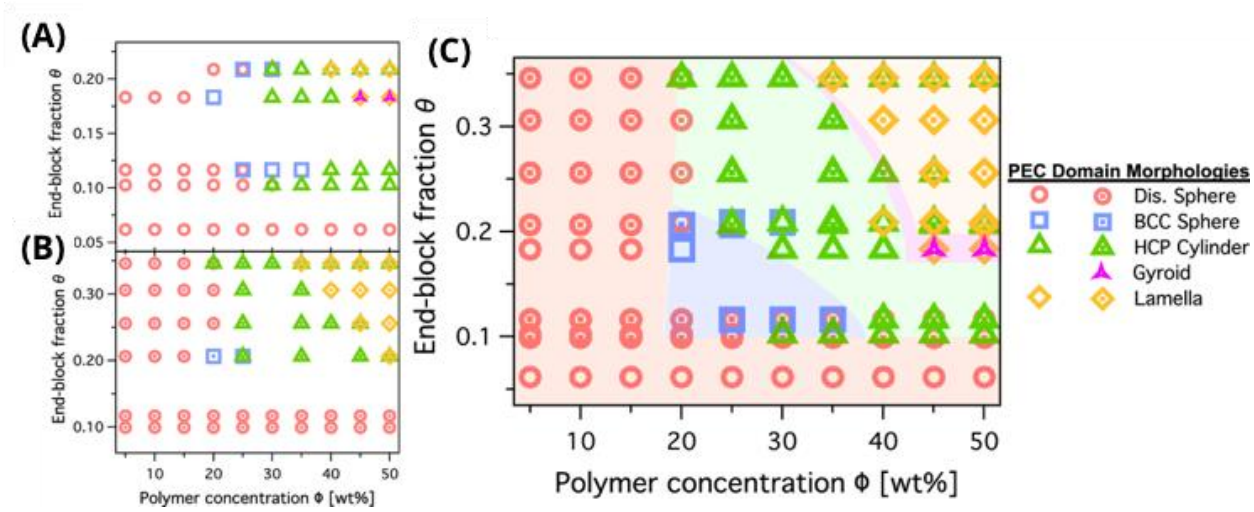

Figure 1.7 Morphology maps showing the structural state of PEC domains as a function of end-block $\theta = N_{PAGE}/(N_{PEO} + N_{PAGE})$ and total polymer concentration Φ (A) PEO midblock n = 455 (B) PEO n = 227 (C) Unified morphology map of both PEO lengths. Adapted from Srivastava et al.[61] Copyright 2020 American Chemical Society.

The influence of block architecture extends beyond equilibrium structures and into assembly pathways for PEC networks derived from triblock polyelectrolytes. Using small-angle neutron scattering (SANS), Srivastava et al. observed that PEC gels form from PAGE-*b*-PEO-*b*-PAGE triblocks at concentrations as low as 0.5 wt. %, with no observed micellar phase proceeding network formation.[62] Simulations predict that in amphiphilic triblock systems, the transition from a polymer solution to a network occurs through an intermediate phase, where flower-like micelles

form and then jam together as the neutral blocks overlap with increasing concentration, which is consistent with experiments.[63] Their work suggests that the individual polyelectrolytes adopt an extended conformation due to the electrostatic repulsion of like-charged end blocks, which favors bridging and network formation instead of looping and micelle formation. By leveraging this unconventional pathway for ordered assembly, multiblock polyelectrolytes could enable ordered materials in challenging conditions and uncover unique morphologies.

1.2.4 Branched and Complex Architectures

In polymer science, branched polymers have been historically pursued for not only their elegant structure and intricate geometry, but also as attractive materials for the diverse range of commercial products spanning viral vectors to rheology modifiers to porogens.[64] In the branched polymer literature, much of the recent interest in exotic architectures has focused on how the connectivity and structural anisotropy of these macromolecules manifests in microphase separation and unique self-assembled structures.[43, 65] The pursuit of more exotic polyelectrolyte architectures that can hierarchically assemble into a wider range of structures has been limited to date. In this section, we describe how the use of polyelectrolytes with star, miktoarm, and bottlebrush architectures as well as geometrically distinct DNA nanostructures can harness specific macromolecular features to direct unique assembly pathways in polyelectrolyte complexation.

1.2.5 Star Polyelectrolytes.

Star polymers are characterized by a central branching point (known as a core) that is surrounded by linear polymer arms with variable length and branching density. This unique architecture results in an array of solution and mechanical properties that are distinct from linear polymers. Excellent accounts of such examples are available elsewhere.[66] Star polymers can be synthesized by different polymerization techniques such as reversible-deactivation radical

polymerization that can increase the density of polymer objects through high branching from the core. For instance, star polyelectrolytes have been used to improve DNA transfection efficiency over conventional alternatives like dendrimers,[67] motivating the need for a more complete understanding of topology effects on polyelectrolyte complexation induced self-assembly for delivery applications.

Star polyelectrolytes incorporated into PECs behave similarly to linear polyelectrolytes, but with important differences that arise from their distinct geometry and higher charge density.[68] When star polyelectrolytes are complexed with an oppositely charged diblock copolymer at a 1:1 charge ratio, a core-shell polyelectrolyte complex micelle (PCM) is formed, similar to those formed by homopolymer-diblock systems of purely linear polyelectrolytes.[69] In contrast, a unique feature of star polyelectrolytes is their ability to form stable nanoparticles solely through complexation with oppositely charged linear polyelectrolytes.[70] In a series of papers, Purgushov et al. complexed PAA star polyelectrolytes containing either 3, 8, or 21 arms with linear polycations of various lengths.[71, 72] Interestingly, they found that stable core-shell PCMs were formed under charge mismatched conditions with excess negative charge. Figure 1.8 A shows a representative size distribution of small complex species and large aggregates from the 8-arm star polycation/linear polyanion via dynamic light scattering.

Careful analysis of the PCMs as a function of the number of arms and ionic strength resulted in a proposed mechanism shown in Figures 1.8 B and C. This was explained by an “arm collapse” mechanism in which whole arms were drawn toward the core to compensate for the linear polycation. The free arms that did not form intermolecular ion complexes provided colloidal stability and formed the shell of the core-shell nanoparticle. Complementary simulation studies supported this unusual mechanism.[73] Purgushov et al. also observed that when the cumulative

degree of polymerization of a star polymer was less than or equal to the linear polyelectrolyte, nanoparticles aggregated between star polymers.[71] This is analogous to recent results in the field of micelleplexes.[74-76] These features of star polyelectrolytes can make them useful as templates for depositing hybrid inorganic particles and core-shell nanoparticles.

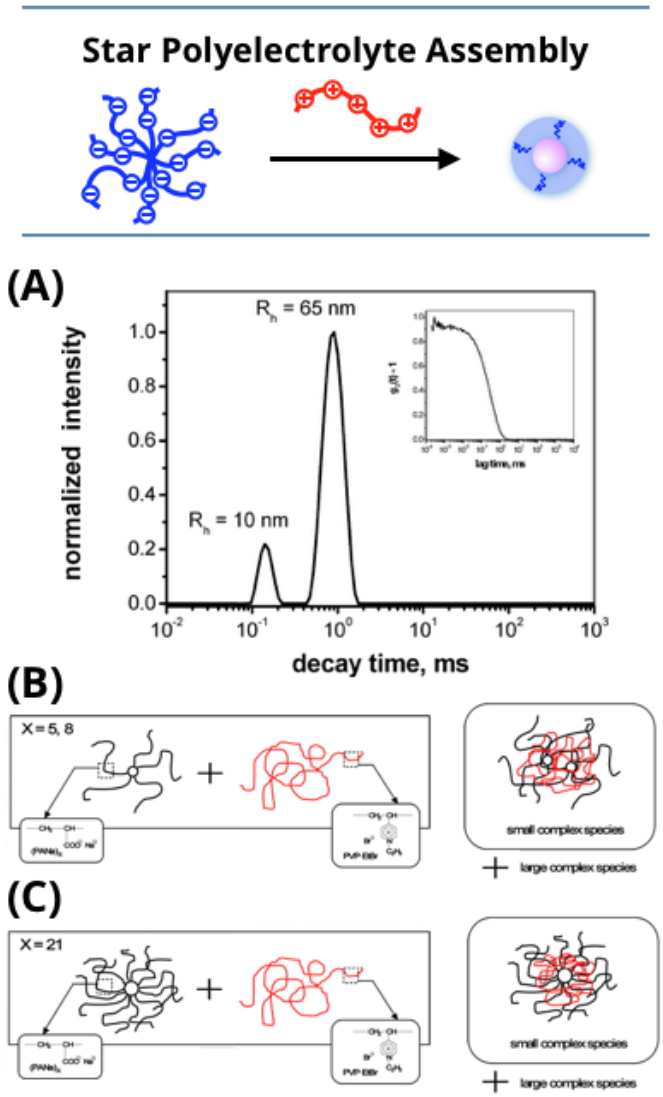

Figure 1.8 (A) Representative intensity distribution of decay times obtained at 90° for the mixture of 8-arm star-shaped poly(acrylic acid) ($(PAA_{100})_8$ in the form of the sodium salt) with poly(N-ethyl-4-vinylpyridinium bromide) (PVP·EtBr); the inset shows the autocorrelation function. (B) Schematic representation of PCMs comprising $(PAA_N)_X$ and PVP·EtBr for (B) X = 5, 8 arms and (C) X = 21 arms. Adapted from Pergushov et al.[72] Copyright 2008 American Chemical Society.

Star polyelectrolytes applied in layer-by-layer PEC coatings form films with precisely tunable features based on processing conditions.[68] Expanding on this strategy, Weinan et al. have utilized star polyelectrolytes to create templated nanoparticles based on layer-by-layer self-assembly of star-linear or linear-linear polyelectrolyte pairs onto a silica nanoparticle.[77] Once assembled, the silica nanoparticles were selectively dissolved and removed, leaving the PEC multilayer microcapsule which was responsive to pH, ionic strength, and temperature. The star-linear polyelectrolyte pairs provided better control over the permeability, higher mechanical stability, and improved colloidal stability compared to the linear-linear system. It is hypothesized that many of these desirable properties are a result of the high charge density in star polyelectrolytes that frustrates complete charge compensation which manifests in excess charged groups that give rise to their improved properties. This type of hierarchically ordered microcapsules are promising as dual-responsive drug carriers and other smart nanomaterials.

1.2.6 Miktoarm Polyelectrolytes.

Miktoarm polymers distinguish themselves from star polymers by incorporating one or more linear branches radiating from the core that is chemically distinct from the rest of the branches. This unique attachment of chemically disparate polymers favors different self-assembly mechanisms than traditional diblock polymers. For example, theory and experiment have reported the propensity for ABC miktoarm triblocks to form a variety of self-assembled structures inaccessible to linear ABC triblocks.[40] Notably, polyelectrolyte complexes formed by double hydrophilic miktoarm polyelectrolytes and oppositely charged diblock or homopolyelectrolytes tend to form vesicular structures instead of the traditional micellar structure. First reported by Plamper et al., this miktoarm polymer system utilizes one PEO arm and varying numbers of quaternized poly(DMAEMA) arms.[78-80] In early reports, vesicle morphology was obtained by

mixing the miktoarm polyelectrolytes with an oppositely charged linear polyelectrolyte. This result was consistent with theory, which suggests that for miktoarm polymers the number of core forming arms is a significant factor in determining the equilibrium structure of assemblies,[81] due to the fact that increasing the number of core forming arms increases the entropic cost for stretching a larger number of core-forming blocks and destabilizes spherical morphologies in favor of worms and vesicles. The prediction was further supported in the PCM literature with work showing that blends of diblock polyelectrolytes and miktoarm polyelectrolytes with an oppositely charged homopolyelectrolyte provide easy access to vesicular, worm and spherical morphologies as the amount of miktoarm polymer is diluted.[78] Conjugating a temperature-responsive block like poly(n-isopropyl acrylamide) to the polyanion provides opportunities to create multi-core spherical or worm-like micelles as a function of temperature and processing method.[82]

Miktoarm polyelectrolytes also present opportunities for advanced encapsulation vehicles. In an evolution of layer-by-layer growth of PEC multilayer microcapsules, Xu et al. utilized a combination of hydrogen bonding and polyelectrolyte complexation driving forces to create hierarchically structured microcapsules capable of encapsulating and sequentially releasing two different types of molecules as a function of the separate stimuli of pH and ionic strength.[83] Figure 1.9A schematically depicts this design process using the PEO-*b*-qPDMAEMA miktoarm system. To construct these microcapsules, they used alternating layers of miktoarm derived, dye-loaded PCM vesicles and tannic acid (TA) to create a multilayer vesicle-TA alternating structure assembled via hydrogen bonding on a sacrificial silica template. The utility of these microcapsules in orthogonally delivering multiple cargo is shown in Figure 1.9B. A dye was loaded and selectively released from the microcapsule by changing pH and protonating the TA layers, which resulted in a more porous structure. Independently, increasing ionic strength can be used to release

cargo, by weakening PEC walls and increasing diffusion out of the polymersomes. Even after both release cycles, the microcapsules retain their structural stability, which paired with the ability to sequentially release cargo makes these materials attractive for a range of therapeutic applications. This provides excellent motivation for future use of both advanced architectures and multiple self-assembly mechanisms as a promising route for future research.

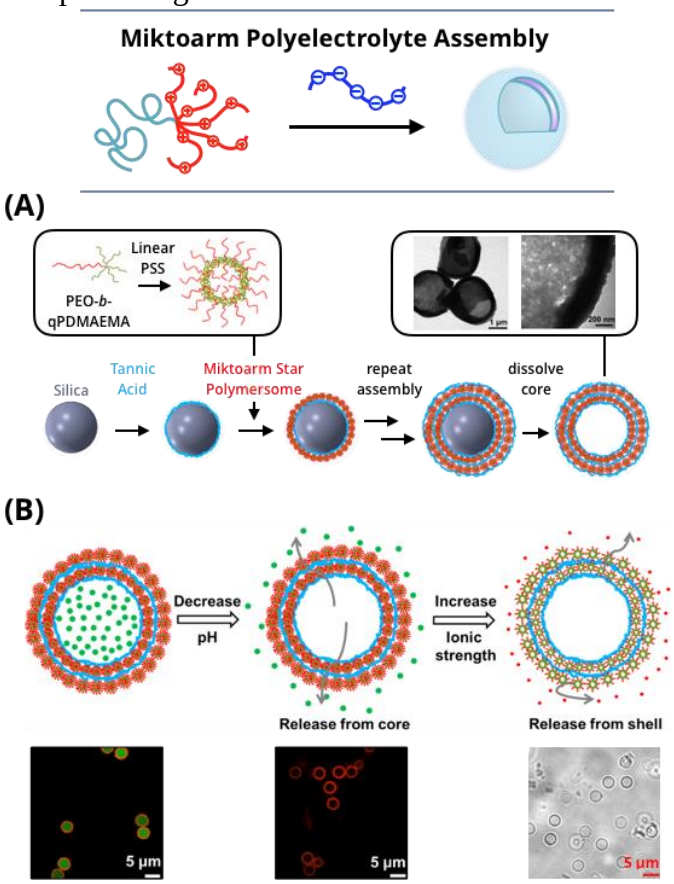

Figure 1.9 Hierarchical assembly of star polyelectrolyte polymersomes into multicompartmental microcapsules. (A) Schematic illustration of the layer-by-layer assembly approach to prepare tannic acid/miktoarm star complex polymersome microcapsules. The inset on the left shows the star poly(ethylene oxide)-*block*-quaternized poly(dimethylaminoethyl methacrylate) (PEO-*b*-qPDMAEMA) and linear poly(styrene sulfonate) (PSS) polymers; the inset on the right shows select TEM images of the layer-by-layer microcapsules. (B) Pathway showing the sequential and independent release of two distinct molecules as a function of pH and ionic strength: anionic fluoroscent molecules (green) from the core followed by cationic fluorescent molecules (red) from the shell of the microcapsules. From left to right, below each cartoon is a confocal laser scanning microscopy image of the microcapsules with combined dual red/green channels, pH-induced release, and microcapsules after both release steps in bright field. Adapted from Xu et al.[83] Copyright 2016 American Chemical Society.

1.2.7 Bottlebrush Polyelectrolytes.

Bottlebrushes polymers present more interesting opportunities for self-assembly, as they possess a unique structural anisotropy due to the independently variable width and length of the macromolecule that can be tuned by structural features such as backbone length, sidechain length, and branching density. Combining these features in bottlebrush polyelectrolytes can open doors to new opportunities in exploring fundamental questions on the interplay between steric and electrostatic repulsion, as well as driving assembly into unprecedented molecular structures. Early work attempted to use bottlebrush polyelectrolytes as rod-like PEC nanoparticles, which often required extremely precise ratios of polymers and polymer concentrations to be successful.[84] Over time, research efforts have evolved beyond efforts to preserve the inherent rod-like architecture of bottlebrush polyelectrolytes and, instead, have explored the unique structures bottlebrush polyelectrolytes can provide as templates in polyelectrolyte complexation induced self-assembly. We detail two specific examples below to show emerging directions of bottlebrush polymers in the realm of PEC materials.

First, bottlebrush polyelectrolytes can be complexed with oppositely charged linear polyelectrolytes to form unique structures that are distinct from more traditional PECs. Larin et al. showed that, like star polyelectrolyte systems, bottlebrush polyelectrolytes undergo an "arm retraction" type complexation mechanism.[85] However, unlike star polyelectrolytes, the bottlebrush architecture has multiple branching points through the length of the backbone, which results in clusters of oppositely charged macromolecules distributed throughout the polymer backbone. This clustering resulted in a pearl necklace-like conformation that was visualized through atomic force microscopy and complementary simulations (Fig. 1.10). Furthermore, like star polyelectrolytes,

the net bottlebrush charge must be in excess relative to the linear polyelectrolyte to ensure colloidal stability against aggregation endowed by the un-complexed bottlebrush arms.

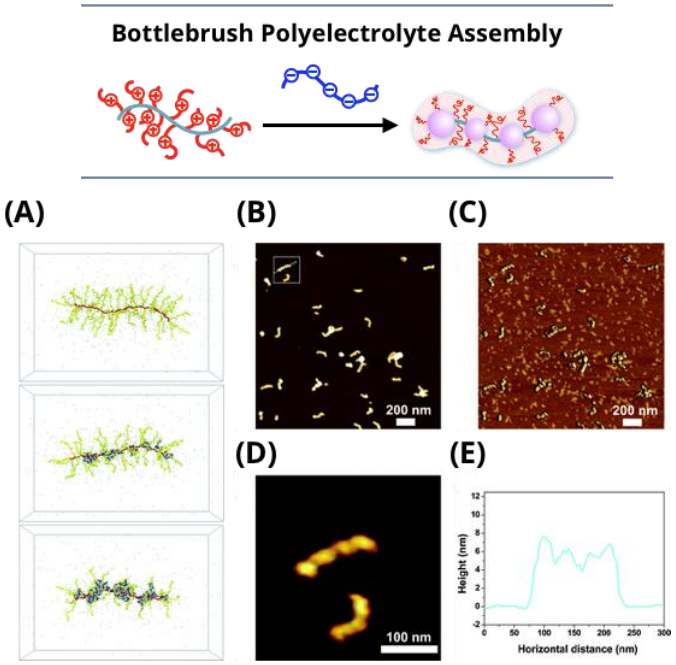

Figure 1.10 (A) Molecular dynamics simulation snapshots of representative conformations of the bare cylindrical polyelectrolyte brush (CPB) and of its complexed state with linear polyelectrolyte (LPE); from top to bottom, Z =[LPE]/[CPB] = 0, 0.25, and 0.5. (B) Atomic force microscopy (AFM) height images of PECs formed by poly([2-(methacryloyl)ethyl]-trimethylammonium iodide) (PMETAI) CPBs and sodium poly(styrene sulfonate) (PSSNa) at Z = 0.75. (C) AFM phase image. (D) Magnified image of selected area in (B). (E) Section analysis of the cursors displayed in (B). Adapted from Larin et al.[85] Copyright 2009 Royal Chemical Society.

1.3 Polyelectrolyte Complex Nanoparticles

1.3.1 Polyelectrolyte Complex Micelles

Controlled self-assembly and compartmentalization on the 1-1000 nm length scale in solution have been longstanding goals in nanotechnology, a field that is beginning to address emerging challenges in energy management,[86] green catalysis,[87] surfactant compatibilizers,[88] and human health.[89] Polymeric micelles, which undergo microphase separation, have provided a rich array of hierarchical nanoaggregates that have been widely recognized as leading candidates to address these issues. These nanoparticles allow cargo to be packaged into discrete domains that can withstand inhospitable environments and transport molecules across otherwise impermeable barriers. Micelle assembly is driven either by amphiphilic polymer association in selective solvents, or by charged polymer interaction in aqueous solution. Significant advances have been made in our fundamental understanding of amphiphilic materials, through foundational works in simulation and modeling,[90-92] scaling theories,[93-95] self-consistent mean field theory,[96-98] and experiments.[99-101] In general, by exploiting the synthetic versatility of block copolymers to tune precisely the energetic components of the (*i*) chain stretching in the core, (*ii*) excluded volume of the corona, and (*iii*) interfacial energy of the micelle in solvent, the micellar size, shape, aggregation number, and chain exchange dynamics can be programmed with high specificity and fidelity for intended applications.

Beyond hydrophobic effects in polymers, other driving forces in non-covalent association have emerged to tailor self-assembly further and expand the selection of sophisticated nanostructures. Complex coacervation has emerged as a promising avenue toward self-assembled materials, garnering interest across interdisciplinary fields including the polymer physics, interface and colloid science, and biology communities.[3] Oppositely charged polyelectrolytes assemble due

to the entropy gain from counterion release,[102] resulting in phase separated polyelectrolyte complex assemblies that exhibit an array of fundamentally unique static and dynamic properties. Polyelectrolyte complex materials can be engineered into polyelectrolyte complex micelles (PCMs), or nanoparticles with a complex core interior and a hydrophilic corona exterior. As shown in Figure 1.11, PCMs typically employ the co-assembly of oppositely charged polymers where at least one polymer in the system has block architecture. In comparison to amphiphilic block copolymer micelles, PCMs are far less quantitatively understood at a molecular level,[103-105] as several underlying features complicate the thermodynamic framework of PCMs. For example, the ionic core consists of two distinct polyelectrolytes that, under stoichiometrically equivalent charge matched conditions, form intrinsic ion pairs that act as physical crosslinks between polycation and polyanion repeat units. These pairings can be disrupted via the addition of salt or by heating, making PCMs highly responsive to changes in the local environment. The low interfacial tension and water solubility of polyelectrolyte chains in complex coacervates means water is present throughout both the core and corona, further complicating efforts to understand the fundamental physics of these nanoparticles, owing to their intrinsically multicomponent nature.[106]

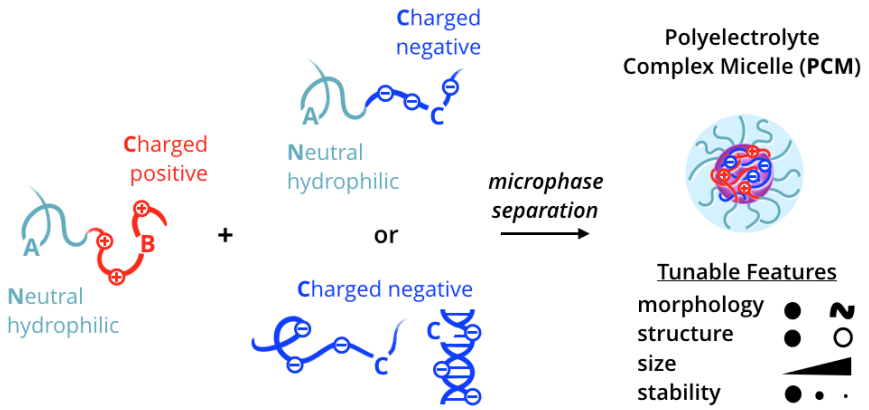

Figure 1.11 Building blocks and microphase separation process of polyelectrolyte complex micelles (PCMs). For nomenclature, A represents a neutral, hydrophilic block, while B/C represents oppositely charged polyelectrolyte blocks. Typical PCMs consist of an AB diblock polycation and either an AC diblock polyanion or a C homopolyanion.

In this chapter, we discuss a collection of recent research articles that shed new light on design strategies for dilute solutions of PCMs using integrated measurement, analysis, and prediction from experimental and computational tools. Special attention is given to the development of (*i*) scaling relationships governing size, shape, and morphological transitions of PCMs, and (*ii*) micellization dynamics in PCM formation/growth, chain exchange, and disassembly pathways. We also provide direct examples of extending polyelectrolyte structure-property principles to impart favorable physiochemical attributes for delivery applications and discuss future directions. Numerous comprehensive reviews[9, 107, 108] on PCM use in gene therapy remain outside the scope of this discussion. These selected works provide blueprints for advancing our fundamental understanding of this important class of self-assembled materials.

1.3.2 PCM Structure-Property Relationships

Controlling the size and structure of PCMs is vital to their success as therapeutic delivery vehicles. Nanoparticles that are smaller than ~10 nm may be removed from the bloodstream by the kidneys, whereas nanoparticles above 200 nm are prone to nonspecific accumulation in the spleen and liver.[36] In addition to avoiding renal clearance, nanoparticle design can have profound impacts on nanoparticle biodistribution and cellular uptake. Recently, Ridolfo et al. explored morphology effects in biological settings by comparing the cellular uptake of amphiphilic spherical, worm-like, vesicular and tubular nanoparticles.[109] They found that higher aspect ratio particles such as worms and tubes performed better than spheres and vesicles because higher aspect ratio nanoparticles diffused faster relative to low aspect ratio nanoparticles. These observations should apply to amphiphilic micelles and PCMs equally well, as these observations do not rely on the assembly mechanism. For these reasons, precise control of PCM size and morphology is a key component to developing efficient PCM encapsulants.

1.3.3 Morphology of PCMs.

The length of each polymer block (A, B, or C in Figure 1.11) can dictate PCM morphology. Roughly, if the length of the neutral block is larger than that of the charged block, i.e. the neutral/charged length ratio (N/C) > 1, self-assembly results in spheroidal micelles for both (AB+AC) and (AB+C) systems. [110-112] When $N/C < 1$ other morphologies can be formed. For most (AB+C) systems, these assemblies are aggregates and complexes similar to bulk assemblies, as the small fraction of neutral polymer does not force microphase separation.[110] However, for (AB+AC) systems, interesting morphologies can be formed in the $N/C < 1$ regime. For example, the Kataoka group observed polyelectrolyte complex vesicles[42, 113, 114] when N/C ~0.5 compared to spheres for the same system with $N/C \sim 2$. Cylindrical and planar assemblies have also been

observed when $N/C < 1$ with a very low poly(ethylene oxide) (PEO, also referred to as poly(ethylene glycol) or PEG) weight fraction.[114] Theory predicts that for $N/C << 1$ morphology scales with degree of ionization (f). [115] As f increases, morphology changes to lamellae, cylinders, crew-cut spherical micelles (corona thickness<<core size), and finally star-like spherical micelles (corona thickness>>core size). At very low f where the free energy gain of complexation is on the order of thermal energy, micellization does not occur and a solution of unimers occurs. Likewise, when charged blocks are very short, experimental results show minimal complexation.[41, 110] Other factors that can also influence micelle morphology are nonlinear polymer architectures,[78, 79] nonstoichiometric charge ratios,[116, 117] salt concentration,[111, 118] chirality,[119] or stimuli-responsive polymers.[120, 121] The idea of block length ratio evokes analogies to classic packing parameter arguments in hydrophobically driven systems,[122, 123] suggesting that commonalities exist despite the drastically different driving forces of self-assembly.

Morphological trends based on N/C are clear from the studies discussed above, but experimentally studying systems exactly at the transition (N/C=1) is quite difficult, due to imprecise polymer synthesis. Recent simulations from the Sing group[124] look at a (AB+C) system with exactly matched block lengths in the block copolymer and find that this length ratio is not the sole driving parameter between macro- and microphase separation. For a $N/C = 1$ system, they predict that at shorter polymer lengths macrophase separation occurs but as length increases past a critical point, microphase separation (micelles) is expected in low salt conditions. While this is hard to replicate experimentally, a reactive polymer system such as poly(allyl glycidyl ether) (PAGE)[57, 125] is a strong candidate to do so, as reactive polymers are powerful tools for achieving architecturally identical neutral, cationic, or anionic polymers.

While the macromolecules considered here are commonly synthetic polymers, biomolecules drive the design and motivation for hydrophilic PCMs and can add additional layers of complexity, for example, polypeptide chirality controlling the phase of bulk polyelectrolyte complexes.[119] There is great interest in PCMs incorporating nucleic acids (often termed "polyplexes") for therapeutic delivery of cargo like plasmid DNA or short interfering RNA (siRNA).[126] Nucleic acids are a densely negatively charged biopolymer, with a phosphate on the backbone between each nucleotide, so they can easily replace a charged block in the general systems scheme described above, as shown in Figure 1.11. Single-stranded nucleic acids behave much like flexible hydrophilic polymers, but double-stranded nucleic acids are substantially more rigid (~50x longer persistence length) and have a much higher charge density, due to the presence of the complementary strand and formation of a double helix.[127, 128] The conformational differences between single- and double-stranded nucleic acids drive a morphological shift within PCMs. DNA hybridization in a bulk system (DNA + poly-L-lysine) forces a phase change between liquid-like coacervates for single-stranded DNA (ssDNA) and solid precipitates for double-stranded DNA (dsDNA)[129], driven by the changes in charge density[129] and rigidity[130]. When single-stranded DNA[10, 41] or RNA[131] is complexed with block copolymers, spheroidal micelles are formed with various charged polymers. However, the double-stranded variant can disrupt micellization as seen with RNA[131] or force a shape change to worm-like cylinders[10, 41, 132] with DNA. When $N/C >> 1$, dsDNA micelles are worm-like cylinders formed with DNA lengths ranging from 10 base-pairs (bp) to 1000s of bp.[10, 41, 132] When N/C is ~1, however, globular micelles can still be formed with dsDNA, as the PEO corona is not crowded enough to force long cylinder formation.[132] The distinction between single-stranded and double-stranded nucleic acids is extremely important for therapeutics delivery, as hybridization can drive therapeutic function.

1.3.4 Structural Properties of Spheroidal PCMs.

The length of each polymer block in a spheroidal micelle can influence its structural properties including size, aggregation number, and stability. In (AB+C) systems, PCM core radius (R_{core}) is directly proportional to the length of the charged block in the block copolymer (N_B),[10, 41, 133] while largely independent of the length of the homopolymer (N_C) below a critical length around N ~ 5000.[110, 118, 133] The size of the neutral block (N_A), which forms the corona, has shown to have a minor effect on the size of the core, but noticeably drives the thickness of the corona (H) and therefore the hydrodynamic radius (R_h), or overall size of the micelle, which is a crucial parameter for controlling biodistribution.[134, 135] Conversely, the aggregation number (P), or number of chains in a given micelle, is shown to decrease as the neutral block size increases for a (AB+C) system.[110, 133-135] To quantify these physical trends, our group developed experimental scaling laws for R_{core}, R_h, H, and P using PCMs containing PEO-pLys paired with ssDNA or pGlu,[133] shown as Equations 1-3, rounded within error. These experimental findings are all consistent with theoretical predictions for PCMs between the star-like and crew-cut regimes,[136-138] which is the case for the vast majority of experiments, and are also consistent with accumulated published data from a variety of synthetic and biological polymers, suggesting the laws are universal, as shown in Figure 1.12. This figure shows a comparison of published data for (AB+C) PCMs and the scaling laws. The data was normalized using the scaling laws for two polymer lengths and plotted against the third length variable. This normalization collapsed all the data to a single trend and is compared to the corresponding scaling law in this figure. N_C was found to have no noticeable effect on any physical parameter, which is convenient for creating versatile delivery systems where the C component is often a therapeutic drug or biomolecule. Polyelectrolyte length is generally reported as degree of polymerization, as it is considered here for physical scaling, but contour length or

physical size are likely a slightly more accurate factor. Understanding how PCM structural properties are controlled by polymer structure can accelerate the design process for tailored carriers.

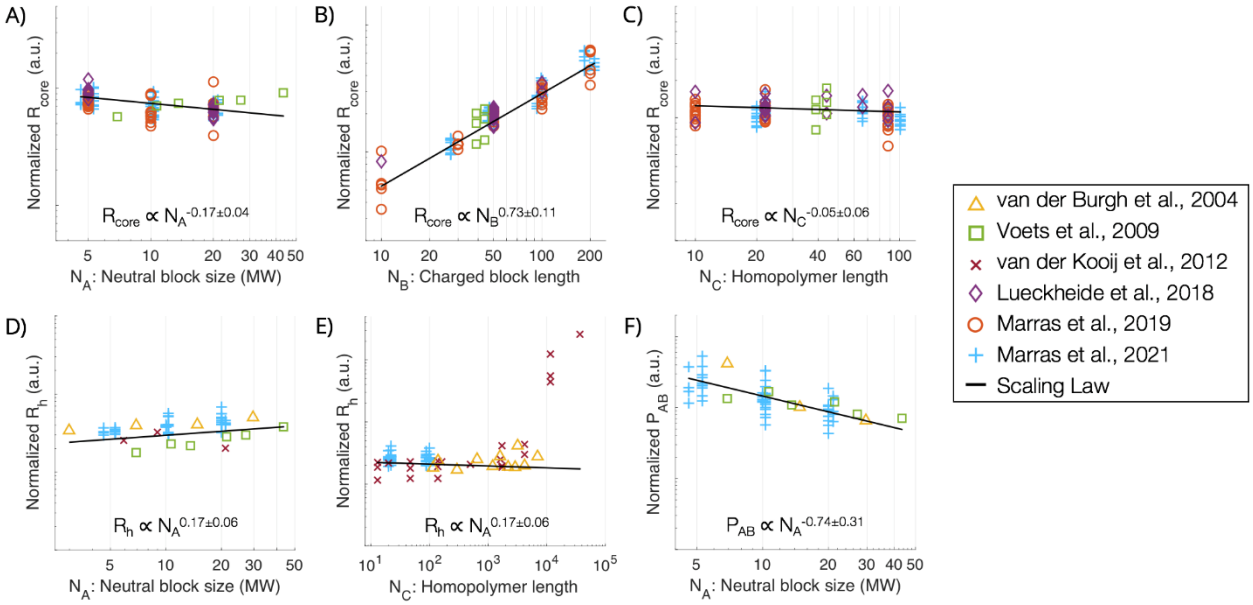

Figure 1.12 Aggregated data from published (AB+C) PCM experimental studies. Size and aggregation number were normalized using scaling laws for two block lengths and plotted against the third block length. The data collapses onto the scaling law for the block length of interest, which is overlayed in black. The available literature provides aggregated data for core size (A-C), hydrodynamic size (D-E), and aggregation number (F). The data represents PCMs from six publications[10, 41, 110, 118, 133, 134] using numerous synthetic and biological polymers and the scaling laws are experimental[133], consistent with theoretical predictions[115] for PCMs between the star-like and crew-cut regimes.

$$R_{core} \propto N_A^{-0.2} N_B^{0.7} \quad [1]$$

$$H \propto N_A^{0.6} \quad [2]$$

$$P \propto N_A^{-0.7} \quad [3]$$

1.3.5 Stability of PCMs.

One aspect of PCM stability is measured by its resistance to nanoparticle degradation in the face of increasing ionic strength in solution. Adding excess counterions from salt competes with ion pairing between polymers to disrupt complexation. In bulk systems (B+C), increasing the length of either charged polymer increases the stability,[129] which can be easily tested with optical microscopy. This is more difficult to study for nanoparticles that are smaller than the diffraction-limited resolution of optical microscopes, but light scattering and small-angle scattering techniques have been used to show a similar effect for PCMs.[118, 139] Likewise, increasing charge density increases complex stability[140] and can drive micellization in PEC systems with charged biomolecules.[141]

PCMs are often discussed as two charged, flexible chains coming together in an entropically favorable process; however, the molecular details of each charged group also play a role in the structure and stability of complex formation.[12] The Choi group used a functionalizable poly(ethylene oxide)-*block*-poly(allyl glycidyl ether) (PEO-PAGE) for a direct comparison of PCMs comprising charged ammonium (pKa = 11), guanidinium (pKa = 14), carboxylate (pKa = 4), and sulfonate (pKa = 1) groups using thiol-ene click chemistry to attach each of the desired side groups onto otherwise identical polymers. The results revealed an increase in core radius and aggregation number as ion pairing interactions become stronger.[125] Our group compared two cationic charged monomers in comparable polymer structures: lysine (primary amine, pKa = 10) and vinylbenzyltrimethylammonium (VBTMA, consisting of a permanently charged ammonium) for complexing DNA at various lengths.[41] Despite the permanent charge and additional hydrophobicity imparted by the aromatic moiety, which have been previously shown to strengthen certain PEC systems,[142, 143] PVBTMA complexed less strongly with DNA, attributed to the steric

hindrance in ion pairing.[144] Crosslinking cationic polymers using glutaraldehyde,[145] disulfide bonds,[146, 147] or other means[148] improves stability after micelle formation and can be reversible. These examples demonstrate that both synthetic polymers and polypeptides are suitable for forming robust PCMs, and that the molecular details must be considered in the design process, as they play a vital role in complexation properties and ultimately, functionality.

Table 1.1. Molecular architecture controls polyelectrolyte complex micelle (PCM) properties. The following physical trends are from both experimental and theoretical publications on PCMs.

Property	Parameter	Notes	References
Core radius	Neutral block length (N_A)	Inverse correlation	115, 133
Core radius	Charged block length (N_B)	Direct correlation	10, 41, 115, 133, 149-151
Core radius	Homopolymer length (N_C)	Independent[a]	10, 41, 110, 118, 133
Corona thickness	Neutral block length (N_A)	Direct correlation	115, 133-135
Aggregation Number	Neutral block length (N_A)	Inverse correlation	110, 133-135
Aggregation Number	Charged block length (N_B)	Direct correlation	115, 133, 152
Aggregation Number	Strength of charge	Direct correlation	125
Polydispersity	Strength of charge	Direct correlation	41, 125
Morphology	N/C>1	Spheroids	110-112
Morphology	N/C<1	Aggregates, vesicles[b], or lamellae[b]	42, 110, 113, 114, 116, 117
Morphology	Polyelectrolyte architecture	Vesicles, cylinders, and more	78, 79
Morphology	DNA hybridization	ssDNA=spheres dsDNA=worm-like cylinders	10, 41
Stability	Polymer length	Direct correlation	139
Stability	Charge density	Direct correlation	140, 141
Stability	Strength of charge	Direct correlation	125
Stability	Cross linking	Direct correlation	145-148

[a]under lengths of ~5000, [b]specific cases.

1.3.6 Dynamics of Micellization and Chain Exchange

For nanocarrier applications, understanding the driving forces of micellization, molecular exchange, and evolution is critical for controlling the exposure of the cargo.[104, 153, 154] A more complete understanding of the PCM equilibration process can enable greater control of the physical self-assembly process, nanocarrier stability over time, and encapsulation/release kinetics. In this section, we focus discussions on several recent developments in PCM dynamics using primarily scattering methods. Small-angle scattering is a powerful tool for gathering multiple orders of magnitude of size information simultaneously for an entire solution and in a precise time-resolved manner. Detailed protocols of small-angle X-ray scattering (SAXS) have been recently outlined by our group to assist in the experimental planning and analysis of the SAXS data.[155, 156] Figure 1.13 A shows the model systems used for these studies. Polyelectrolytes include poly(ethylene oxide)-*block*-poly(vinyl benzyl trimethylammonium chloride) (PEO-*b*-PVBTMA), sodium poly(acrylate) (PAA), poly(ethylene oxide)-*block*-poly(sodium 4-styrenesulfonate) (PEO-*b*-PSS), and poly(sodium 4-styrenesulfonate) (PSS). We have previously provided experimental details of the controlled synthesis of these polyelectrolytes in water,[157, 158] so that precise lengths of neutral and charged blocks can be prepared with low dispersity in the molar mass distribution. Depending on the block lengths and pairing of the PEO-*b*-PVBTMA polycation with PAA, PEO-*b*-PSS, or PSS polyanion, the assemblies that form can resemble spherical, core/shell PCMs or polydisperse colloidal aggregates. Both classes of nanostructures will be discussed in detail below, along with open-ended questions that these results raise for the physical chemistry community.

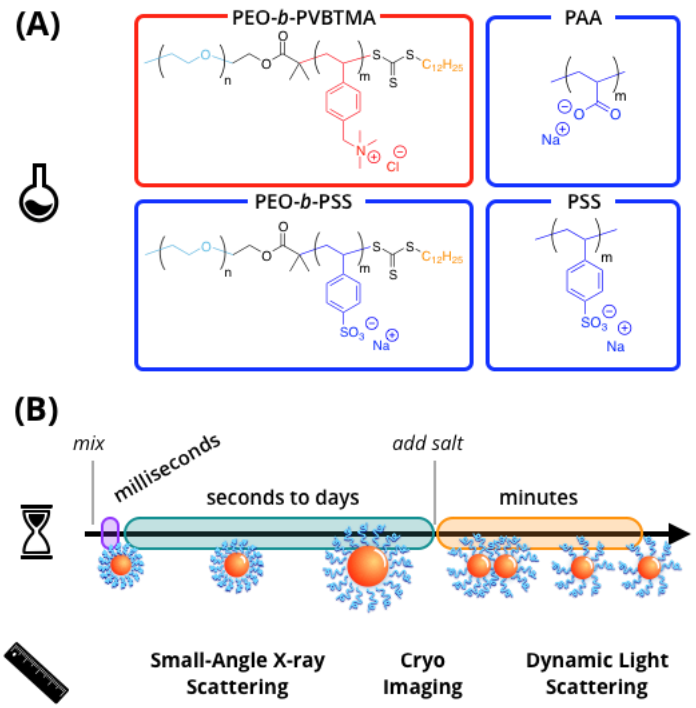

Figure 1.13 Dynamics of polyelectrolyte complex micelles (PCMs). (A) Chemical structures of poly(ethylene oxide)-*block*-poly(vinyl benzyl trimethylammonium chloride) (PEO-*b*-PVBTMA, boxed in red), sodium poly(acrylate) (PAA, boxed in blue), poly(ethylene oxide)-*block*-poly(sodium 4-styrenesulfonate) (PEO-*b*-PSS, boxed in blue), and poly(sodium 4-styrenesulfonate) (PSS, boxed in blue). (B) Illustration of the relevant time and length scales investigated in PCM formation (purple), chain exchange (green), and disassembly (orange), ranging from milliseconds to minutes using small-angle X-ray scattering, cryogenic imaging, and dynamic light scattering.

Following established stopped-flow protocols from the amphiphilic block copolymer literature, the ultrafast formation of PCMs can be monitored *in situ* using time-resolved small-angle X-ray scattering (TR-SAXS) with millisecond temporal resolution (Fig. 1.13 B). Here, solutions of oppositely charged polymers are loaded into separate syringes, pumped into a turbulent mixer, and dispensed into a capillary cell without further flow for scattering measurements. This technique has provided new physical insights into ionic nanomaterial behavior, including complex coacervate coalescence of poly(allylamine hydrochloride) and PAA as a function of added NaCl salt.[159] However, it was only very recently that the initial complexation of block polyelectrolytes have been reported. The chemical and electrostatic nature of the

polyelectrolyte pairing appears to greatly influence the kinetic pathway of micellization, demonstrating the importance of mindful polymer selection in constructing PCM nanocarriers. Two independent cases that illustrate completely different pathways are shown in Figure 1.14.

In the first case, Wu and coworkers investigated the spatiotemporal formation kinetics of PEO-*b*-PVBTMA with PAA.[160] Using a stopped-flow apparatus with high-throughput data collection capabilities at the Stanford Synchrotron Radiation Lighthouse (SSRL, SLAC National Accelerator Laboratory),[161] they directly observed the assembly kinetics and SAXS profiles of PEO-*b*-PVBTMA / PAA PCMs via TR-SAXS from 100 ms to 5 s, which exhibited spherical particles ($\sim q^0$ power law dependence of intensity for $q < 0.01$ Å^{-1}) that grew in size over time (Fig. 1.14 A). The structural evolution of PCMs was evaluated by determining the apparent Guinier radius of gyration (R_g), which showed incremental micelle growth from R_g ~10 to 12 nm over 5 s by gradual insertion of either unimer chains or ion-paired clusters. For the second case, Amann and coworkers examined PCMs comprising PEO-PVBTMA and PSS.[162] Using a SFM-400 stopped-flow apparatus at the European Synchrotron Radiation Facility (ESRF), the researchers reported the TR-SAXS formation of metastable aggregates for internal charge neutralization at 3 ms, preceding rearrangement and pinch-off into small micellar particles over the course of 30 s (Fig. 1.14 B). The equilibration data was described by these relaxation processes as a function of the degree of polymerization (N) of PVBTMA from $N = 6$ to 19, where rearrangement of unimer chains or ion-paired clusters becomes increasingly unfavorable as block length increased. In a previous report, Wu et al. showed that PEO-*b*-PVBTMA and PEO-b-PSS at $N \approx 50$ for the charged blocks form nonequilibrium complexes, far from well-defined spheres by fitting the SAXS data.[163] Altogether, these examples illustrate only two of many possible formation pathways that lead to charge-driven micellization. Expanding TR-SAXS to study more PCM systems and varying

parameters like polyelectrolyte selection, block lengths, molecular architecture, can help move PCM design toward more efficacious and predictive encapsulation of cargo.

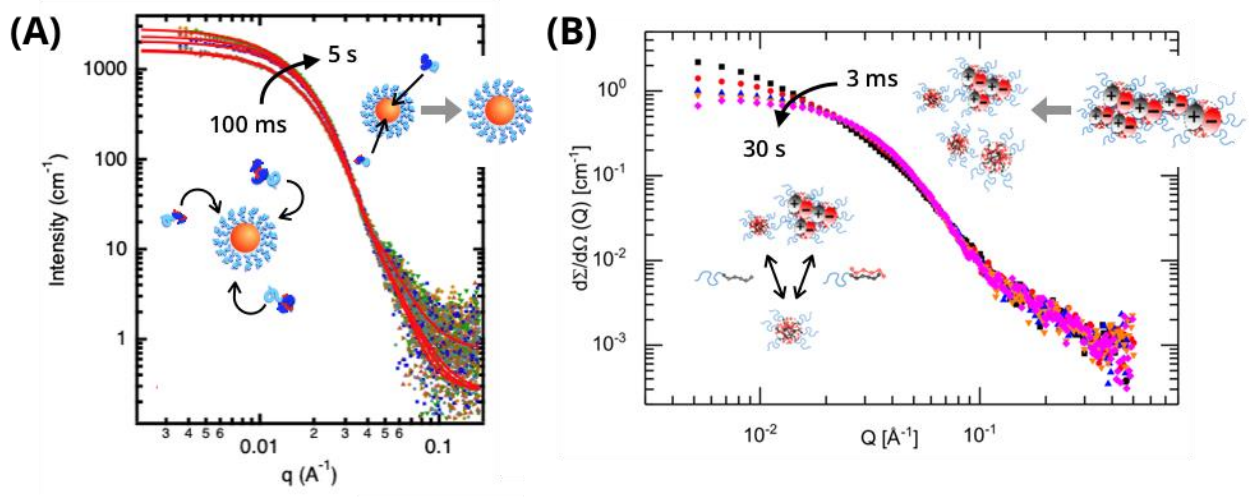

Figure 1.14 Time-resolved small-angle X-ray scattering (TR-SAXS) reveals distinct formation pathways of polyelectrolyte complex micelles (PCMs). (A) For PEO-*b*-PVBTMA/PAA systems, within 100 ms well-defined spherical micelles incrementally grow into larger micellar entities, as denoted by the black arrow. Adapted from Wu et al.[160] Copyright 2020 American Chemical Society. (B) For PEO-*b*-PVBTMA/PSS systems, within 3 ms aggregates break apart into smaller micellar entities, as denoted by the black arrow. Adapted from Amann et al.[162] Copyright 2019 American Chemical Society.

Understanding chain exchange in dilute micelle solutions is crucial towards their development as efficient delivery vehicles, as the rate and method by which sequestered therapeutic molecules are exposed to the surrounding environment will control their efficacy. In general, chain exchange between equilibrium polymeric micelles proceeds via two primary mechanisms: chain expulsion/insertion and micelle fusion/fission.[164-166] While chain exchange processes have been probed with amphiphilic polymer assemblies, to the extent of our knowledge no experimental studies have examined chain exchange for PCMs. We have previously shown how interparticle effects emerge in the form of a structure factor in SAXS profiles for concentrated micelle solutions and thereby maintain PCM stability over time,[167] but the molecular details of unimer chain exchange or fusion/fission cannot be unveiled with these experiments alone.

However, advances in molecular dynamic simulations have offered new insights to potential mechanisms of exchange in which electrostatics interplay with other competing non-covalent interactions.

Bos et al. performed coarse-grain dynamics simulations on a model diblock-homopolymer PCM system and outlined physical characteristics influencing the mode of chain exchange and PCM stability.[168] In these Langevin dynamics simulations, non-electrostatic interactions (i.e., hydrogen bonding or hydrophobicity) tended to disfavor the chain expulsion mechanism, as these additional interactions generate an enthalpic cost which counteracts the entropic gain that drives small neutral complex cluster expulsion from PCMs (Fig. 1.15 A). Interestingly, these effects depended on the non-electrostatic interactions (represented by the Lennard-Jones potential ε_{LJ}) being intermolecular and changed when the interactions were modified to be solely intramolecular. In the case where one polyelectrolyte displayed significant non-electrostatic interactions with itself but not the oppositely charged polyelectrolyte, chain expulsion and fusion/fission events increased, suggesting that the PCM became less stable. Meanwhile, macromolecular design parameters such as block length have divergent effects on the two mechanisms as ε_{LJ} was increased, shown in Figure 1.15 B. Chain expulsion was sensitive to the relative length of the charged blocks in the system, displaying a distinct increase for matching lengths relative to unmatched chain lengths. Fusion/fission, on the other hand, appeared insensitive to the ratio of the block lengths, but instead depended on the total length of the homopolymer. Taken together, simulation and experiment provide a strong case for the careful consideration of non-electrostatic interactions between polyelectrolytes and polyelectrolyte length.

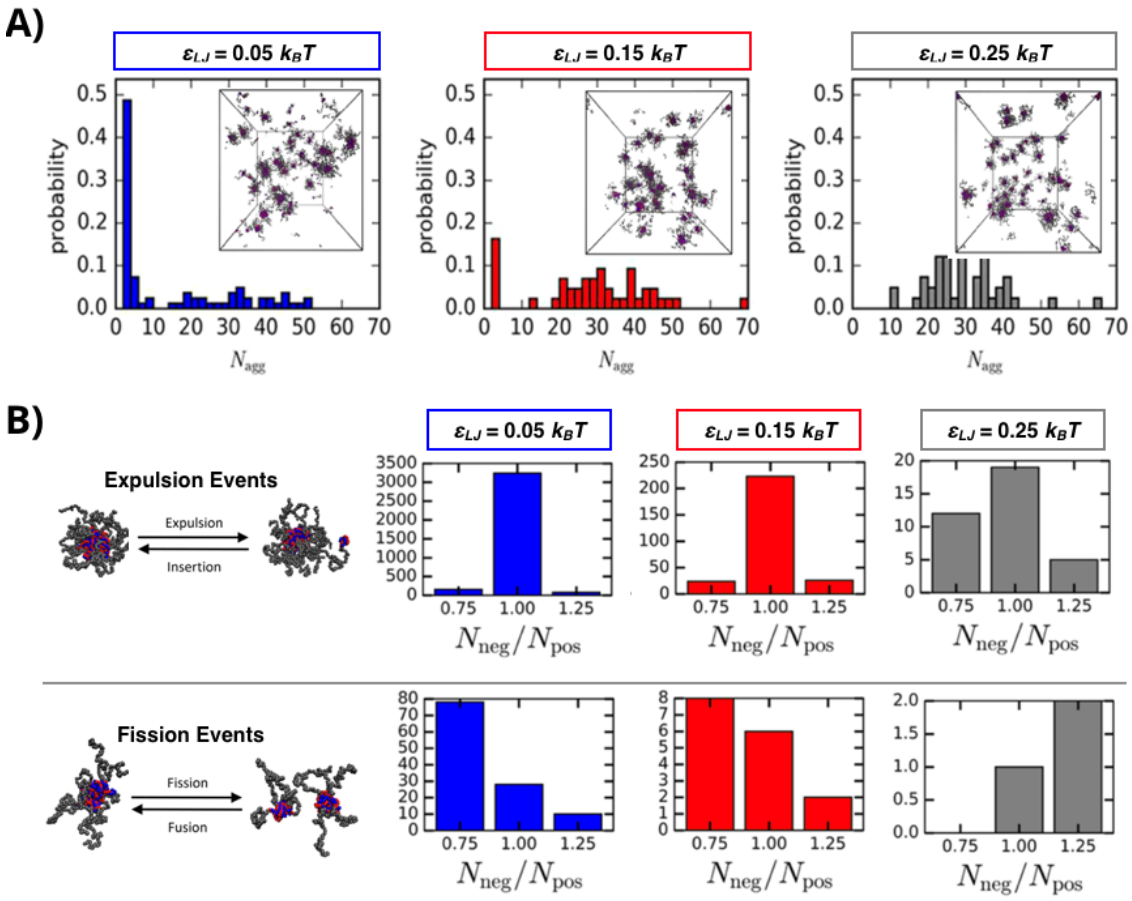

Figure 1.15 Chain exchange of polyelectrolyte complex micelles (PCMs) upon formation as a function of electrostatic interactions, non-electrostatic interactions, and polyelectrolyte length using Langevin dynamics simulations. (A) Histograms of the PCM size distribution varying non-electrostatic attraction strength between polyelectrolytes at $\varepsilon_{LJ} = 0.05k_BT$ (blue), $\varepsilon_{LJ} = 0.15k_BT$ (red), and $\varepsilon_{LJ} = 0.25k_BT$ (gray); insets show snapshots of the simulated PCMs with $N_{\text{negative}} = N_{\text{positive}} = 20$ and $N_{\text{netural}} = 50$. (B) Comparison of the number of chain expulsion/insertion and micelle fission/fusion events for PCMs as a function of polyelectrolyte length ratio ($N_{\text{negative}} / N_{\text{positive}}$) at increasing non-electrostatic attraction strengths. Adapted from Bos et al.[168] Copyright 2019 American Chemical Society.

For PCMs containing nucleic acids, an important practical consequence of dynamic chain exchange between micellar assemblies is the potential displacement of nucleic acids over time upon immersion in different biological settings. Because of the complicated delivery pathways involved with overcoming various biological barriers, molecular engineering approaches to boost stability in nanocarriers is non-trivial. However, simplified fundamental experiments can provide revealing structure-property relationships for constructing more stable PCMs. For example, can

foreign polyelectrolytes with a strong tendency of association into PCM hosts result in mixed micelles? If so, what features are consequential for this feature of macromolecular exchange? To the extent of our knowledge, there are only a handful of published works that have examined such questions. Dautzenberg et al. conducted polyanion exchange reactions involving PCMs containing model oligophosphates and competing higher MW polymers (PSS and DNA) at physiological salt conditions.[169] Another study by Harada and Kataoka exploited polymer architecture to show how diblock polyelectrolytes displace homopolyelectrolytes in PCMs formed with an oppositely charged diblock polyelectrolyte, suggesting increased association in (AB+AC) PCM systems compared to (AB+C) systems.[170] These examples provide insight on how PCM chain exchange can arise from molecular recognition based on polyelectrolyte compatibility and dynamics, an area in which advances in non-invasive characterization techniques such as small-angle neutron scattering,[171] fluorescence microscopy,[172] and liquid-phase transmission electron microscopy[173] are well-equipped to provide key leaps forward in our understanding of polyelectrolyte complex micellization and chain exchange.

1.4 References

1. Muthukumar, M. 50th Anniversary Perspective: A Perspective on Polyelectrolyte Solutions. *Macromolecules* **2017**, *50* 24, 9528-9560. DOI: 10.1021/acs.macromol.7b01929.

2. Fu, J.; Schlenoff, J. B. Driving Forces for Oppositely Charged Polyion Association in Aqueous Solutions: Enthalpic, Entropic, but Not Electrostatic. *Journal of the American Chemical Society* **2016**, *138* 3, 980-990. DOI: 10.1021/jacs.5b11878.

3. Sing, C. E.; Perry, S. L. Recent progress in the science of complex coacervation. *Soft Matter* **2020**, *16* 12, 2885-2914, 10.1039/D0SM00001A. DOI: 10.1039/D0SM00001A.

4. Chang, L.-W.; Lytle, T. K.; Radhakrishna, M.; Madinya, J. J.; Vélez, J.; Sing, C. E.; Perry, S. L. Sequence and entropy-based control of complex coacervates. *Nature communications* **2017**, *8* 1, 1-8.

5. Li, L.; Srivastava, S.; Andreev, M.; Marciel, A. B.; de Pablo, J. J.; Tirrell, M. V. Phase Behavior and Salt Partitioning in Polyelectrolyte Complex Coacervates. *Macromolecules* **2018**, *51* 8, 2988-2995. DOI: 10.1021/acs.macromol.8b00238.

6. Li, L.; Rumyantsev, A. M.; Srivastava, S.; Meng, S.; de Pablo, J. J.; Tirrell, M. V. Effect of solvent quality on the phase behavior of polyelectrolyte complexes. *Macromolecules* **2020**, *54* 1, 105-114.

7. Wang, Q.; Schlenoff, J. B. The polyelectrolyte complex/coacervate continuum. *Macromolecules* **2014**, *47* 9, 3108-3116.

8. Ishii, S.; Kaneko, J.; Nagasaki, Y. Dual Stimuli-Responsive Redox-Active Injectable Gel by Polyion Complex Based Flower Micelles for Biomedical Applications. *Macromolecules* **2015**, *48* 9, 3088-3094. DOI: 10.1021/acs.macromol.5b00305.

9. Lachelt, U.; Wagner, E. Nucleic Acid Therapeutics Using Polyplexes: A Journey of 50 Years (and Beyond). *Chem Rev* **2015**, *115* 19, 11043-11078. DOI: 10.1021/cr5006793.

10. Lueckheide, M.; Vieregg, J. R.; Bologna, A. J.; Leon, L.; Tirrell, M. V. Structure-Property Relationships of Oligonucleotide Polyelectrolyte Complex Micelles. *Nano Letters* **2018**, *18* 11, 7111-7117. DOI: 10.1021/acs.nanolett.8b03132.

11. Zhou, Z.; Yeh, C.-F.; Mellas, M.; Oh, M.-J.; Zhu, J.; Li, J.; Huang, R.-T.; Harrison, D. L.; Shentu, T.-P.; Wu, D.; et al. Targeted polyelectrolyte complex micelles treat vascular complications in vivo. *Proceedings of the National Academy of Sciences* **2021**, *118* 50, e2114842118. DOI: 10.1073/pnas.2114842118.

12. Fu, J. C.; Fares, H. M.; Schlenoff, J. B. Ion-Pairing Strength in Polyelectrolyte Complexes. *Macromolecules* **2017**, *50* 3, 1066-1074.

13. Yang, M.; Shi, J.; Schlenoff, J. B. Control of Dynamics in Polyelectrolyte Complexes by Temperature and Salt. *Macromolecules* **2019**, *52* 5, 1930-1941. DOI: 10.1021/acs.macromol.8b02577.

14. Zhang, Y.; Li, F.; Valenzuela, L. D.; Sammalkorpi, M.; Lutkenhaus, J. L. Effect of Water on the Thermal Transition Observed in Poly (allylamine hydrochloride)–Poly (acrylic acid) Complexes. *Macromolecules* **2016**, *49* 19, 7563-7570.

15. Chang, L.-W.; Lytle, T. K.; Radhakrishna, M.; Madinya, J. J.; Vélez, J.; Sing, C. E.; Perry, S. L. Sequence and entropy-based control of complex coacervates. *Nature Communications* **2017**, *8* 1. DOI: 10.1038/s41467-017-01249-1.

16. Akkaoui, K.; Yang, M.; Digby, Z. A.; Schlenoff, J. B. Ultraviscosity in Entangled Polyelectrolyte Complexes and Coacervates. *Macromolecules* **2020**, *53* 11, 4234-4246. DOI: 10.1021/acs.macromol.0c00133.

17. Van der Gucht, J.; Spruijt, E.; Lemmers, M.; Stuart, M. A. C. Polyelectrolyte complexes: Bulk phases and colloidal systems. *Journal of colloid and interface science* **2011**, *361* 2, 407-422.

18. Meng, S.; Ting, J. M.; Wu, H.; Tirrell, M. V. Solid-to-Liquid Phase Transition in Polyelectrolyte Complexes. *Macromolecules* **2020**, *53* 18, 7944-7953. DOI: 10.1021/acs.macromol.0c00930.

19. Neitzel, A. E.; Fang, Y. N.; Yu, B.; Rumyantsev, A. M.; de Pablo, J. J.; Tirrell, M. V. Polyelectrolyte complex coacervation across a broad range of charge densities. *Macromolecules* **2021**, *54* 14, 6878-6890.

20. Marciel, A. B.; Srivastava, S.; Tirrell, M. V. Structure and rheology of polyelectrolyte complex coacervates. *Soft Matter* **2018**, *14* 13, 2454-2464.

21. Rubinstein, M.; Liao, Q.; Panyukov, S. Structure of liquid coacervates formed by oppositely charged polyelectrolytes. *Macromolecules* **2018**, *51* 23, 9572-9588.

22. Spruijt, E.; Cohen Stuart, M. A.; van der Gucht, J. Linear viscoelasticity of polyelectrolyte complex coacervates. *Macromolecules* **2013**, *46* 4, 1633-1641.

23. Huang, J.; Morin, F. J.; Laaser, J. E. Charge-Density-Dominated Phase Behavior and Viscoelasticity of Polyelectrolyte Complex Coacervates. *Macromolecules* **2019**, *52* 13, 4957-4967. DOI: 10.1021/acs.macromol.9b00036.

24. Liu, Y.; Santa Chalarca, C. F.; Carmean, R. N.; Olson, R. A.; Madinya, J.; Sumerlin, B. S.; Sing, C. E.; Emrick, T.; Perry, S. L. Effect of Polymer Chemistry on the Linear Viscoelasticity of Complex Coacervates. *Macromolecules* **2020**, *53* 18, 7851-7864. DOI: 10.1021/acs.macromol.0c00758.

25. Larson, R. G.; Liu, Y.; Li, H. Linear viscoelasticity and time-temperature-salt and other superpositions in polyelectrolyte coacervates. *Journal of Rheology* **2021**, *65* 1, 77-102.

26. Suarez-Martinez, P. C.; Batys, P.; Sammalkorpi, M.; Lutkenhaus, J. L. Time–temperature and time–water superposition principles applied to poly (allylamine)/poly (acrylic acid) complexes. *Macromolecules* **2019**, *52* 8, 3066-3074.

27. Tekaat, M.; Bütergerds, D.; Schönhoff, M.; Fery, A.; Cramer, C. Scaling properties of the shear modulus of polyelectrolyte complex coacervates: a time-pH superposition principle. *Physical Chemistry Chemical Physics* **2015**, *17* 35, 22552-22556.

28. Hillmyer, M. Editorial. *Macromolecules* **2020**, *53* 1, 1-1. DOI: 10.1021/acs.macromol.9b02714.

29. Rowan, S. J. Happy 100th Anniversary to Polymer Science and Engineering. *ACS Macro Letters* **2020**, *9* 1, 122-122. DOI: 10.1021/acsmacrolett.9b01029.

30. Schubert, U. S.; Zechel, S. The Year of Polymers – 100 Years of Macromolecular Chemistry. *Macromolecular Rapid Communications* **2020**, *41* 1. DOI: 10.1002/marc.201900620.

31. Frey, H.; Johann, T. Celebrating 100 years of "polymer science": Hermann Staudinger's 1920 manifesto. *Polymer Chemistry* **2020**, *11* 1, 8-14. DOI: 10.1039/c9py90161b.

32. Berry, G. C.; Bockstaller, M. R.; Matyjaszewski, K. Celebrating 100 years of polymer science. *Progress in Polymer Science* **2020**, *100*. DOI: 10.1016/j.progpolymsci.2019.101193.

33. Bates, F. S.; Hillmyer, M. A.; Lodge, T. P.; Bates, C. M.; Delaney, K. T.; Fredrickson, G. H. Multiblock Polymers : Panacea or Pandora's Box? *Science* **2012**, *336* April, 434-440. DOI: 10.1126/science.1215368.

34. Bates, F. S.; Fredrickson, G. H. Block Copolymers—Designer Soft Materials. *Physics Today* **1999**, *52* 2, 32-38. DOI: 10.1063/1.882522.

35. Bates, C. M.; Bates, F. S. 50th Anniversary Perspective: Block Polymers—Pure Potential. *Macromolecules* **2017**, *50* 1, 3-22. DOI: 10.1021/acs.macromol.6b02355.

36. Cabral, H.; Miyata, K.; Osada, K.; Kataoka, K. Block Copolymer Micelles in Nanomedicine Applications. *Chem Rev* **2018**, *118* 14, 6844-6892. DOI: 10.1021/acs.chemrev.8b00199.

37. Kuo, C. H.; Leon, L.; Chung, E. J.; Huang, R. T.; Sontag, T. J.; Reardon, C. A.; Getz, G. S.; Tirrell, M.; Fang, Y. Inhibition of atherosclerosis-promoting microRNAs via targeted polyelectrolyte complex micelles. *J Mater Chem B* **2014**, *2* 46, 8142-8153. DOI: 10.1039/C4TB00977K.

38. Min, H. S.; Kim, H. J.; Naito, M.; Ogura, S.; Toh, K.; Hayashi, K.; Kim, B. S.; Fukushima, S.; Anraku, Y.; Miyata, K.; et al. Systemic Brain Delivery of Antisense Oligonucleotides across

the Blood-Brain Barrier with a Glucose-Coated Polymeric Nanocarrier. *Angew Chem Int Ed Engl* **2020**, *59* 21, 8173-8180. DOI: 10.1002/anie.201914751.

39. Bates, F. S.; Fredrickson, G. Block copolymers-designer soft materials. *Physics today* **2000**, *52*.

40. Moughton, A. O.; Hillmyer, M. A.; Lodge, T. P. Multicompartment Block Polymer Micelles. *Macromolecules* **2012**, *45* 1, 2-19. DOI: 10.1021/ma201865s.

41. Marras, A. E.; Vieregg, J. R.; Ting, J. M.; Rubien, J. D.; Tirrell, M. V. Polyelectrolyte Complexation of Oligonucleotides by Charged Hydrophobic-Neutral Hydrophilic Block Copolymers. *Polymers-Basel* **2019**, *11* 1, 83. DOI: 10.3390/polym11010083.

42. Koide, A.; Kishimura, A.; Osada, K.; Jang, W. D.; Yamasaki, Y.; Kataoka, K. Semipermeable polymer vesicle (PICsome) self-assembled in aqueous medium from a pair of oppositely charged block copolymers: physiologically stable micro-/nanocontainers of water-soluble macromolecules. *J Am Chem Soc* **2006**, *128* 18, 5988-5989. DOI: 10.1021/ja057993r.

43. Polymeropoulos, G.; Zapsas, G.; Ntetsikas, K.; Bilalis, P.; Gnanou, Y.; Hadjichristidis, N. 50th Anniversary Perspective: Polymers with Complex Architectures. *Macromolecules* **2017**, *50* 4, 1253-1290. DOI: 10.1021/acs.macromol.6b02569.

44. Tritschler, U.; Pearce, S.; Gwyther, J.; Whittell, G. R.; Manners, I. 50th Anniversary Perspective: Functional Nanoparticles from the Solution Self-Assembly of Block Copolymers. *Macromolecules* **2017**, *50* 9, 3439-3463. DOI: 10.1021/acs.macromol.6b02767.

45. Kim, K.; Schulze, M. W.; Arora, A.; Lewis, R. M.; Hillmyer, M. A.; Dorfman, K. D.; Bates, F. S. Thermal processing of diblock copolymer melts mimics metallurgy. *Science* **2017**, *356* 6337, 520. DOI: 10.1126/science.aam7212.

46. Grubbs, R. B.; Grubbs, R. H. 50th Anniversary Perspective: Living Polymerization—Emphasizing the Molecule in Macromolecules. *Macromolecules* **2017**, *50* 18, 6979-6997. DOI: 10.1021/acs.macromol.7b01440.

47. Kawamoto, K.; Zhong, M.; Gadelrab, K. R.; Cheng, L.-C.; Ross, C. A.; Alexander-Katz, A.; Johnson, J. A. Graft-through Synthesis and Assembly of Janus Bottlebrush Polymers from A-Branch-B Diblock Macromonomers. *Journal of the American Chemical Society* **2016**, *138* 36, 11501-11504. DOI: 10.1021/jacs.6b07670.

48. Haque, F. M.; Grayson, S. M. The synthesis, properties and potential applications of cyclic polymers. *Nature Chemistry* **2020**, *12* 5, 433-444. DOI: 10.1038/s41557-020-0440-5.

49. Wei, H.; Chu, D. S. H.; Zhao, J.; Pahang, J. A.; Pun, S. H. Synthesis and Evaluation of Cyclic Cationic Polymers for Nucleic Acid Delivery. *ACS Macro Letters* **2013**, *2* 12, 1047-1050. DOI: 10.1021/mz400560y.

50. Levi, A. E.; Lequieu, J.; Horne, J. D.; Bates, M. W.; Ren, J. M.; Delaney, K. T.; Fredrickson, G. H.; Bates, C. M. Miktoarm Stars via Grafting-Through Copolymerization: Self-Assembly and the Star-to-Bottlebrush Transition. *Macromolecules* **2019**, *52* 4, 1794-1802. DOI: 10.1021/acs.macromol.8b02321.

51. Li, Z.; Kesselman, E.; Talmon, Y.; Hillmyer, M. A.; Lodge, T. P. Multicompartment Micelles from ABC Miktoarm Stars in Water. *Science* **2004**, *306*, 98-101.

52. Marciel, A. B.; Chung, E. J.; Brettmann, B. K.; Leon, L. Bulk and nanoscale polypeptide based polyelectrolyte complexes. *Adv Colloid Interface Sci* **2017**, *239*, 187-198. DOI: 10.1016/j.cis.2016.06.012.

53. Hammond, P. T. Engineering materials layer-by-layer: Challenges and opportunities in multilayer assembly. *AIChE Journal* **2011**, *57* 11, 2928-2940. DOI: 10.1002/aic.12769.

54. Harada, A.; Kataoka, K. Polyion complex micelle formation from double-hydrophilic block copolymers composed of charged and non-charged segments in aqueous media. *Polym J* **2018**, *50* 1, 95-100. DOI: 10.1038/pj.2017.67.

55. Banerjee, S. L.; Hoskins, R.; Swift, T.; Rimmer, S.; Singha, N. K. A self-healable fluorescence active hydrogel based on ionic block copolymers prepared: Via ring opening polymerization and xanthate mediated RAFT polymerization. *Polymer Chemistry* **2018**, *9* 10, 1190-1205. DOI: 10.1039/c7py01883e.

56. Banerjee, S. L.; Singha, N. K. A new class of dual responsive self-healable hydrogels based on a core crosslinked ionic block copolymer micelle prepared: Via RAFT polymerization and Diels-Alder "click" chemistry. *Soft Matter* **2017**, *13* 47, 9024-9035. DOI: 10.1039/c7sm01906h.

57. Hunt, J. N.; Feldman, K. E.; Lynd, N. A.; Deek, J.; Campos, L. M.; Spruell, J. M.; Hernandez, B. M.; Kramer, E. J.; Hawker, C. J. Tunable, high modulus hydrogels driven by ionic coacervation. *Advanced Materials* **2011**, *23* 20, 2327-2331. DOI: 10.1002/adma.201004230.

58. Krogstad, D. V.; Lynd, N. A.; Choi, S. H.; Spruell, J. M.; Hawker, C. J.; Kramer, E. J.; Tirrell, M. V. Effects of polymer and salt concentration on the structure and properties of triblock copolymer coacervate hydrogels. *Macromolecules* **2013**, *46* 4, 1512-1518. DOI: 10.1021/ma302299r.

59. Krogstad, D. V.; Choi, S. H.; Lynd, N. A.; Audus, D. J.; Perry, S. L.; Gopez, J. D.; Hawker, C. J.; Kramer, E. J.; Tirrell, M. V. Small Angle Neutron Scattering Study of Complex Coacervate Micelles and Hydrogels Formed from Ionic Diblock and Triblock Copolymers. *Journal of Physical Chemistry B* **2014**, *118* 45, 13011-13018. DOI: 10.1021/jp509175a.

60. Krogstad, D. V.; Lynd, N. A.; Miyajima, D.; Gopez, J.; Hawker, C. J.; Kramer, E. J.; Tirrell, M. V. Structural evolution of polyelectrolyte complex core micelles and ordered-phase bulk materials. *Macromolecules* **2014**, *47* 22, 8026-8032. DOI: 10.1021/ma5017852.

61. Srivastava, S.; Levi, A. E.; Goldfeld, D. J.; Tirrell, M. V. Structure, Morphology, and Rheology of Polyelectrolyte Complex Hydrogels Formed by Self-Assembly of Oppositely Charged Triblock Polyelectrolytes. *Macromolecules* **2020**.

62. Srivastava, S.; Andreev, M.; Levi, A. E.; Goldfeld, D. J.; Mao, J.; Heller, W. T.; Prabhu, V. M.; De Pablo, J. J.; Tirrell, M. V. Gel phase formation in dilute triblock copolyelectrolyte complexes. *Nature Communications* **2017**, *8*. DOI: 10.1038/ncomms14131.

63. Balsara, N. P.; Tirrell, M.; Lodge, T. P. Micelle formation of BAB triblock copolymers in solvents that preferentially dissolve the A block. *Macromolecules* **1991**, *24* 8, 1975-1986. DOI: 10.1021/ma00008a040.

64. Seo, S. E.; Hawker, C. J. The Beauty of Branching in Polymer Science. *Macromolecules* **2020**, *53* 9, 3257-3261. DOI: 10.1021/acs.macromol.0c00286.

65. Lungwitz, U.; Breunig, M.; Blunk, T.; Gopferich, A. Polyethylenimine-based non-viral gene delivery systems. *Eur J Pharm Biopharm* **2005**, *60* 2, 247-266. DOI: 10.1016/j.ejpb.2004.11.011.

66. Ren, J. M.; McKenzie, T. G.; Fu, Q.; Wong, E. H. H.; Xu, J.; An, Z.; Shanmugam, S.; Davis, T. P.; Boyer, C.; Qiao, G. G. Star Polymers. *Chemical Reviews* **2016**, *116* 12, 6743-6836. DOI: 10.1021/acs.chemrev.6b00008.

67. Li, J.; Qian, J.; Xu, Y.; Yan, S.; Shen, J.; Yin, M. A Facile-Synthesized Star Polycation Constructed as a Highly Efficient Gene Vector in Pest Management. *ACS Sustainable Chemistry & Engineering* **2019**, *7* 6, 6316-6322. DOI: 10.1021/acssuschemeng.9b00004.

68. Choi, I.; Suntivich, R.; Plamper, F. A.; Synatschke, C. V.; Müller, A. H. E.; Tsukruk, V. V. pH-Controlled Exponential and Linear Growing Modes of Layer-by-Layer Assemblies of Star Polyelectrolytes. *Journal of the American Chemical Society* **2011**, *133* 24, 9592-9606. DOI: 10.1021/ja203106c.

69. Babin, I. A.; Pergushov, D. V.; Wolf, A.; Plamper, F. A.; Schmalz, H.; Müller, A. H. E.; Zezin, A. B. Micellar interpolyelectrolyte complexes formed by star-shaped poly(acrylic acid) with double hydrophilic cationic diblock copolymer1. *Doklady Physical Chemistry* **2011**, *441* 1, 219-223. DOI: 10.1134/S0012501611110030.

70. Pergushov, D. V.; Babin, I. A.; Plamper, F. A.; Schmalz, H.; Müller, A. H. E.; Zezin, A. B. Water-soluble complex macromolecular structures based on star-shaped poly(acrylic acid). *Doklady Physical Chemistry* **2009**, *425* 1, 57-61. DOI: 10.1134/S0012501609030038.

71. Pergushov, D. V.; Babin, I. A.; Zezin, A. B.; Müller, A. H. E. Water-soluble macromolecular co-assemblies of star-shaped polyelectrolytes. John Wiley and Sons Ltd: 2013; Vol. 62, pp 13-21.

72. Pergushov, D. V.; Babin, I. A.; Plamper, F. A.; Zezin, A. B.; Müller, A. H. E. Water-soluble complexes of star-shaped poly(acrylic acid) with quaternized poly(4-vinylpyridine). *Langmuir* **2008**, *24* 13, 6414-6419. DOI: 10.1021/la800959s.

73. Larin, S. V.; Darinskii, A. A.; Zhulina, E. B.; Borisov, O. V. Interpolyelectrolyte complexes between starlike and linear macromolecules: A structural model for nonviral gene vectors. *Langmuir* **2009**, *25* 4, 1915-1918. DOI: 10.1021/la8037022.

74. Laaser, J. E.; Jiang, Y.; Petersen, S. R.; Reineke, T. M.; Lodge, T. P. Interpolyelectrolyte Complexes of Polycationic Micelles and Linear Polyanions: Structural Stability and Temporal Evolution. *J Phys Chem B* **2015**, *119* 52, 15919-15928. DOI: 10.1021/acs.jpcb.5b09010.

75. Laaser, J. E.; Lohmann, E.; Jiang, Y.; Reineke, T. M.; Lodge, T. P. Architecture-Dependent Stabilization of Polyelectrolyte Complexes between Polyanions and Cationic Triblock Terpolymer Micelles. *Macromolecules* **2016**, *49* 17, 6644-6654. DOI: 10.1021/acs.macromol.6b01408.

76. Jiang, Y.; Lodge, T. P.; Reineke, T. M. Packaging pDNA by Polymeric ABC Micelles Simultaneously Achieves Colloidal Stability and Structural Control. *J Am Chem Soc* **2018**, *140* 35, 11101-11111. DOI: 10.1021/jacs.8b06309.

77. Xu, W.; Ledin, P. A.; Plamper, F. A.; Synatschke, C. V.; Müller, A. H. E.; Tsukruk, V. V. Multiresponsive microcapsules based on multilayer assembly of star polyelectrolytes. *Macromolecules* **2014**, *47* 22, 7858-7868. DOI: 10.1021/ma501853c.

78. Steinschulte, A. A.; Gelissen, A. P. H.; Jung, A.; Brugnoni, M.; Caumanns, T.; Lotze, G.; Mayer, J.; Pergushov, D. V.; Plamper, F. A. Facile Screening of Various Micellar Morphologies by Blending Miktoarm Stars and Diblock Copolymers. *Acs Macro Lett* **2017**, *6* 7, 711-715. DOI: 10.1021/acsmacrolett.7b00328.

79. Plamper, F. A.; Gelissen, A. P.; Timper, J.; Wolf, A.; Zezin, A. B.; Richtering, W.; Tenhu, H.; Simon, U.; Mayer, J.; Borisov, O. V.; et al. Spontaneous Assembly of Miktoarm Stars into Vesicular Interpolyelectrolyte Complexes. *Macromol Rapid Comm* **2013**, *34* 10, 855-860. DOI: 10.1002/marc.201300053.

80. Gelissen, A. P. H.; Pergushov, D. V.; Plamper, F. A. Janus-like interpolyelectrolyte complexes based on miktoarm stars. *Polymer* **2013**, *54* 26, 6877-6881. DOI: 10.1016/j.polymer.2013.11.004.

81. Zhulina, E. B.; Borisov, O. V. Effect of Block Copolymer Architecture on Morphology of Self-Assembled Aggregates in Solution. *ACS Macro Letters* **2013**, *2* 4, 292-295. DOI: 10.1021/mz400035k.

82. Dähling, C.; Lotze, G.; Drechsler, M.; Mori, H.; Pergushov, D. V.; Plamper, F. A. Temperature-induced structure switch in thermo-responsive micellar interpolyelectrolyte

complexes: toward core–shell–corona and worm-like morphologies. *Soft Matter* **2016**, *12* 23, 5127-5137, 10.1039/C6SM00757K. DOI: 10.1039/C6SM00757K.

83. Xu, W.; Steinschulte, A. A.; Plamper, F. A.; Korolovych, V. F.; Tsukruk, V. V. Hierarchical Assembly of Star Polymer Polymersomes into Responsive Multicompartmental Microcapsules. *Chemistry of Materials* **2016**, *28* 3, 975-985. DOI: 10.1021/acs.chemmater.5b04934.

84. Störkle, D.; Duschner, S.; Heimann, N.; Maskos, M.; Schmidt, M. Complex formation of DNA with oppositely charged polyelectrolytes of different chain topology: Cylindrical brushes and dendrimers. *Macromolecules* **2007**, *40* 22, 7998-8006. DOI: 10.1021/ma0711689.

85. Larin, S. V.; Pergushov, D. V.; Xu, Y.; Darinskii, A. A.; Zezin, A. B.; Müller, A. H. E.; Borisov, O. V. Nano-patterned structures in cylindrical polyelectrolyte brushes assembled with oppositely charged polyions. *Soft Matter* **2009**, *5* 24, 4938-4943. DOI: 10.1039/b913944c.

86. Orilall, M. C.; Wiesner, U. Block copolymer based composition and morphology control in nanostructured hybrid materials for energy conversion and storage: solar cells, batteries, and fuel cells. *Chem Soc Rev* **2011**, *40* 2, 520-535. DOI: 10.1039/c0cs00034e.

87. Dwars, T.; Paetzold, E.; Oehme, G. Reactions in micellar systems. *Angew Chem Int Ed Engl* **2005**, *44* 44, 7174-7199. DOI: 10.1002/anie.200501365.

88. Mortensen, K. PEO-related block copolymer surfactants. *Colloids Surf.* **2001**, *183-185*, 277-292.

89. Kataoka, K. H., Atsushi; Nagasaki, Yukio. Block copolymer micelles for drug delivery: design, characterization and biological significance. *Adv. Drug Deliv. Rev.* **2001**, *477*, 113-131.

90. McCullagh, M. P., T.; Tonzani, S.; Winter, N. D.; Schatz, G. C. Modeling Self-Assembly Processes Driven by Nonbonded Interactions in Soft Materials. *J. Phys. Chem. B* **2008**, *112*, 10388-10398.

91. Haliloğlu, T. B., Ivet; Erman, Burak; Mattice, Wayne L. Mechanisms of the Exchange of Diblock Copolymers between Micelles at Dynamic Equilibrium. *Macromolecules* **1996**, *29*, 4764-4771.

92. Wang, Y. M., W. L.; Napper, D. H. Simulation of the Formation of Micelles by Diblock Copolymers under Weak Segregation. *Langmuir* **1993**, *9*, 66-70.

93. De Gennes, P. G. Scaling theory of polymer adsorption. *Journal de Physique* **1976**, *37* 12, 1445-1452. DOI: 10.1051/jphys:0197600370120144500.

94. De Gennes, P. G. Conformation of Polymers Attached to an Interface. *Macromolecules* **1980**, *13*, 1069-1075.

95. Halperin, A. Polymeric Micelles: A Star Model. *Macromolecules* **1987**, *20*, 2943-2946.

96. Noolandi, J. H., K. M. Theory of Block Copolymer Micelles in Solution. *Macromolecules* **1983**, *16*, 1443-1448.

97. Leibler, L. O., H.; Wheeler, J. C. Theory of critical micelle concentration for solutions of block copolymers. *J Chem Phys* **1983**, *79*, 3550. DOI: 10.1063/1.4940687.

98. Pépin, M. P. W., M. D. Monte Carlo and Mean Field Study of Diblock Copolymer Micelles. *Macromolecules* **2000**, *33*, 8644-8653.

99. Cantu, L. C., M.; Salina, P. Direct measurement of the formation time of mixed micelles. *J. Phys. Chem.* **1991**, *95*, 5981–5983.

100. Won, Y.-Y. D., H. T.; Bates, F. S. Molecular Exchange in PEO-PB Micelles in Water. *Macromolecules* **2003**, *36*, 953-955.

101. Lund, R. W., Lutz; Richter, Dieter; Dormidontova, Elena E. Equilibrium Chain Exchange Kinetics of Diblock Copolymer Micelles: Tuning and Logarithmic Relaxation. *Macromolecules* **2006**, *39*, 4566-4575.

102. Fu, J.; Schlenoff, J. B. Driving Forces for Oppositely Charged Polyion Association in Aqueous Solutions: Enthalpic, Entropic, but Not Electrostatic. *J Am Chem Soc* **2016**, *138* 3, 980-990. DOI: 10.1021/jacs.5b11878.

103. Voets, I. K.; de Keizer, A.; Cohen Stuart, M. A. Complex coacervate core micelles. *Adv Colloid Interfac* **2009**, *147-148*, 300-318. DOI: 10.1016/j.cis.2008.09.012.

104. Sproncken, C. C. M.; Magana, J. R.; Voets, I. K. 100th Anniversary of Macromolecular Science Viewpoint: Attractive Soft Matter: Association Kinetics, Dynamics, and Pathway Complexity in Electrostatically Coassembled Micelles. *Acs Macro Lett* **2021**, 167-179. DOI: 10.1021/acsmacrolett.0c00787.

105. Magana, J. R.; Sproncken, C. C. M.; Voets, I. K. On Complex Coacervate Core Micelles: Structure-Function Perspectives. *Polymers (Basel)* **2020**, *12* 9. DOI: 10.3390/polym12091953.

106. Riggleman, R. A.; Kumar, R.; Fredrickson, G. H. Investigation of the interfacial tension of complex coacervates using field-theoretic simulations. *J Chem Phys* **2012**, *136* 2, 024903. DOI: 10.1063/1.3674305.

107. Wei, H.; Pahang, J. A.; Pun, S. H. Optimization of brush-like cationic copolymers for nonviral gene delivery. *Biomacromolecules* **2013**, *14* 1, 275-284. DOI: 10.1021/bm301747r.

108. Van Bruggen, C.; Hexum, J. K.; Tan, Z.; Dalai, R. J.; Reineke, T. M. Nonviral Gene Delivery with Cationic Glycopolymers. *Accounts of Chemical Research* **2019**, *52* 5, 1347-1358.

109. Ridolfo, R.; Tavakoli, S.; Junnuthula, V.; Williams, D. S.; Urtti, A.; van Hest, J. C. Exploring the impact of morphology on the properties of biodegradable nanoparticles and their diffusion in complex biological medium. *Biomacromolecules* **2020**.

110. van der Burgh, S.; de Keizer, A.; Cohen Stuart, M. A. Complex coacervation core micelles. Colloidal stability and aggregation mechanism. *Langmuir* **2004**, *20* 4, 1073-1084. DOI: 10.1021/la035012n.

111. Aloi, A.; Guibert, C.; Olijve, L. L. C.; Voets, I. K. Morphological evolution of complex coacervate core micelles revealed by iPAINT microscopy. *Polymer* **2016**, *107*, 450-455. DOI: 10.1016/j.polymer.2016.08.002.

112. Harada, A.; Kataoka, K. Formation of Polyion Complex Micelles in an Aqueous Milieu from a Pair of Oppositely-Charged Block-Copolymers with Poly(Ethylene Glycol) Segments. *Macromolecules* **1995**, *28* 15, 5294-5299. DOI: DOI 10.1021/ma00119a019.

113. Anraku, Y.; Kishimura, A.; Oba, M.; Yamasaki, Y.; Kataoka, K. Spontaneous formation of nanosized unilamellar polyion complex vesicles with tunable size and properties. *J Am Chem Soc* **2010**, *132* 5, 1631-1636. DOI: 10.1021/ja908350e.

114. Wibowo, A.; Osada, K.; Matsuda, H.; Anraku, Y.; Hirose, H.; Kishimura, A.; Kataoka, K. Morphology Control in Water of Polyion Complex Nanoarchitectures of Double-Hydrophilic Charged Block Copolymers through Composition Tuning and Thermal Treatment. *Macromolecules* **2014**, *47* 9, 3086-3092. DOI: 10.1021/ma500314d.

115. Rumyantsev, A. M.; Zhulina, E. B.; Borisov, O. V. Scaling Theory of Complex Coacervate Core Micelles. *ACS Macro Letters* **2018**, *7* 7, 811-816. DOI: 10.1021/acsmacrolett.8b00316.

116. Takahashi, R.; Sato, T.; Terao, K.; Yusa, S. Intermolecular Interactions and Self-Assembly in Aqueous Solution of a Mixture of Anionic-Neutral and Cationic-Neutral Block Copolymers. *Macromolecules* **2015**, *48* 19, 7222-7229. DOI: 10.1021/acs.macromol.5b01368.

117. Takahashi, R.; Sato, T.; Terao, K.; Yusa, S. Reversible Vesicle-Spherical Micelle Transition in a Polyion Complex Micellar System Induced by Changing the Mixing Ratio of Copolymer Components. *Macromolecules* **2016**, *49* 8, 3091-3099. DOI: 10.1021/acs.macromol.6b00308.

118. van der Kooij, H. M.; Spruijt, E.; Voets, I. K.; Fokkink, R.; Cohen Stuart, M. A.; van der Gucht, J. On the stability and morphology of complex coacervate core micelles: from spherical to wormlike micelles. *Langmuir* **2012**, *28* 40, 14180-14191. DOI: 10.1021/la303211b.

119. Perry, S. L.; Leon, L.; Hoffmann, K. Q.; Kade, M. J.; Priftis, D.; Black, K. A.; Wong, D.; Klein, R. A.; Pierce, C. F., 3rd; Margossian, K. O.; et al. Chirality-selected phase behaviour in ionic polypeptide complexes. *Nat Commun* **2015**, *6*, 6052. DOI: 10.1038/ncomms7052.

120. Shah, S.; Leon, L. Structural transitions and encapsulation selectivity of thermoresponsive polyelectrolyte complex micelles. *J Mater Chem B* **2019**, *7* 41, 6438-6448. DOI: 10.1039/c9tb01194c.

121. Rodriguez-Hernandez, J.; Lecommandoux, S. Reversible inside-out micellization of pH-responsive and water-soluble vesicles based on polypeptide diblock copolymers. *J Am Chem Soc* **2005**, *127* 7, 2026-2027. DOI: 10.1021/ja043920g.

122. Holder, S. J.; Sommerdijk, N. A. J. M. New micellar morphologies from amphiphilic block copolymers: disks, toroids and bicontinuous micelles. *Polymer Chemistry* **2011**, *2* 5, 1018-1028. DOI: 10.1039/c0py00379d.

123. Srivastava, S.; Tirrell, M. V. Polyelectrolyte Complexation. In *Advances in Chemical Physics*, Rice, S. A., Dinner, A. R. Eds.; Advances in Chemical Physics, Vol. 161; John Wiley & Sons, Inc., 2016; pp 499-544.

124. Sing, C. E. Micro- to macro-phase separation transition in sequence-defined coacervates. *J Chem Phys* **2020**, *152* 2, 024902. DOI: 10.1063/1.5140756.

125. Heo, T. Y.; Kim, I.; Chen, L.; Lee, E.; Lee, S.; Choi, S. H. Effect of Ionic Group on the Complex Coacervate Core Micelle Structure. *Polymers-Basel* **2019**, *11* 3. DOI: 10.3390/polym11030455.

126. Burke, P. A.; Pun, S. H.; Reineke, T. M. Advancing polymeric delivery systems amidst a nucleic acid therapy renaissance. *Acs Macro Lett* **2013**, *2* 10, 928-934. DOI: 10.1021/mz400418j.

127. Hays, J. B.; Magar, M. E.; Zimm, B. H. Persistence Length of DNA. *Biopolymers* **1969**, *8* 4, 531-536. DOI: DOI 10.1002/bip.1969.360080410.

128. Tinland, B.; Pluen, A.; Sturm, J.; Weill, G. Persistence length of single-stranded DNA. *Macromolecules* **1997**, *30* 19, 5763-5765. DOI: DOI 10.1021/ma970381+.

129. Vieregg, J. R.; Lueckheide, M.; Marciel, A. B.; Leon, L.; Bologna, A. J.; Rivera, J. R.; Tirrell, M. V. Oligonucleotide-Peptide Complexes: Phase Control by Hybridization. *Journal of the American Chemical Society* **2018**, *140* 5, 1632-1638. DOI: 10.1021/jacs.7b03567.

130. Shakya, A.; King, J. T. DNA Local-Flexibility-Dependent Assembly of Phase-Separated Liquid Droplets. *Biophysical Journal* **2018**, *115* 10, 1840-1847.

131. Hayashi, K.; Chaya, H.; Fukushima, S.; Watanabe, S.; Takemoto, H.; Osada, K.; Nishiyama, N.; Miyata, K.; Kataoka, K. Influence of RNA Strand Rigidity on Polyion Complex Formation with Block Catiomers. *Macromol Rapid Comm* **2016**, *37* 6, 486-493. DOI: 10.1002/marc.201500661.

132. Takeda, K. M.; Osada, K.; Tockary, T. A.; Dirisala, A.; Chen, Q.; Kataoka, K. Poly(ethylene glycol) Crowding as Critical Factor To Determine pDNA Packaging Scheme into

Polyplex Micelles for Enhanced Gene Expression. *Biomacromolecules* **2017**, *18* 1, 36-43. DOI: 10.1021/acs.biomac.6b01247.

133. Marras, A. E.; Campagna, T. R.; Vieregg, J. R.; Tirrell, M. V. Physical Property Scaling Relationships for Polyelectrolyte Complex Micelles. *ChemRxiv. Preprint. DOI:10.26434/chemrxiv.13721719* **2021**. DOI: 10.26434/chemrxiv.13721719.

134. Voets, I. K.; de Vries, R.; Fokkink, R.; Sprakel, J.; May, R. P.; de Keizer, A.; Cohen Stuart, M. A. Towards a structural characterization of charge-driven polymer micelles. *Eur Phys J E Soft Matter* **2009**, *30* 4, 351-359. DOI: 10.1140/epje/i2009-10533-4.

135. Voets, I. K.; van der Burgh, S.; Farago, B.; Fokkink, R.; Kovacevic, D.; Hellweg, T.; de Keizer, A.; Stuart, M. A. C. Electrostatically driven coassembly of a diblock copolymer and an oppositely charged homopolymer in aqueous solutions. *Macromolecules* **2007**, *40* 23, 8476-8482. DOI: 10.1021/ma071356z.

136. Nagarajan, R.; Ganesh, K. Block Copolymer Self-Assembly in Selective Solvents - Spherical Micelles with Segregated Cores. *J Chem Phys* **1989**, *90* 10, 5843-5856. DOI: 10.1063/1.456390.

137. Zhulina, E. B.; Adam, M.; LaRue, I.; Sheiko, S. S.; Rubinstein, M. Diblock copolymer micelles in a dilute solution. *Macromolecules* **2005**, *38* 12, 5330-5351. DOI: 10.1021/ma048102n.

138. Zhulina, E. B.; Borisov, O. V. Theory of Block Polymer Micelles: Recent Advances and Current Challenges. *Macromolecules* **2012**, *45* 11, 4429-4440. DOI: 10.1021/ma300195n.

139. Holley, A. C.; Parsons, K. H.; Wan, W. M.; Lyons, D. F.; Bishop, G. R.; Correia, J. J.; Huang, F. Q.; McCormick, C. L. Block ionomer complexes consisting of siRNA and aRAFT-synthesized hydrophilic-block-cationic copolymers: the influence of cationic block length on gene suppression. *Polymer Chemistry* **2014**, *5* 24, 6967-6976. DOI: 10.1039/c4py00940a.

140. Parsons, K. H.; Holley, A. C.; Munn, G. A.; Flynt, A. S.; McCormick, C. L. Block ionomer complexes consisting of siRNA and aRAFT-synthesized hydrophilic-block-cationic copolymers II: the influence of cationic block charge density on gene suppression. *Polymer Chemistry* **2016**, *7* 39, 6044-6054. DOI: 10.1039/c6py01048b.

141. Horn, J. M.; Kapelner, R. A.; Obermeyer, A. C. Macro- and Microphase Separated Protein-Polyelectrolyte Complexes: Design Parameters and Current Progress. *Polymers-Basel* **2019**, *11* 4. DOI: 10.3390/polym11040578.

142. Sadman, K.; Wang, Q. F.; Chen, Y. Y.; Keshavarz, B.; Jiang, Z.; Shull, K. R. Influence of Hydrophobicity on Polyelectrolyte Complexation. *Macromolecules* **2017**, *50* 23, 9417-9426. DOI: 10.1021/acs.macromol.7b02031.

143. Fernandez-Villamarin, M.; Sousa-Herves, A.; Porto, S.; Guldris, N.; Martinez-Costas, J.; Riguera, R.; Fernandez-Megia, E. A dendrimer-hydrophobic interaction synergy improves the stability of polyion complex micelles. *Polymer Chemistry* **2017**, *8* 16, 2528-2537. DOI: 10.1039/c7py00304h.

144. Izumrudov, V. A.; Zhiryakova, M. V.; Kudaibergenov, S. E. Controllable stability of DNA-containing polyelectrolyte complexes in water-salt solutions. *Biopolymers* **1999**, *52* 2, 94-108.

145. Kim, B. S.; Chuanoi, S.; Suma, T.; Anraku, Y.; Hayashi, K.; Naito, M.; Kim, H. J.; Kwon, I. C.; Miyata, K.; Kishimura, A.; et al. Self-assembly of siRNA/PEG-b-catiomer at integer molar ratio into 100 nm-sized vesicular polyion complexes (siRNAsomes) for RNAi and codelivery of cargo macromolecules. *J Am Chem Soc* **2019**. DOI: 10.1021/jacs.8b13641.

146. Miyata, K.; Kakizawa, Y.; Nishiyama, N.; Harada, A.; Yamasaki, Y.; Koyama, H.; Kataoka, K. Block catiomer polyplexes with regulated densities of charge and disulfide cross-linking directed to enhance gene expression. *J Am Chem Soc* **2004**, *126* 8, 2355-2361. DOI: 10.1021/ja0379666.

147. Wang, Y.; Ma, B.; Abdeen, A. A.; Chen, G.; Xie, R.; Saha, K.; Gong, S. Versatile Redox-Responsive Polyplexes for the Delivery of Plasmid DNA, Messenger RNA, and CRISPR-Cas9 Genome-Editing Machinery. *ACS Appl Mater Interfaces* **2018**, *10* 38, 31915-31927. DOI: 10.1021/acsami.8b09642.

148. Bronich, T. K.; Keifer, P. A.; Shlyakhtenko, L. S.; Kabanov, A. V. Polymer micelle with cross-linked ionic core. *J Am Chem Soc* **2005**, *127* 23, 8236-8237. DOI: 10.1021/ja043042m.

149. Dey, D.; Kumar, S.; Banerjee, R.; Maiti, S.; Dhara, D. Polyplex formation between PEGylated linear cationic block copolymers and DNA: equilibrium and kinetic studies. *J Phys Chem B* **2014**, *118* 25, 7012-7025. DOI: 10.1021/jp501234p.

150. Dhande, Y. K.; Wagh, B. S.; Hall, B. C.; Sprouse, D.; Hackett, P. B.; Reineke, T. M. N-Acetylgalactosamine Block-co-Polycations Form Stable Polyplexes with Plasmids and Promote Liver-Targeted Delivery. *Biomacromolecules* **2016**, *17* 3, 830-840. DOI: 10.1021/acs.biomac.5b01555.

151. Sprouse, D.; Reineke, T. M. Investigating the Effects of Block versus Statistical Glycopolycations Containing Primary and Tertiary Amines for Plasmid DNA Delivery. *Biomacromolecules* **2014**, *15* 7, 2616-2628. DOI: 10.1021/bm5004527.

152. Kramarenko, E. Y.; Khokhlov, A. R.; Reineker, P. Stoichiometric polyelectrolyte complexes of ionic block copolymers and oppositely charged polyions. *J Chem Phys* **2006**, *125* 19, 194902. DOI: 10.1063/1.2387173.

153. Bos, I.; Timmerman, M.; Sprakel, J. FRET-Based Determination of the Exchange Dynamics of Complex Coacervate Core Micelles. *Macromolecules* **2020**. DOI: 10.1021/acs.macromol.0c02387.

154. Takahashi, R.; Narayanan, T.; Yusa, S.-i.; Sato, T. Kinetics of Morphological Transition between Cylindrical and Spherical Micelles in a Mixture of Anionic–Neutral and Cationic–Neutral Block Copolymers Studied by Time-Resolved SAXS and USAXS. *Macromolecules* **2018**, *51* 10, 3654-3662.

155. Marras, A. E.; Vieregg, J. R.; Tirrell, M. V. Assembly and Characterization of Polyelectrolyte Complex Micelles. *J Vis Exp* **2020**, 157, e60894. DOI: 10.3791/60894.

156. Marciel, A. B.; Srivastava, S.; Ting, J. M.; Tirrell, M. V. SAXS methods for investigating macromolecular and self-assembled polyelectrolyte complexes. Methods in Enzymology, 2020.

157. Ting, J. M.; Wu, H.; Herzog-Arbeitman, A.; Srivastava, S.; Tirrell, M. V. Synthesis and Assembly of Designer Styrenic Diblock Polyelectrolytes. *Acs Macro Lett* **2018**, *7* 6, 726-733. DOI: 10.1021/acsmacrolett.8b00346.

158. Ting, J. M.; Marras, A. E.; Mitchell, J. D.; Campagna, T. R.; Tirrell, M. V. Comparing Zwitterionic and PEG Exteriors of Polyelectrolyte Complex Micelles. *Molecules* **2020**, *25* 11. DOI: 10.3390/molecules25112553.

159. Takahashi, R.; Narayanan, T.; Sato, T. Growth Kinetics of Polyelectrolyte Complexes Formed from Oppositely-Charged Homopolymers Studied by Time-Resolved Ultra-Small-Angle X-ray Scattering. *J Phys Chem Lett* **2017**, *8* 4, 737-741. DOI: 10.1021/acs.jpclett.6b02957.

160. Wu, H.; Ting, J. M.; Yu, B.; Jackson, N. E.; Meng, S.; de Pablo, J. J.; Tirrell, M. V. Spatiotemporal Formation and Growth Kinetics of Polyelectrolyte Complex Micelles with Millisecond Resolution. *ACS Macro Letters* **2020**, *9* 11, 1674-1680. DOI: 10.1021/acsmacrolett.0c00543.

161. Smolsky, I. L.; Liu, P.; Niebuhr, M.; Ito, K.; Weiss, T. M.; Tsuruta, H. Biological small-angle X-ray scattering facility at the Stanford Synchrotron Radiation Laboratory. *Journal of Applied Crystallography* **2007**, *40* s1, s453-s458. DOI: 10.1107/s0021889807009624.

162. Amann, M.; Diget, J. S.; Lyngsø, J.; Pedersen, J. S.; Narayanan, T.; Lund, R. Kinetic Pathways for Polyelectrolyte Coacervate Micelle Formation Revealed by Time-Resolved Synchrotron SAXS. *Macromolecules* **2019**, *52* 21, 8227-8237.

163. Wu, H.; Ting, J. M.; Werba, O.; Meng, S.; Tirrell, M. V. Non-equilibrium phenomena and kinetic pathways in self-assembled polyelectrolyte complexes. *J Chem Phys* **2018**, *149* 16, 163330. DOI: 10.1063/1.5039621.

164. Lund, R.; Willner, L.; Monkenbusch, M.; Panine, P.; Narayanan, T.; Colmenero, J.; Richter, D. Structural observation and kinetic pathway in the formation of polymeric micelles. *Phys Rev Lett* **2009**, *102* 18, 188301. DOI: 10.1103/PhysRevLett.102.188301.

165. Dormidontova, E. E. Micellization Kinetics in Block Copolymer Solutions: Scaling Model. *Macromolecules* **1999**, *32*, 7630-7644.

166. Aniansson, E. A. G. W., S. N. Kinetics of step-wise micelle association. *The Journal of Physical Chemistry* **1974**, *78*, 1024-1030.

167. Wu, H.; Ting, J. M.; Weiss, T. M.; Tirrell, M. V. Interparticle Interactions in Dilute Solutions of Polyelectrolyte Complex Micelles. *ACS Macro Letters* **2019**, *8* 7, 819-825. DOI: 10.1021/acsmacrolett.9b00226.

168. Bos, I.; Sprakel, J. Langevin Dynamics Simulations of the Exchange of Complex Coacervate Core Micelles: The Role of Nonelectrostatic Attraction and Polyelectrolyte Length. *Macromolecules* **2019**, *52* 22, 8923-8931. DOI: 10.1021/acs.macromol.9b01442.

169. Dautzenberg, H.; Konak, C.; Reschel, T.; Zintchenko, A.; Ulbrich, K. Cationic graft copolymers as carriers for delivery of antisense-oligonucleotides. *Macromolecular Bioscience* **2003**, *3* 8, 425-435. DOI: 10.1002/mabi.200350014.

170. Harada, A.; Kataoka, K. Selection between block- and homo-polyelectrolytes through polyion complex formation in aqueous medium. *Soft Matter* **2008**, *4* 1, 162-167. DOI: 10.1039/b713853a.

171. Carl, N.; Prévost, S.; Schweins, R.; Huber, K. Contrast variation of micelles composed of Ca2+ and block copolymers of two negatively charged polyelectrolytes. *Colloid and Polymer Science* **2020**, *298* 7, 663-679. DOI: 10.1007/s00396-019-04596-1.

172. Qiang, Z.; Wang, M. 100th Anniversary of Macromolecular Science Viewpoint: Enabling Advances in Fluorescence Microscopy Techniques. *ACS Macro Letters* **2020**, *9* 9, 1342-1356. DOI: 10.1021/acsmacrolett.0c00506.

173. Parent, L. R.; Gnanasekaran, K.; Korpanty, J.; Gianneschi, N. C. 100th Anniversary of Macromolecular Science Viewpoint: Polymeric Materials by In Situ Liquid-Phase Transmission Electron Microscopy. *ACS Macro Letters* **2020**, *10* 1, 14-38. DOI: 10.1021/acsmacrolett.0c00595.

Chapter 2

Effect of Charged Block Length Mismatch on Double Diblock Polyelectrolyte Complex Micelle Cores

2.1 Introduction

Understanding the self-assembly of polyelectrolytes remains an outstanding problem in polymer science with widespread implications.[1, 2] The ubiquity of ion-containing biopolymers with remarkably complex structures has long fascinated polymer scientists seeking to emulate the intricate self-assembly that enables cellular compartmentalization, enzymatic catalysis, and viral delivery.[2] Unfortunately, in many situations biomimicry remains either impractical or unattainable in scope, so polymer scientists often focus on developing synthetic systems that interface with biology instead.[3] To this end, a great deal of effort has been devoted to developing nanocarriers to delivery therapeutics in a variety of clinical applications.[4, 5] The most common approach has been the utilization of amphiphilic molecules. With judicious placement, the hydrophobic groups of these molecules can self-assemble in aqueous environments to form hydrophobic domains capable of sequestering hydrophobic cargo. While successful in certain instances, amphiphilic assembly can require complex protocols or materials to encapsulate hydrophilic therapeutics and may suffer from poor circulation or toxicity, motivating the development of alternative approaches to biomaterials.[3] A more complete understanding of polyelectrolyte assemblies could address key knowledge gaps and enable the development of next generation biomaterials.

Polyelectrolyte complexes (PECs) stand out as a promising biomaterials platform since a host of therapeutic molecules are charge-bearing, and many adverse biological interactions are known or suspected to be mediated by charge-charge interactions.[6, 7] PECs form spontaneously upon the mixture of oppositely charged polyelectrolytes due to associations between oppositely

charged polyelectrolytes and the entropic gain resulting from the release of small molecule counterions, resulting in a hydrated polymer-rich phase. [8-13] If desired, blocky and non-linear architectures can be incorporated to induce phase separation at smaller scales, resulting in ordered gels and nanoparticles with PEC domains. Among these structured PEC materials, polyelectrolyte complex micelles (PCMs) have gained particular interest for their ability to partition hydrophilic biomolecules such as nucleic acids (e.g., new DNA or RNA genes, oligonucleotide gene modulators, or gene editors) or charged proteins within core-shell nanoparticles aiding protection, shielding, and biodistribution. [14-17] PCMs were pioneered by Harada and Kataoka in the 1990s, and since that time single diblock (AB + C) and double diblock (AB + AC) PCMs have emerged as the two primary micelle formulations. [18-21] As the names suggest, single diblock PCMs (S-PCMs) employ one diblock polyelectrolyte (with a neutral A block and charged B block) complexing with an oppositely charged homopolyelectrolyte (C block) to create core-shell nanostructures, [3, 18, 22,-25] whereas double diblock PCMs (D-PCMs) utilize two oppositely charged AB and AC diblocks. [20 26-33]

The differences between single and D-PCMs may seem trivial, but the covalent attachment of charged and neutral blocks in every constituent polyelectrolyte establishes the most important structural interplay for D-PCM structure: namely, the competition between charge neutralization within the core and strict core-shell segregation. . [34, 35] This interplay results in D-PCMs having smaller particle size, lower resistance to dissolution by salt and smaller aggregation numbers than comparable S-PCMs. [21, 34, 35] Fascinating studies of the fundamental assembly properties of D-PCMs have demonstrated unique behavior such as homogeneous mixing of immiscible corona forming blocks and homopolymer displacement from S-PCMs to favor D-PCMs. These studies suggest that a complex interplay of thermodynamic properties distinguish S-PCMs from D-PCMs

and have prompted the exploration of these materials in a variety of storage and delivery applications.

Within the growing literature on double-diblock PEC nanostructures, few have examined the effect of blending two diblocks with mismatched charged block lengths, despite the potential understanding and utility that unmatched block lengths could provide. In seminal work on D-PCMs, Harada and Kataoka reported that when mismatched charged length diblock polyelectrolytes were mixed, no PCMs formed. [36] Instead, small aggregates were formed. The same group concluded that the aggregates are "unit polyionic complexes" by calculating their molecular weight using light scattering. [35] These small aggregates were hypothesized to be composed of one long diblock compensated by enough short diblocks to neutralize charge (Fig. 2.1). The neutral length of all polymers was the same. These unit polyionic complexes were theorized to be an intermediate stage of PCMs formation that were unable to proceed to well-defined core shell structures due to an inability to reconcile the need for charge compensation and core-shell segregation. Chain length recognition, the term used to describe the unique ability of matched diblocks to grow past small aggregates and form uniform D-PCMs, shaped many experimental studies that followed. Since the publication of these results, a majority of D-PCM studies focus on polyelectrolyte pairs with less than 10% difference in oppositely charged block length. To accommodate the restrictions of chain length recognition, some works make structurally identical but oppositely charged polyelectrolytes by using reactive precursor polymers which are subsequently functionalized using click chemistry. [28-30, 37, 38] Overall, this result has been hugely consequential in the design of ordered PEC structures from gels to PCMs, but recent results in PCM dynamics lead us to question some foundational assumptions behind chain length recognition.

Some assume that since PCMs form spontaneously upon mixing, they rapidly reach thermodynamic equilibrium, and thus the failure of mismatched diblocks to form PCMs is due to poor chain length recognition and not kinetics. [36] However, this interpretation is at odds with recent chain exchange measurements in PCMs which suggest large energetic barriers to molecular rearrangement in low salt environments, as well as studies of micelle formation that demonstrate the role of kinetic barriers in PCM formation and equilibration. [26, 39-41] Furthermore, our group has shown that PCMs formed by rapidly mixing polyelectrolyte solutions do not form PCMs with consistent and reproducible structures. Taken together, these studies confirm that many PCMs are not at equilibrium on the timescale of experiment, despite forming spontaneously in water. [15] To circumvent this issue, our group developed annealing protocols which gave PCMs the necessary mobility to rearrange and reach their minimum energy states, leading to reproducible PCMs. [15, 42, 43] In this work, we use directed salt annealing to abandon the limitations of chain length recognition and explore a wide ratio of diblock polyelectrolytes with mismatched charged block lengths and discover unique interdependent trends as a function of charged block length in the core of D-PCMs (Fig. 2.1).

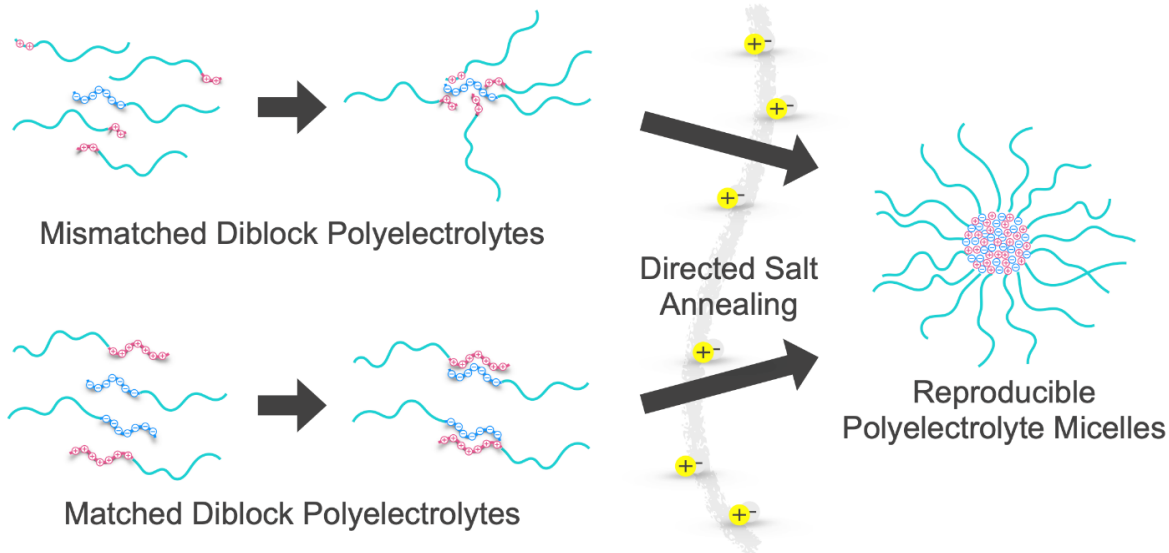

Figure 2.1 Schematic model for the formation of mismatched and matched PCMs through salt annealing.

2.2 Results and Discussion

To understand the influence of charged block length mismatch on D-PCMs, we created a library of diblock polyelectrolytes with poly(ethylene oxide) (PEO) as the neutral block and poly(glutamic acid) (P(*D*,*L*)E), poly(aspartic acid) (P(*D*,*L*)D), poly(lysine) (P*L*K) and poly((vinylbenzyl)trimethylammonium chloride) (PVB) as the charged blocks (Fig. 2.2). We chose to study diblock polymers with a consistent neutral block length of approximately 5 kg/mol PEO and charged block lengths of 25-200 units to examine charged block lengths that spanned an order of magnitude and are within the typical size range for PCM studies (Table 2.1). [44] To refer to data concisely, we use the shorthand of E, D, K and V to refer to PEO-*b*-P(*D*,*L*)E, PEO-*b*-P(*D*,*L*)D, PEO-*b*-P*L*K and PEO-*b*-PVB, respectively. For example, micelles composed of combinations of PEO-*b*-P*L*K and PEO-*b*-P(*D*,*L*)D will be referred to as KD pairings for brevity. In addition, the term set block length is used throughout the discussion to refer to the charged block length that is held constant within a data set.

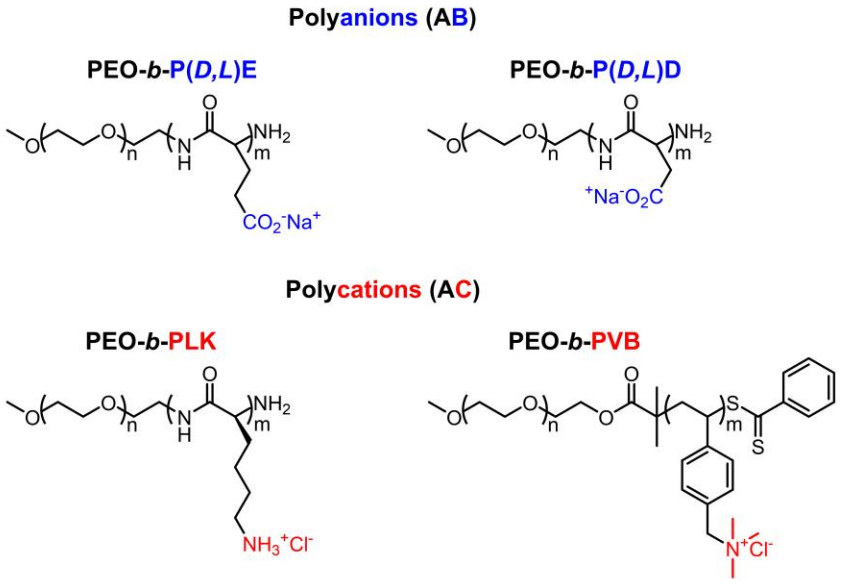

Figure 2.2 Chemical structures of polyelectrolytes examined in this work: PEO-*b*-P(*D*,*L*)D (**D**), PEO-*b*-P(*D*,*L*)E (**E**), PEO-*b*-P*L*K (**K**), and PEO-*b*-PVB (**V**).

Table 2.1 Polymer characterization data provided by Alamanda Polymers, INC.

Polymer	Charged DP	M_n of mPEG-NH_2 (kg/mol)	Mn by NMR (kg/mol)	PDI by GPC
K25	27	5.3	9.7	1.05
K50	51	4.6	13.0	1.09
K100	101	4.6	21.2	1.05
K200	194	4.6	36.5	1.07
D50	45	5.3	11.5	1.02
D100	100	4.6	18.3	1.04
D200	220	5.0	35.1	1.01
E25	25	5.0	8.7	N/A
E50	46	5.3	12.2	1.05
E100	92	5.1	19.0	1.02
E200	208	5.1	36.5	1.02

Previous work in our group has shown that the dominant form of micelle preparation, rapid mixing, can lead to kinetically trapped PCMs, leading to inconsistent micelle structure. [15] To address this issue, we developed salt-annealing protocols for PCMs where the oppositely charged polymers are prepared in a high salt environment and then dialyzed to the final salt concentration over the course of days. This method ensures that the micelles have ample freedom to rearrange and avoid kinetic restrictions and has been shown to produce thermodynamically stable, reproducible PCMs. [15, 43] To prepare our PCMs, diblock polyelectrolytes were first mixed at a 1:1 charge ratio at an ionic strength high enough to minimize complexation of PCMs and then slowly dialyzed to the final buffer concentration of 50 mM NaCl in 10 mM HEPES.

To fully characterize the shape, structural features, and aggregation number of our PCMs, we use a combination of small angle X-ray scattering (SAXS), dynamic light scattering (DLS) and cryogenic transmission electron microscopy (cryo-TEM). Most diblock polyelectrolyte pairings assemble into well-defined spheroidal core-shell micelles regardless of charged block length

symmetry. However, KE pairings do not form monodisperse spherical PCMs, but instead form aggregates with rodlike structures according to SAXS, possibly due to the formation of beta sheets in the PCM core.[45] These ineffective pairings represent a small minority of the total polyelectrolyte pairs studied and were not included in our analysis.

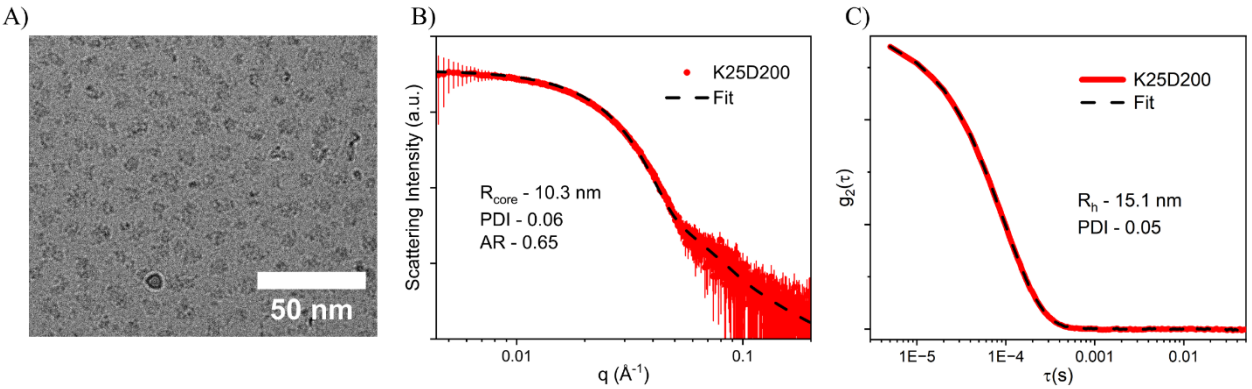

Figure 2.3 PCM characterization (A) Cryo-transmission electron microscopy (cryo-TEM) images of the PCMs formed by mixing 5kPEG-*b*-P*L*K$_{25}$ and 5kPEG-*b*-P(*D*,*L*)D$_{200}$ (K25D200). Cryo-TEM shows PCM cores but is unable to resolve PCM coronas due to the low contrast between PEG and water. Scale bar = 50 nm. (B) Experimental small-angle X-ray scattering (SAXS) data and fit used to determine the PCM core radius R_{core}, polydispersity index (PDI) and aspect ratio (AR) for K25D200 (C) Dynamic light scattering (DLS) and fit provide total particle size through R_h, which can be used to calculate PCM shell thickness ($H = R_h - R_{core}$).

The remaining PCMs formed compact, spheroidal nanoparticles as visualized by representative TEM images in Fig. 2.3A and Fig. 2.4. As detailed in Table 2.2, the scattering contrast between the core-forming polyelectrolyte repeat units and water is an order of magnitude stronger than that of PEO. As a result, SAXS patterns of these systems are dominated by scattering contributions from the PCM core, as has been shown previously.[15, 42, 43, 46, 47] Our collected SAXS data was then fit with a spheroidal form factor to model the PCM core supplemented with a high q power law fit to account for scattering from neutralized polymer chains within the core.[15, 42, 43] The data and model fits show excellent agreement, as shown in Fig. 2.3B and Fig. 2.5. A majority of PCM fits had core radii values that ranged from 9-25 nm with aspect ratios from 0.5-1.0 and

narrow polydispersity indexes. To measure the hydrodynamic radius of our PCMs, we utilized DLS and obtained sizes of 10-60 nm. Figure 2.3C shows the fitting of a representative autocorrelation function. Combining SAXS and DLS allows us to calculate the corona thickness by subtracting the core radius from the hydrodynamic radius, resulting in shell thicknesses that mostly ranged from 4-15 nm. A detailed list of complete PCM features can be found in Table 2.3.

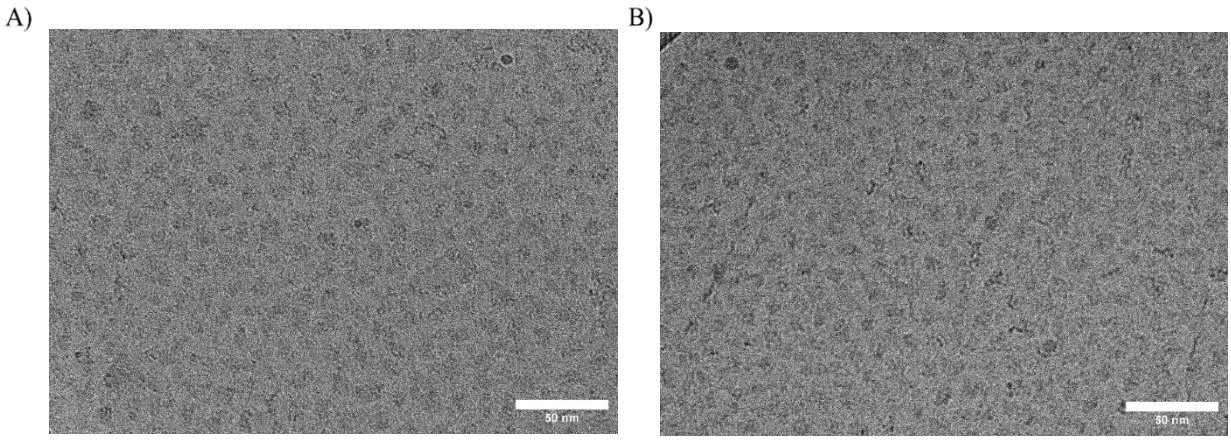

Figure 2.4 Cryo-TEM images of (A) K200D50 and (B) K50E50.

Table 2.2 Scattering Length Density (SLD)

Material	SLD (ρ) (10^{10} cm^{-2})	Contrast $(\Delta\rho)^2$ (10^{10} cm-2)2
Lysine	12.71	10.82
VBTMA	12.11	7.24
Aspartic Acid	12.62	10.24
Glutamic Acid	12.34	8.53
PEG	10.36	0.88
Solvent	9.42	0.00

The built-in density calculator from the Irena scattering plugin package within Igor was used to obtain Scattering Length Density (SLD) and contrast values, which are used below in the derivation for n_{ip}. SLD, $\boldsymbol{\rho}$) was calculated in Origin using the built-in contrast calculator within the Irena plugin bundle for Igor by inputting the chemical composition for each material and solvent. Contrast values **($\Delta\boldsymbol{\rho}$)** in Table S1 are proportional to SAXS scattering intensity. The values in table S1 support our assumption that PEG contributes minimally to our SAXS data and that the models fit to our data only represent PCM cores.

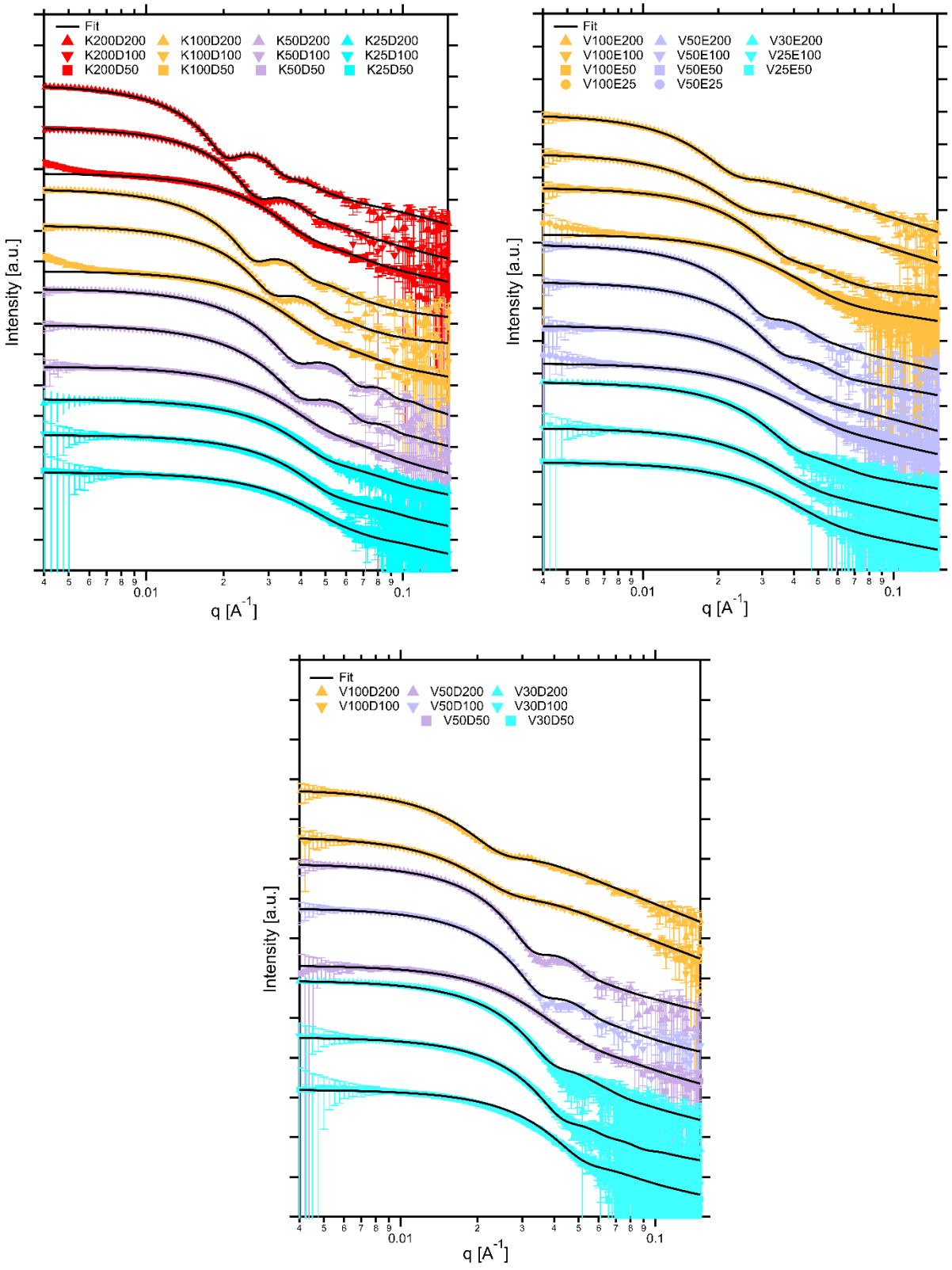

Figure 2.5 SAXS patterns and fits of double-diblock PCMs.

Table 2.3 Fitting results for SAXS and DLS data of mismatched PCMs

PCM components	Core structure from SAXS				Hydrodynamic size from DLS		
Sample Label	**Intensity (q=0)**	**R_{core}: Mean Radius (nm)**	**PDI**	**Aspect Ratio**	**R_h: Mean Radius (nm)**	**PDI**	**H: Corona Thickness (nm)**
K25D50	0.157	9.3	0.05	0.53	12.5	0.09	3.2
K25D100	0.255	10.0	0.04	0.60	14.3	0.05	4.3
K25D200	0.344	10.3	0.06	0.65	15.1	0.05	4.7
K50D50	0.415	11.3	0.03	0.61	18.0	0.03	6.6
K50D100	0.919	13.6	0.01	0.69	22.4	0.07	8.8
K50D200	1.289	14.2	0.01	0.70	18.5	0.02	4.3
K100D50	0.583	12.0	0.03	0.61	22.2	0.25	10.2
K100D100	1.546	15.3	0.02	0.88	21.8	0.03	6.5
K100D200	2.363	19.0	0.01	0.77	24.7	0.02	5.7
K200D50	0.803	13.1	0.03	0.62	57.8	0.42	44.7
K200D100	2.274	18.8	0.01	0.72	24.6	0.03	5.8
K200D200	5.525	24.4	0.01	0.77	30.5	0.05	6.1
V25E25	-	-	-	-	-	-	-
V25E50	0.192	9.6	0.09	0.62	42.0	0.85	32.4
V25E100	0.631	11.6	0.05	0.64	16.8	0.23	4.2
V25E200	0.551	13.1	0.02	0.65	17.0	0.23	3.9
V50E25	0.227	9.9	0.08	0.54	20.6	0.54	10.7
V50E50	0.283	12.3	0.14	0.62	17.6	0.17	5.4
V50E100	0.633	14.1	0.10	0.73	19.5	0.07	5.4
V50E200	0.89	16.4	0.07	0.75	22.3	0.06	5.9
V100E25	0.227	9.9	0.10	0.62	15.2	0.19	5.3
V100E50	0.494	13.6	0.12	0.72	19.1	0.07	5.5
V100E100	0.549	17.8	0.16	0.74	24.5	0.12	6.7
V100E200	0.831	20.6	0.12	0.72	25.9	0.05	5.3
V25D50	0.183	9.2	0.09	0.67	19.7	0.50	10.5
V25D100	0.35	12.2	0.02	0.63	17.9	0.21	5.7
V25D200	0.873	13.2	0.01	0.67	19.9	0.40	6.7
V50D50	0.231	11.4	0.12	0.53	16.9	0.15	5.5
V50D100	0.604	14.0	0.07	0.75	21.8	0.11	7.8

V50D200	0.768	15.0	0.06	0.75	22.6	0.11	7.6
V100D50	-	-	-	-	-	-	-
V100D100	0.359	14.9	0.25	0.81	25.9	0.18	11.0
V100D200	0.595	16.7	0.26	0.89	25.1	0.15	8.4

Tabulated results for each PCM (Figures 2.3-7). PCM core size and aggregation number were characterized via SAXS and modeled in the Irena[1] plugin for Igor Pro according to previous methods.[2, 3] DLS data were fit using a cumulant fitting algorithm. Corona thickness was calculated as $H=R_h-R_{core}$.

2.2.1 Core Growth

To investigate the relationship between charged block length mismatch and PCM structural features, we first looked at the relationship between total charged block length and PCM core radius. Intuitively, one might expect that a micelle feature like core radius would scale with the sum of the charged block lengths of the constituent polyelectrolytes, as both charged blocks contribute to core size. However, there is a poor relationship between the total charged block length and core size (Fig. 2.6). Instead, we grouped our PCMs into sets where one charged block length is held constant as the oppositely charged block length is varied.

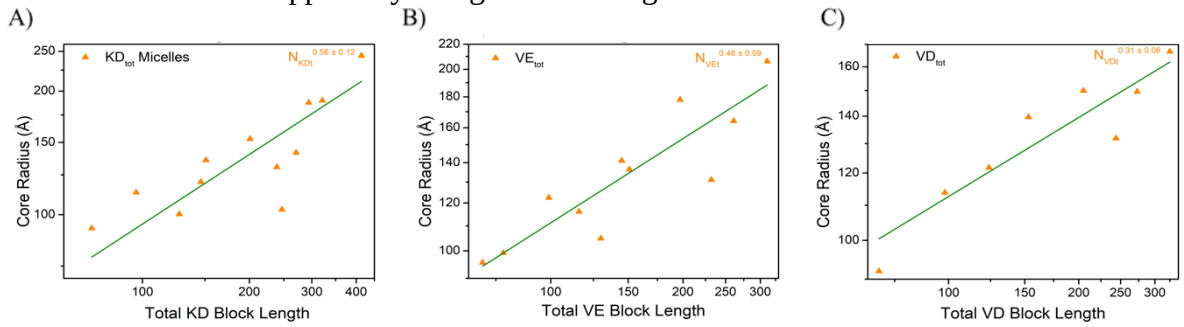

Figure 2.6 Power law fits for set block length vs ion pair aggregation number from SAXS data.

Since each of these micelles is composed of two diblock polyelectrolytes (AB + AC), there are two ways to examine each set of data: either a fixed AB polymer length and variable AC length, or the converse. For example, in Fig. 2.7A we plot the core radius results of the KD dataset in the frame of reference holding the block lengths of PEO-*b*-P(*D*,*L*)D constant at D50 (open red), D100 (open blue), D200 (open pink) and varying P*L*K block lengths from 25 to 200. Fig. 2.7B represents

the same data visualized with closed symbols by holding PEO-*b*-P*L*K block length constant at K25 (black), K50 (red), K100 (blue), and K200 (pink) and varying P(*D*,*L*)D block length from 50 to 200. Both perspectives of the data were fit with a power law, as shown in the text labels of each plot. To remove bias towards one polyelectrolyte, we also consolidated the datasets from the left two columns of Fig. 2.7 into the right column (Fig. 2.7C,F,I), such that in Fig. 2.7C, the KD50 dataset is a composite of the D50 set from Fig. 2.7A (open symbols) and the K50 set from Fig. 2.7B (closed symbols). This gives a chemically agnostic description of the growth of the PCM cores without biasing towards one polyelectrolyte and allows us to evaluate the influence of diblock mismatch.

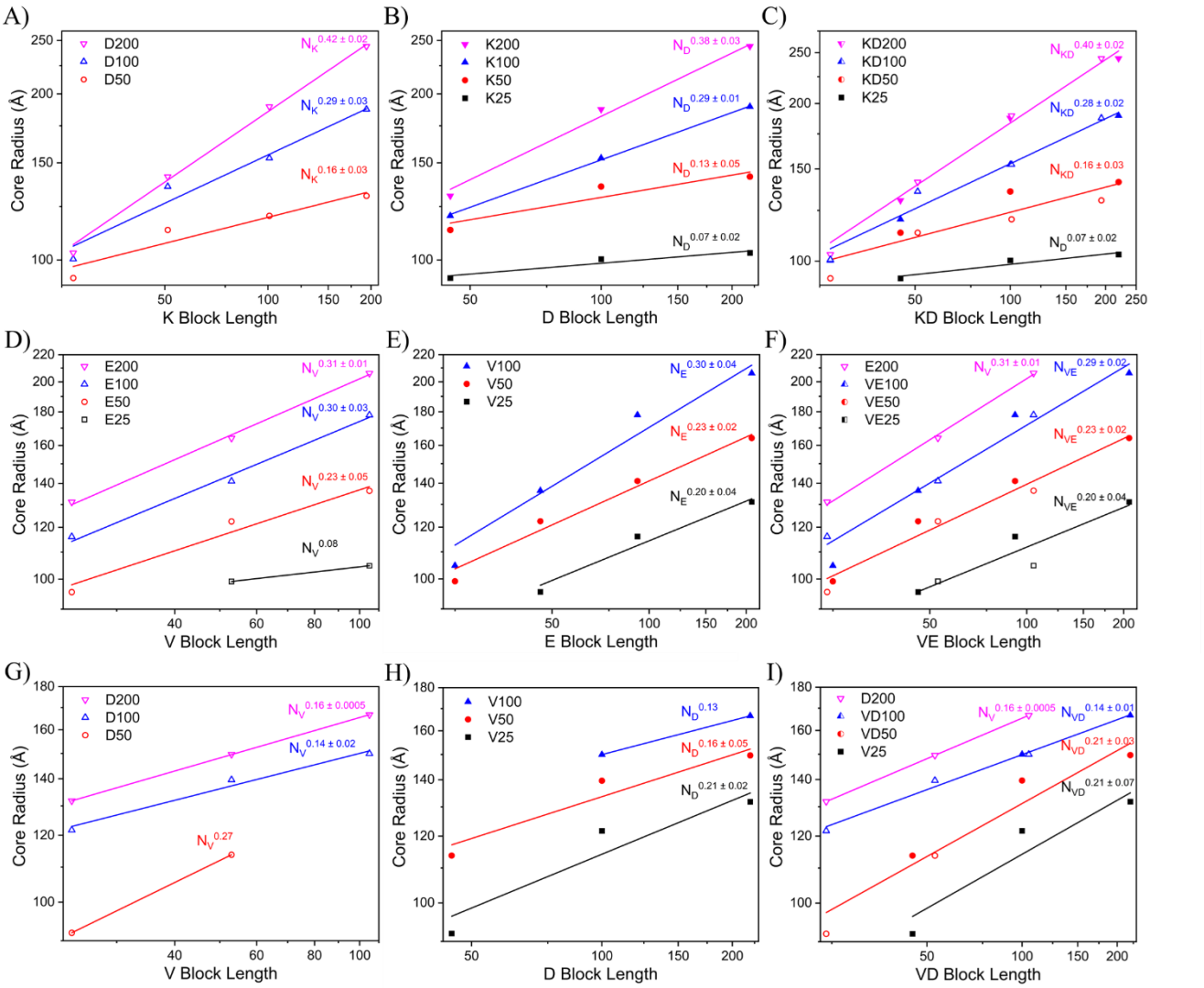

Figure 2.7 Core radius vs block length determined by fitting SAXS data and plotting the results against charged block length. A power law fit was applied to each data set, which are divided into separate colors/symbols. Every diblock polyelectrolyte has a neutral PEO block length of ~5k. Charged block length names are abbreviated from P*L*K to K, PVB to V, P(*D*,L)D to D and P(*D*,*L*)E to E for brevity. Across all datasets the datapoints/fits are represented by colors, with black representing DP~25, red symbols representing DP~50, blue symbols representing DP~100 and pink symbols representing DP~200. Open datapoints signify an anionic frame of reference, where the data are grouped into sets of constant anionic block length and plotted against varying cationic block length. Filled data signify a cationic frame of reference, where data are grouped into sets of constant cationic block length and plotted against varying anionic block lengths. Half-filled data signify a composite dataset where both anionic and cationic frames of reference are represented in the same color and are fit together. (A-C) show the KD pairing. (A) and (B) show the distinct frames of reference and in (C) both datasets are overlayed to remove any preference for one diblock when fitting the results. (D-F) and (G-I) repeat the same graphing pattern for VE and VD polyelectrolyte pairings.

2.2.2 Interdependent Core Growth

Our data shows that larger charged block lengths lead to increased core size in all sets regardless of polyelectrolyte pairing. However, unlike single diblock PCMs, the different sets cannot be normalized and combined into a single predictive scaling law because the exponential value of the power law fits varies as a function of set block length. For example, in the KD system, the power law fit applied to the sets grows from 0.07 ± 0.02 to 0.40 ± 0.02 as the set block length grows from 25 to 200. The systematically increasing growth rate as a function of set block length suggests that AB + AC micelle cores grow via a uniquely interdependent mechanism, whereby the size of AB polyelectrolytes modulate the ability of AC polyelectrolytes to contribute to core growth.

To the best of our knowledge, this interdependent behavior has not been observed in uncharged AB + AC amphiphilic systems. Furthermore, interdependent growth in uncharged systems may prove extremely difficult to observe due to the tendency of chemically dissimilar neutral polymers to undergo macrophase separation upon mixing. PCMs, on the other hand, exhibit dynamic, uniform mixing of chemically distinct polymers within a hydrated micelle core. This allows us to observe how the charged block length of AB polyelectrolytes enhances or inhibits the ability of AC polyelectrolytes to contribute to the core size as a function of charged block length. To better understand this phenomenon, we examined the relationship between set block length and core growth for different polyelectrolyte chemistries.

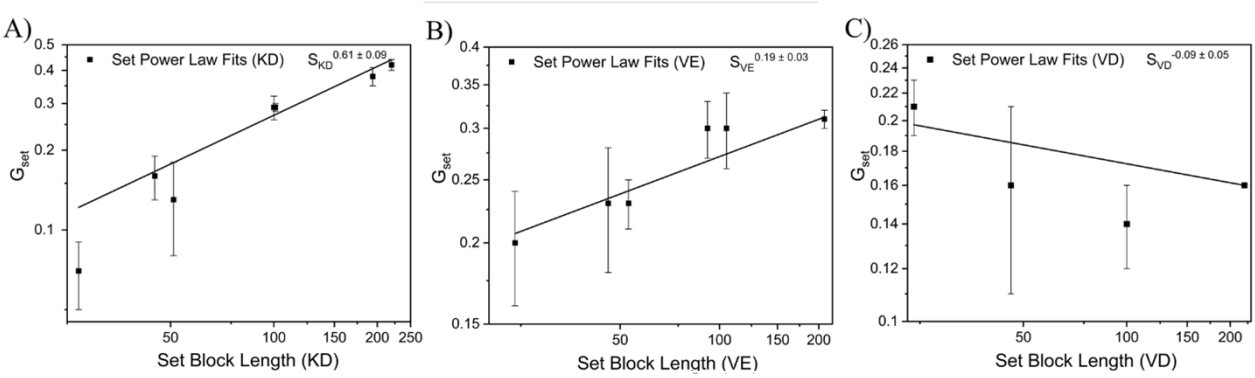

Figure 2.8 Set power law fits vs set block length for core radius from sets of data found in Fig. 2.7 A,B,D,E,G and H. Polyelectrolyte pairings of PEO-*b*-P*L*K and PEO-*b*-P(*D*,*L*)D, PEO-*b*-PVB and PEO-*b*-P(*D*,*L*)E and PEO-*b*-PVB and PEO-*b*-P(*D*,*L*)D are denoted with KD, VE, and VD, respectively. A power law fit was applied to each data set. Sets from Figure 2.7 with fewer than three data points were excluded from this analysis. Error bars represent standard error.

To develop a systematic understanding of the effect of polyelectrolyte chemistry on interdependent PCM growth, we examined the relationship between the scaling exponents of each data set in Fig. 2.7 and set block length. Fitting the combined data in Fig. 2.8 allows us to extract an interdependent growth relationship (IGR) which serves to quantify how the set block length influencs PCM core growth between sets (e.g. K100 vs. K200) and how polyelectrolyte chemistry influences across polyelectrolyte pairings (e.g. KD vs. VE). For example, the positive relationsip between PCM growth per set of micelles (G_{set}) and set block length for KD micelles suggests that if one increased the block length held constant from K200 to K300 and examined a series of PCMs formed from pairing K300 with D50-D200, one should expect the scaling exponent of that new data set to follow the IGR for KD of $S_{KD}^{0.61\pm0.09}$ (Fig. 2.8A) The new relationship between set block length and core growth for the K300 set should grow with PRD block length (N_{PRD}) by approximately, $R_{core}\ \alpha\ N_{PRD}^{0.49\pm0.09}$ assuming no significant morphological transition occurs as a result of the longer K block. In addition, we can use the magnitude of the IGRs of KD ($S_{KD}^{0.61 \pm 0.09}$) and VE ($S_{VE}^{0.19 \pm 0.03}$) to conclude that the effect of set block length is about three times more pronounced in KD polyelectrolyte pairings than in VE pairings. Interestingly, the IGR of VD

micelles is slightly negative at $S_{VD}^{-0.09 \pm 0.05}$, contrary to the positive values of KD and VE IGRs, suggesting there is a wide range of potential IGRs which are extremely sensitive to polyelectrolyte chemistry.

The behavior of different polyelectrolyte pairings on AB + AC micelle core growth stands in stark contrast to behavior observed in AB + C systems, where the influence of block length on micelle features can be predictied with a high degree of certainty independently of the polyelectrolyte chemistry.[43] It remains unclear which chemical features of the different polyelectrolyte pairs change the growth rates of the PCM cores a priori. If one were to conclude that more hydrophilic polyelectrolyte chains promoted larger PCM cores from comparing the IGRs of the KD and VE system, one would then expect that the IGR of the VD system would be a positive value larger than that of the VE system, due to the margnially more hydrophilic backbone of the P(*D*,*L*)D chain relative to P*L*E. But Fig. 2.8 shows that not only is the IGR for VD smaller than the VE system, it is the only polyelectrolyte pair with a negative IGR. These trends highlight the pronounced difference in growth behavior between S-PCM and D-PCM cores.

2.2.3 Ion Pair Aggregation Number

In an attempt to understand the origin of the difference between single and D-PCM core growth, we examined aggregation number evolution as a function of constant block length. The aggregation number represents the number of polymers associating within each nanoparticle. This quantity can be calculated from the forward scattering intensity of SAXS experiments, as described in the Table 2.3. Calculating aggregation numbers in our systems requires us to assume that the cores of our micelles are charge neutral and that essentially all polyelectrolytes in our system contribute to micelle formation. These assumptions are reinforced by the typically low critical

micelle concentration for PCMs[20] and the neutral zeta potential measurements in our system (Fig. 2.9 and Table 2.4). Using these assumptions, Marras et al.[41] derived the following expression:

$$n_{ip} \propto \frac{1}{I(0)} R^6 \Delta\rho^2 \quad (1)$$

Where n_{ip} is the number of ion pairs per micelle, R is the core radius of the PCM, $I(0)$ is the forward scattering intensity from SAXS and $\Delta\rho$ is the calculated scattering contrast between polymer and solvent (Table 2.2).

This ion pair aggregation number (n_{ip}) data was visualized using the same naming and color conventions as Fig. 2.7. The n_{ip} increases with larger block length in most samples. Much like the data in Fig. 2.7, the different sets in Fig. 2.10 cannot be normalized to a single predictive curve because the slope of each set shows a systematic dependence on set block length, increasing with set block length. The dependence of the data set fits on set block length gives an interdependent monomeric aggregation number relationship (IAR) for each polyelectrolyte chemistry (Fig. 2.11). Interestingly, there is no straightforward trend between the IAR and the IGR for each chemistry. One would expect that if density was held constant, the growth of aggregation number and core size should be related such that the trends between IAR and IGR were similar. This led us to investigate the relationship of aggregation number and core growth through the framework of monomer density within the PCM core.

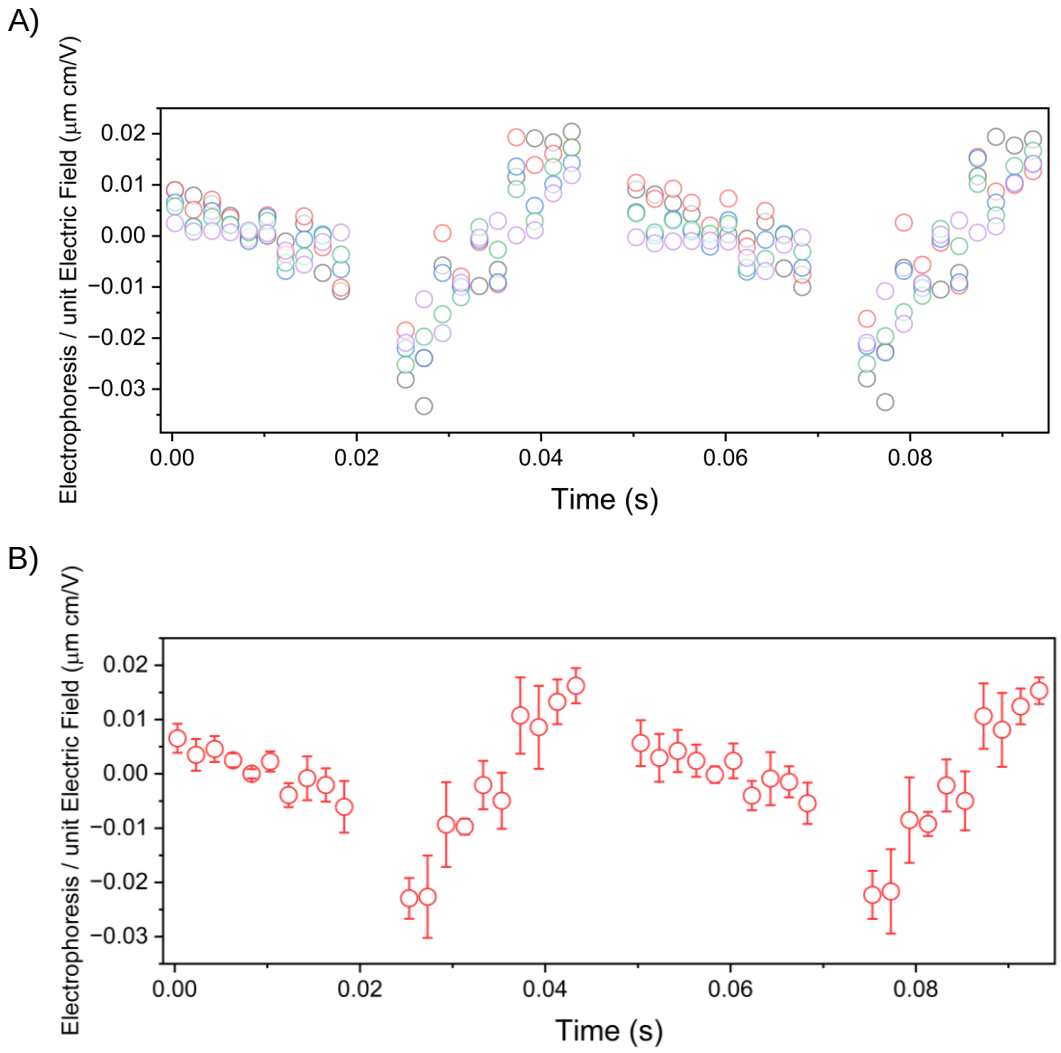

Figure 2.9 Representative mobility curve for V100E25 micelle. A) Raw data from 5 separate measurements. B) Averaged data and standard deviation.

Table 2.4 Zeta potential values. All values are averages and standard deviations from 5 measurements.

Micelle Name	Mobility (µm cm/s V)	Zeta Potential (mV)	Conductivity (mS/cm)	PALS Amplitude (mV)
V100E25	0.0 ± 0.05	0.00 ± 0.63	5.98 ± 0.08	78.7 ± 20.1
V100E50	$4x10^{-3}$ ± 0.03	0.09 ± 0.38	5.86 ± 0.04	97.12 ± 0.51
V100E100	$4x10^{-3}$ ± 0.11	0.06 ± 1.44	5.88 ± 0.08	109 ± 6.29
V100E200	$-2x10^{-3}$ ± 0.04	-0.03 ± 0.46	5.48 ± 0.05	167 ± 79.53

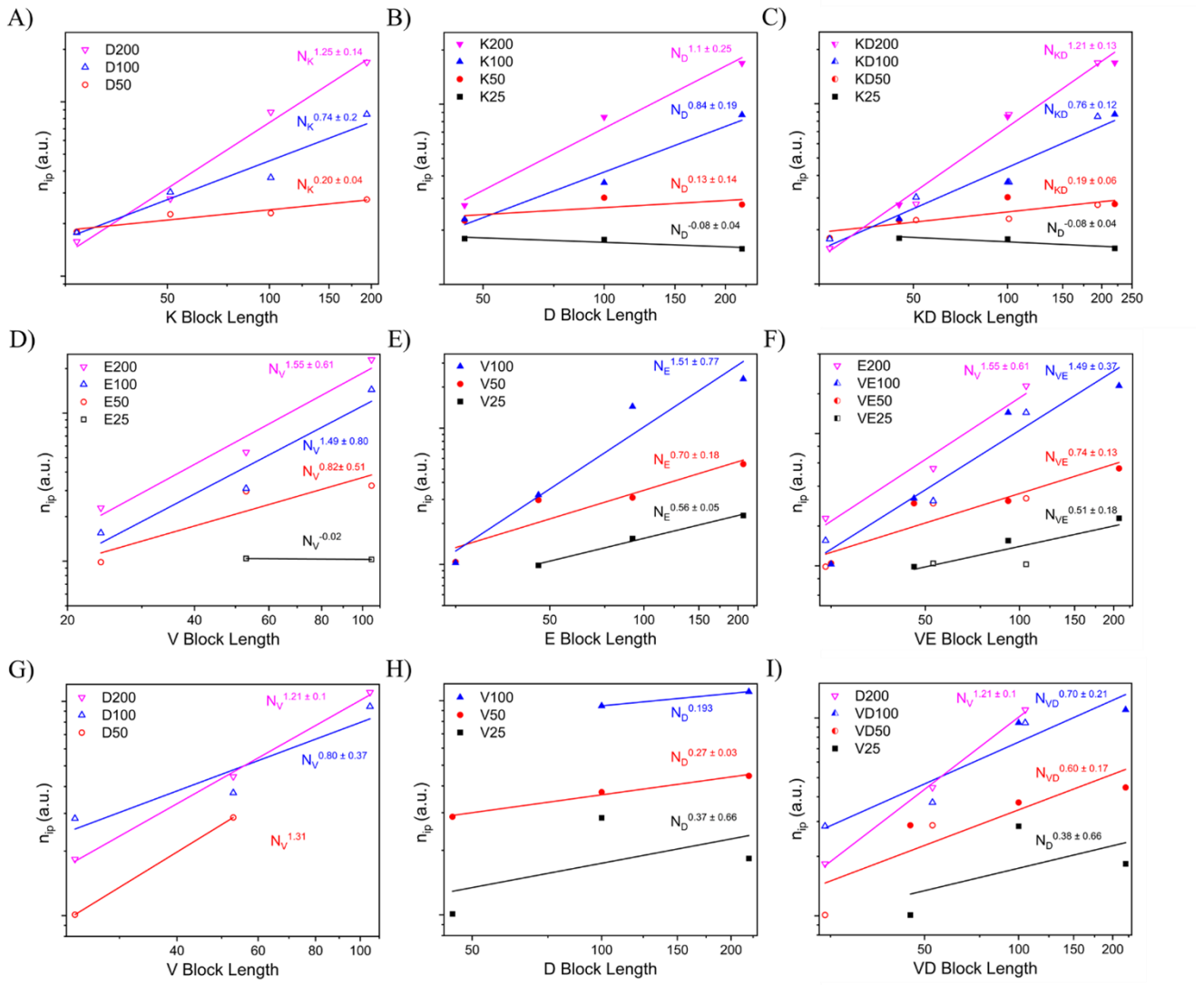

Figure 2.10 Aggregation number vs block length determined by fitting I(0) SAXS data and plotting the results against charged block length. A power law fit was applied to each data set, which are divided into separate colors/symbols. Every diblock polyelectrolyte has a neutral PEO block length of ~5k. Charged block length names are abbreviated from P*LK* to K, PVB to V, P(*D*,L)D to D and P(*D*,*L*)E to E for brevity. Across all datasets the datapoints/fits are represented by colors, with black representing DP~25, red symbols representing DP~50, blue symbols representing DP~100 and pink symbols representing DP~200. Open datapoints signify an anionic frame of reference, where the data are grouped into sets of constant anionic block length and plotted against varying cationic block length. Filled data signify a cationic frame of reference, where data are grouped into sets of constant cationic block length and plotted against varying anionic block lengths. Half-filled data signify a composite dataset where both anionic and cationic frames of reference are represented in the same color and are fit together. (A-C) show the KD pairing. (A) and (B) show the distinct frames of reference and in (C) both datasets are overlayed to remove any preference for one diblock when fitting the results. (D-F) and (G-I) repeat the same graphing pattern for VE and VD polyelectrolyte pairings.

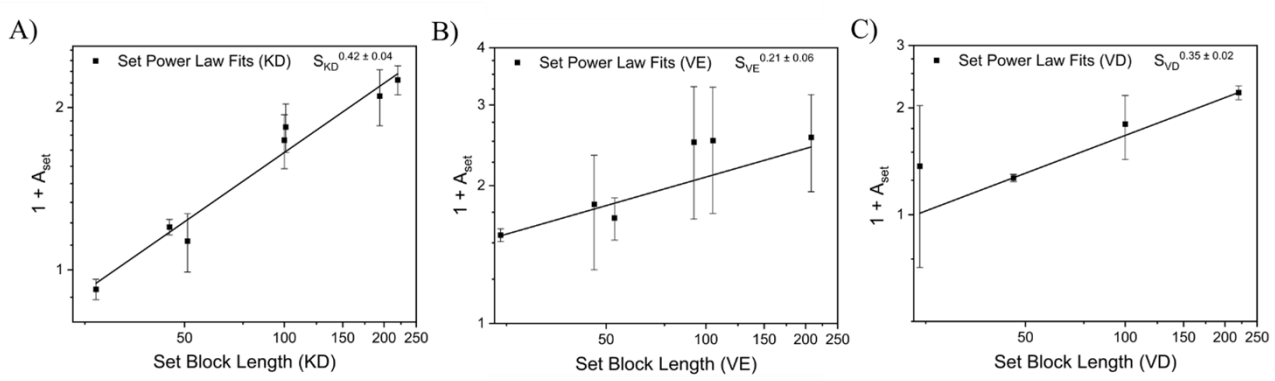

Figure 2.11 Set block length vs 1 + A_{set} where A_{set} is defined as the fits of ion pair aggregation number vs charged block length for each set from Fig. 6 A,B,D,E,G and H. Polyelectrolyte pairings of PEO-*b*-P*L*K and PEO-*b*-P(*D*,*L*)D, PEO-*b*-PVB and PEO-*b*-P(*D*,*L*)E and PEO-*b*-PVB and PEO-*b*-P(*D*,*L*)D are denoted with KD, VE, and VD, respectively. A power law fit was applied to each data set. Sets from Figure 6 with fewer than three data points were excluded from this analysis. Error bars represent standard error.

2.2.4 Core Density

If we consider the PCM core to be a homogenously distributed sphere of ion pairs with no higher order structure, then PCM core density should be related to the size and number of ion pairs within the core. Figs. 7, 8, 10 and 11 suggest that the core radius (*R*) and ion pair aggregation number (n_{ip}) do not grow with the $n_{ip} \sim R^3$ relationship one would expect if the monomer density within the PCM core were to remain constant. To understand how these trends relate to each other, we sought to create a variable D_{set} to represent the change in micelle density over each data set:

$$D_{set} \sim \frac{A_{set}}{G_{set}^3} \quad (2)$$

Here, A_{set} is the power law fit value for n_{ip} within the core for each PCM set in Fig. 10, and G_{set} is the PCM core radius fit value for each set in Fig. 7 where R^3 ~ PCM core volume. The value of D_{set} describes how the density within the core of a micelle changes over a single data set. A constant D_{set} across set block lengths would mean the extent that PCM core density changes PCM core density consistently across each set of micelles for that polyelectrolyte pair. Fitting the

data allows us to extract an interdependent density relationship (IDR) which can be used to compare how the density changes evolve as set block length grows for each chemistry explored here (Fig. 12). Unfortunately, the calculations for D_{set} propagate too much error for us to make definitive conclusions between different polyelectrolyte chemistries using the data in Fig. 12.

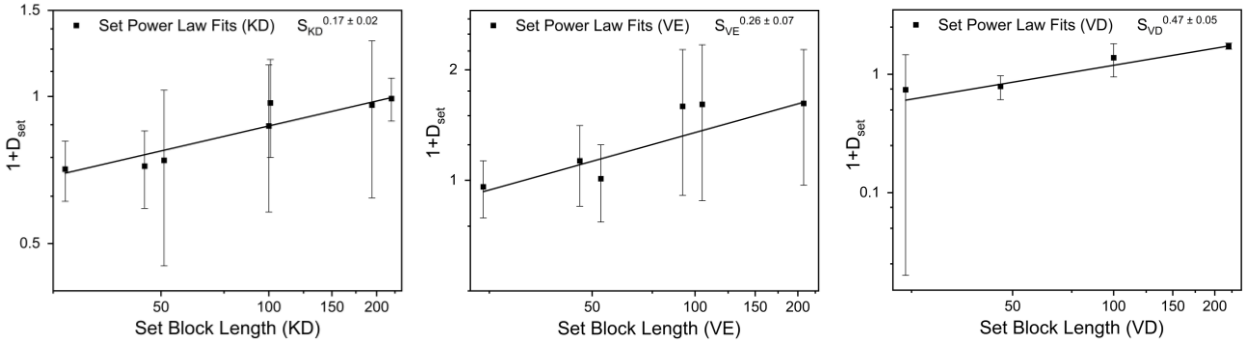

Figure 2.12 Set block length vs 1 + D_{set} where D_{set} is defined as $\frac{A_{set}}{G_{set}^3}$ where A_{set} is defined as the fits of ion pair aggregation number vs charged block length for each set from Fig. 10 A,B,D,E,G and H and G_{set} is the fit of core radius from sets of data found in Fig. 7 A,B,D,E,G and H. Polyelectrolyte pairings of PEO-*b*-P*L*K and PEO-*b*-P(*D*,*L*)D, PEO-*b*-PVB and PEO-*b*-P(*D*,*L*)E and PEO-*b*-PVB and PEO-*b*-P(*D*,*L*)D are denoted with KD, VE, and VD, respectively. A power law fit was applied to each data set. Sets from Fig. 10 with fewer than three data points were excluded from this analysis. Error bars represent standard error.

Table 2.5 Summary of Interdependent Relationships for Core Growth, Aggregation Number and Core Density.[a]

Polyelectrolyte Pair	IGR	IAR	IDR*
KD	0.61 ± 0.09	0.42 ± 0.04	0.17 ± 0.02
VE	0.19 ± 0.03	0.21 ± 0.06	0.26 ± 0.07
VD	-0.9 ± 0.05	0.35 ± 0.02	0.47 ± 0.05

[a]All interdependent relationships are power law fits obtained from Figures 8, 11 and 12. *Some datapoints within the trendlines for IDR have large error propagation from equation 1. IDR is therefore more suggestive than conclusive and is tabulated here for ease of comparison with IGR.

While it is not possible to make definitive conclusions from the values of D_{set} due to error propagation, there is a consistent trend in the data whereby polyelectrolyte pairs with the largest IGRs have the lowest IDRs (Table 2.5). This suggests that if the core density growth were constant for every set block length, the effect of block length on core size would be quite large. However,

if core density depends on block length, the relationship between block length and core size can decrease or even become negative. On a physical level, this relationship between core growth and density change could be explained by the molecular rearrangements required to simultaneously accommodate charge neutralization and strict core-shell separation in mismatched micelles. Greater understanding of how polyelectrolyte chemistry affects micelle core density could provide a route to predictive understanding of the interdependent micelle behavior of more general AB + AC systems. More meaningful exploration of this mechanism could perhaps be achieved through simulations and modeling.

2.2.5 Comparison Between Double and Single Diblock PCMs

In preceding sections, we detailed how D-PCMs, unlike S-PCMs, show a variety of interdependent structure property relationships that cannot be simplified into a unifying scaling law. It is well known from decades of experiments that D-PCMs tend to have smaller core sizes and polymer aggregation numbers than S-PCMs of similar composition. However, little is known about how the trends in S-PCM and D-PCM structure property relationships differ quantitatively. In Table 6 we compare the scaling laws derived by Marras et al. for S-PCMs and compare them to the range of growth behaviors observed in this work for D-PCMs (Tables 2.7-9).[41] Interestingly, it seems that not only do D-PCMs have smaller core sizes than S-PCMs, but they also grow at a slower rate as a function of charged block length. As one would expect, the aggregation number growth is also smaller for the D-PCMs, although the largest values fall within error of S-PCMs. It is difficult to decipher if the density values differ from those of S-PCMs due to the large error in the scaling law for the ion pair density. Taken together, the results in Table 2.6 suggest that D-PCM geometries not only reduce the size and ion pair aggregation number relative to S-PCMs, but the D-PCM configuration also restricts the growth of these structural features as a function of

charged block length. The differences between S-PCMs and D-PCMs could be attributed to the attachment of corona-forming blocks to every core forming block in the case of D-PCMs. Presumably, this leads to D-PCMs being less able to accommodate the competing demands of core packing, charge matching and core-shell segregation over ranges of varying chain lengths than S-PCMs. Importantly, the comparisons in Table 2.6 cannot be easily generalized to chemistries beyond those explored in this work.

Table 2.6 Comparison of Structure-Property Relationships for S-PCMs and D-PCM Cores.[a,]

	S-PCMs ($\propto N_B$)	D-PCMs ($\propto N_{B/C}$) min	D-PCMs ($\propto N_{B/C}$) max
R_{core}	0.73 ± 0.11	0.07 ± 0.02	0.42 ± 0.02
n_{ip}	2.37 ± 0.41	-0.08 ± 0.04	1.55 ± 0.61
Φ_{ip}	0.18 ± 0.74	-0.29 ± 0.10	0.73 ± 0.21

[a]Since single diblock scaling laws describe data from multiple discrete sets of PCMs, errors for single diblock PCM scaling relationships are standard deviations, whereas the errors for single diblocks are standard error.

Table 2.7 Power law fits for set block length vs core size for KD, VE and VD micelle.

Set Label (KD)	Fit	Set Label (VE)	Fit	Set Label (VD)	Fit
K25(D)	0.07 ± 0.02	V25(E)	0.20 ± 0.04	V25(D)	0.21 ± 0.02
K50(D)	0.13 ± 0.05	V50(E)	0.23 ± 0.02	V50(D)	0.1 ± 0.05
K100(D)	0.29 ± 0.01	V100(E)	0.30 ± 0.04	V100(D)	0.13
K200(D)	0.38 ± 0.03	E25(V)	0.08	D50(V)	0.27
D50(K)	0.16 ± 0.03	E50(V)	0.23 ± 0.05	D100(V)	0.14 ± 0.02
D100(K)	0.29 ± 0.03	E100(V)	0.30 ± 0.03	D200(V)	0.16 ± 5E-4
D200(K)	0.42 ± 0.02	E200(V)	0.31 ± 0.01	VD50	0.21 ± 0.03
KD50	0.16 ± 0.03	VE25	0.2 ± 0.04	VD100	0.14 ± 0.01
KD100	0.28 ± 0.02	VE50	0.23 ± 0.02	S_{rad}(VD)	-0.9 ± 0.05
KD200	0.40 ± 0.02	VE100	0.29 ± 0.02	-	-
S_{rad}(KD)	0.61 ± 0.09	S_{rad}(VE)	0.19 ± 0.03	-	-

Table 2.8 Power law fits for ion pair aggregation number vs core size for KD, VE and VD

Set Label (KD)	Fit	Set Label (VE)	Fit	Set Label (VD)	Fit
K25(D)	-0.08 ± 0.04	V25(E)	0.56 ± 0.05	V25(D)	0.37 ± 0.66
K50(D)	0.13 ± 0.14	V50(E)	0.70 ± 0.18	V50(D)	0.27 ± 0.03
K100(D)	0.84 ± 0.19	V100(E)	1.51 ± 0.77	V100(D)	0.193
K200(D)	1.1 ± 0.25	E25(V)	-0.02	D50(V)	1.31
D50(K)	0.2 ± 0.04	E50(V)	0.82 ± 0.51	D100(V)	0.80 ± 0.37
D100(K)	0.74 ± 0.2	E100(V)	1.49 ± 0.80	D200(V)	1.21 ± 0.10
D200(K)	1.25 ± 0.04	E200(V)	1.55 ± 0.61	VD50	0.60 ± 0.17
KD50	0.19 ± 0.06	VE25	0.51 ± 0.18	VD100	0.70 ± 0.21
KD100	0.76 ± 0.12	VE50	0.74 ± 0.13	S_{agg}(VD)	0.35 ± 0.02
KD200	1.21 ± 0.13	VE100	1.49 ± 0.37	-	-
S_{agg}(KD)	0.42 ± 0.04	S_{agg}(VE)	0.21 ± 0.06	-	-

Table 2.9 Power law fits for ion pair aggregation number vs core size for KD, VE and VD

Set Label (KD)	Fit	Set Label (VE)	Fit	Set Label (VD)	Fit
K25(D)	-0.29 ± 0.1	V25(E)	-0.04 ± 0.17	V25(D)	-0.26 ± 0.72
K50(D)	-0.26 ± 0.29	V50(E)	0.01 ± 0.24	V50(D)	-0.21 ± 0.18
K100(D)	-0.03 ± 0.22	V100(E)	0.61 ± 0.89	V100(D)	-
K200(D)	-0.04 ± 0.34	E25(V)	-	D50(V)	-
D50(K)	-0.28 ± 0.04	E50(V)	0.13 ± 0.66	D100(V)	0.38 ± 0.43
D100(K)	-0.13 ± 0.29	E100(V)	0.59 ± 0.89	D200(V)	0.73 ± 0.10
D200(K)	-0.01 ± 0.1	E200(V)	0.62 ± 0.64	S_{den}(VD)	0.47 ± 0.05
S_{den}(KD)	0.17 ± 0.02	S_{den}(VE)	0.26 ± 0.07	-	-

2.3 Conclusions

Our results demonstrate that D-PCMs can be formed from a wide range of mismatched charged block lengths using a variety of chemistries; something that was previously thought to be unattainable for PCMs. This work analyzes structures formed by pairs of polyelectrolytes with block length mismatches of up to ~1000% (K25D200), moving far beyond the <10% charged block length difference usually chosen for PEC self-assembly. We see a correlation between PCM core radius and charged block length, as expected, and uncover a unique relationship between these two parameters. Instead of constant scaling as a function of the core forming block length, we observe an interdependent growth mechanism whereby one charged block length influences the ability of the other charged block length to contribute to core growth. Examining the relationship between power law fits and block lengths revealed interdependent growth behaviors which estimate PCM core size as each charged block length is varied for PCMs of the same chemistry. These behaviors also illustrate the effect of block length on PCM core radius between different PCM chemistries. This unique interdependent behavior extends to the aggregation number of these micelles with a similar trend. Finally, we use the combination of aggregation number and growth patterns to estimate a relationship for core density. We postulate that the effects seen on changes in core size growth could be an indirect consequence of changes in core density but are unable to verify this experimentally due to propagated error. We encourage contributions using simulations and theory to gain further mechanistic insight and understanding to this open question. Finally, we compare the scaling relationships observed for S-PCMs to the interdependent growth behaviors extracted for D-PCMs and find that R_{core} and n_{ip} grow at a reduced rate in D-PCMs compared to S-PCMs.

Our results have broad implications for the design of nanostructured PEC materials. We show that processing conditions can overcome the limitations of chain length recognition, and that introducing mismatched block lengths in a PEC nanostructure can lead to unique behavior within PCM cores, which we quantify here. The implications of these findings raise questions about how mismatched charged block lengths affect the mechanical structure of PEC gels, the chain exchange of PCMs and the permeability and delivery efficacy of PEC polymersomes, as the density and size of PEC domains is central to all these phenomena. Further work on the role of design parameters like neutral block length and polymer concentration on mismatched D-PCMs could serve to deepen our understanding of structure-property relationships within D-PCMs and charged assemblies more broadly.

2.4 Experimental

2.4.1 Materials Poly(ethylene oxide)-*b*-poly(*L*-lysine hydrochloride) (PEO-*b*-PLK), Poly(ethylene oxide)-*b*-(poly(*D,L* glutamic acid) (PEO-*b*-P(*D,L*)E) and poly(ethylene oxide)-*b*-poly(*D,L* aspartic acid) (PEO-*b*-P(*D,L*)D) were purchased from Alamanda Polymers and used as received. Degree of polymerization provided from the manufacturer is used in all calculations (Table S5). Poly(ethylene oxide)-*b*-((vinylbenzyl) trimethylammonium chloride) (PEO-*b*-PVBTMA) were synthesized via reversible addition-fragmentation chain-transfer (RAFT) polymerization of (vinylbenzyl) trimethylammonium chloride monomer from 5000 g/mol PEO trithiocarybonyl macro-CTA according to previous conditions. [48]

2.4.2 Polyelectrolyte Complex Micelle Preparation Stock solutions were prepared by mixing the desired amount of polymer and water, vortexing for 1 minute and sonicating for 5 minutes, per the instructions provided by Alamanda Polymers. Stock solutions of polymer, salt and N-(2-hydroxyethyl)piperazine-N'-ethanesulfonic acid (HEPES) were mixed such that the final solutions were 5 M NaCl, 2mM charge concentration for each polymer, and 10 mM HEPES buffer (pH 7.4). These high salt mixtures were then dialyzed over the course of days until a final concentration of 50 mM NaCl and 10 mM HEPES in water was reached, following our published protocols. [42] These solutions were stored at 4^{o}C and allowed to equilibrate for at least 2 hours at room temperature before any experiments were performed.

2.4.3 Dynamic Light Scattering (DLS) Dynamic light scattering measurements were performed on a Brookhaven Instruments BI-200SM Research Goniometer System with an incident wavelength of 637 nm and a 90° scattering angle. Dust-free decalin was used as a bath to match the refractive index of the glass sample tubes. The Stokes-Einstein relationship was used to calculate the hydrodynamic radius under Brownian diffusion. Autocorrelation functions were analyzed via cumulant analysis in MATLAB.

2.4.4 Zeta Potential ζ-potential measurements were performed on a Wyatt Mobius Dynamic/Electrophoretic Light Scattering instrument using Dynamics (Version 7.4.072) software. Micelle samples were loaded into a quartz cuvette for ζ-potential measurements. A voltage amplitude of 2 V was applied at a frequency of 10 Hz and collected for 15 seconds at 25° C five separate times. Three scans were averaged together and converted to ζ-potentials via the Smoluchowski equation.

2.4.5 Small-Angle X-ray Scattering SAXS measurements were made at Argonne National Laboratory's Advanced Photon Source at beamline 12-ID-B. To minimize radiation damage, SAXS samples were prepared at 1% glycerol by volume. Micelles were irradiated in a thin-walled glass capillary flow cell with a 14 keV photon energy. Data reduction, background subtraction and data fitting were performed using the Irena plugin package within Igor Pro as described in reference 40. Raw SAXS data will be uploaded to the Materials Data Facility. [49]

2.4.6 Transmission Electron Microscopy To obtain cryo-TEM images, 3.5 μl of PCM sample was blotted onto a plasma cleaned Quantifoil copper grid 200 mesh 1.2/1.3, blotted for 1 second, and plunged into liquid ethane. Images were taken on a Thermo Titan Krios G3i at 300kV at 81,000x with a Gatan K3 direct detector.

2.5 References

1. Lodge, T. P. Celebrating 50 Years of Macromolecules. *Macromolecules* **2017**, *50* 24, 9525-9527. DOI: 10.1021/acs.macromol.7b02507.

2. Muthukumar, M. 50th Anniversary Perspective: A Perspective on Polyelectrolyte Solutions. *Macromolecules* **2017**, *50* 24, 9528-9560. DOI: 10.1021/acs.macromol.7b01929.

3. Cabral, H.; Miyata, K.; Osada, K.; Kataoka, K. Block Copolymer Micelles in Nanomedicine Applications. *Chemical Reviews* **2018**, *118* 14, 6844-6892. DOI: 10.1021/acs.chemrev.8b00199.

4. Mitchell, M. J.; Billingsley, M. M.; Haley, R. M.; Wechsler, M. E.; Peppas, N. A.; Langer, R. Engineering precision nanoparticles for drug delivery. *Nature Reviews Drug Discovery* **2021**, *20* 2, 101-124. DOI: 10.1038/s41573-020-0090-8.

5. Tritschler, U.; Pearce, S.; Gwyther, J.; Whittell, G. R.; Manners, I. 50th Anniversary Perspective: Functional Nanoparticles from the Solution Self-Assembly of Block Copolymers. *Macromolecules* **2017**, *50* 9, 3439-3463. DOI: 10.1021/acs.macromol.6b02767.

6. Sing, C. E.; Perry, S. L. Recent progress in the science of complex coacervation. *Soft Matter* **2020**, *16* 12, 2885-2914. DOI: 10.1039/d0sm00001a.

7. Blocher, W. C.; Perry, S. L. Complex coacervate-based materials for biomedicine. *WIREs Nanomedicine and Nanobiotechnology* **2017**, *9* 4, e1442. DOI: 10.1002/wnan.1442.

8. Chang, L.-W.; Lytle, T. K.; Radhakrishna, M.; Madinya, J. J.; Vélez, J.; Sing, C. E.; Perry, S. L. Sequence and entropy-based control of complex coacervates. *Nature Communications* **2017**, *8* 1. DOI: 10.1038/s41467-017-01249-1.

9. Fu, J.; Schlenoff, J. B. Driving Forces for Oppositely Charged Polyion Association in Aqueous Solutions: Enthalpic, Entropic, but Not Electrostatic. *Journal of the American Chemical Society* **2016**, *138* 3, 980-990. DOI: 10.1021/jacs.5b11878.

10. Lou, J.; Friedowitz, S.; Qin, J.; Xia, Y. Tunable Coacervation of Well-Defined Homologous Polyanions and Polycations by Local Polarity. *ACS Cent Sci* **2019**, *5* 3, 549-557. DOI: 10.1021/acscentsci.8b00964.

11. Marciel, A. B.; Srivastava, S.; Tirrell, M. V. Structure and rheology of polyelectrolyte complex coacervates. *Soft Matter* **2018**, *14* 13, 2454-2464. DOI: 10.1039/c7sm02041d.

12. Meng, S.; Ting, J. M.; Wu, H.; Tirrell, M. V. Solid-to-Liquid Phase Transition in Polyelectrolyte Complexes. *Macromolecules* **2020**, *53* 18, 7944-7953. DOI: 10.1021/acs.macromol.0c00930.

13. Srivastava, S.; Tirrell, M. V. Polyelectrolyte Complexation. In *Advances in Chemical Physics*, Rice, S. A., Dinner, A. R. Eds.; Advances in Chemical Physics, Vol. 161; John Wiley & Sons, Inc., 2016; pp 499-544.

14. Zhou, Z.; Yeh, C.-F.; Mellas, M.; Oh, M.-J.; Zhu, J.; Li, J.; Huang, R.-T.; Harrison, D. L.; Shentu, T.-P.; Wu, D.; et al. Targeted polyelectrolyte complex micelles treat vascular complications in vivo.

Proceedings of the National Academy of Sciences **2021**, *118* 50, e2114842118. DOI: 10.1073/pnas.2114842118.

15. Lueckheide, M.; Vieregg, J. R.; Bologna, A. J.; Leon, L.; Tirrell, M. V. Structure-Property Relationships of Oligonucleotide Polyelectrolyte Complex Micelles. *Nano Letters* **2018**, *18* 11, 7111-7117. DOI: 10.1021/acs.nanolett.8b03132.

16 Kuo, C. H.; Leon, L.; Chung, E. J.; Huang, R. T.; Sontag, T. J.; Reardon, C. A.; Getz, G. S.; Tirrell, M.; Fang, Y. Inhibition of atherosclerosis-promoting microRNAs via targeted polyelectrolyte complex micelles. *J Mater Chem B* **2014**, *2* 46, 8142-8153. DOI: 10.1039/C4TB00977K.

17. Sproncken, C. C. M.; Magana, J. R.; Voets, I. K. 100th Anniversary of Macromolecular Science Viewpoint: Attractive Soft Matter: Association Kinetics, Dynamics, and Pathway Complexity in Electrostatically Coassembled Micelles. *ACS Macro Letters* **2021**, 167-179. DOI: 10.1021/acsmacrolett.0c00787.

18. Kataoka, K.; Togawa, H.; Harada, A.; Yasugi, K.; Matsumoto, T.; Katayose, S. Spontaneous Formation of Polyion Complex Micelles with Narrow Distribution from Antisense Oligonucleotide and Cationic Block Copolymer in Physiological Saline. *Macromolecules* **1996**, *29* 26, 8556-8557. DOI: 10.1021/ma961217+.

19. Harada, A.; Kataoka, K. Formation of Polyion Complex Micelles in an Aqueous Milieu from a Pair of Oppositely-Charged Block-Copolymers with Poly(Ethylene Glycol) Segments. *Macromolecules* **1995**, *28* 15, 5294-5299. DOI: DOI 10.1021/ma00119a019.

20. Voets, I. K.; de Keizer, A.; Cohen Stuart, M. A. Complex coacervate core micelles. *Advances in Colloid and Interface Science* **2009**, *147-148*, 300-318. DOI: 10.1016/j.cis.2008.09.012.

21. Harada, A.; Kataoka, K. Polyion complex micelle formation from double-hydrophilic block copolymers composed of charged and non-charged segments in aqueous media. *Polym J* **2018**, *50* 1, 95-100. DOI: 10.1038/pj.2017.67.

22. Hayashi, K.; Chaya, H.; Fukushima, S.; Watanabe, S.; Takemoto, H.; Osada, K.; Nishiyama, N.; Miyata, K.; Kataoka, K. Influence of RNA Strand Rigidity on Polyion Complex Formation with Block Catiomers. *Macromolecular Rapid Communications* **2016**, *37* 6, 486-493. DOI: 10.1002/marc.201500661.

23. Wang, Y. P.; Cheng, Y. T.; Cao, C.; Oliver, J. D.; Stenzel, M. H.; Chapman, R. Polyion Complex-Templated Synthesis of Cross-Linked Single-Enzyme Nanoparticles. *Macromolecules* **2020**, *53* 13, 5487-5496. DOI: 10.1021/acs.macromol.0c00528.

24. Holley, A. C.; Parsons, K. H.; Wan, W. M.; Lyons, D. F.; Bishop, G. R.; Correia, J. J.; Huang, F. Q.; McCormick, C. L. Block ionomer complexes consisting of siRNA and aRAFT-synthesized hydrophilic-block-cationic copolymers: the influence of cationic block length on gene suppression. *Polymer Chemistry* **2014**, *5* 24, 6967-6976. DOI: 10.1039/c4py00940a.

25. Parsons, K. H.; Holley, A. C.; Munn, G. A.; Flynt, A. S.; McCormick, C. L. Block ionomer complexes consisting of siRNA and aRAFT-synthesized hydrophilic-block-cationic copolymers II: the influence of cationic block charge density on gene suppression. *Polymer Chemistry* **2016**, *7* 39, 6044-6054. DOI: 10.1039/c6py01048b.

26. Heo, T.-Y.; Kim, S.; Chen, L.; Sokolova, A.; Lee, S.; Choi, S.-H. Molecular Exchange Kinetics in Complex Coacervate Core Micelles: Role of Associative Interaction. *ACS Macro Letters* **2021**, *10* 9, 1138-1144. DOI: 10.1021/acsmacrolett.1c00482.

27. Bos, I.; Sprakel, J. Langevin Dynamics Simulations of the Exchange of Complex Coacervate Core Micelles: The Role of Nonelectrostatic Attraction and Polyelectrolyte Length. *Macromolecules* **2019**, *52* 22, 8923-8931. DOI: 10.1021/acs.macromol.9b01442.

28. Krogstad, D. V.; Choi, S. H.; Lynd, N. A.; Audus, D. J.; Perry, S. L.; Gopez, J. D.; Hawker, C. J.; Kramer, E. J.; Tirrell, M. V. Small Angle Neutron Scattering Study of Complex Coacervate Micelles and Hydrogels Formed from Ionic Diblock and Triblock Copolymers. *Journal of Physical Chemistry B* **2014**, *118* 45, 13011-13018. DOI: 10.1021/jp509175a.

29. Krogstad, D. V.; Lynd, N. A.; Miyajima, D.; Gopez, J.; Hawker, C. J.; Kramer, E. J.; Tirrell, M. V. Structural evolution of polyelectrolyte complex core micelles and ordered-phase bulk materials. *Macromolecules* **2014**, *47* 22, 8026-8032. DOI: 10.1021/ma5017852.

30. Heo, T. Y.; Kim, I.; Chen, L.; Lee, E.; Lee, S.; Choi, S. H. Effect of Ionic Group on the Complex Coacervate Core Micelle Structure. *Polymers-Basel* **2019**, *11* 3. DOI: 10.3390/polym11030455.

31. Koide, A.; Kishimura, A.; Osada, K.; Jang, W. D.; Yamasaki, Y.; Kataoka, K. Semipermeable polymer vesicle (PICsome) self-assembled in aqueous medium from a pair of oppositely charged block copolymers: physiologically stable micro-/nanocontainers of water-soluble macromolecules. *J Am Chem Soc* **2006**, *128* 18, 5988-5989. DOI: 10.1021/ja057993r.

32. Anraku, Y.; Kishimura, A.; Oba, M.; Yamasaki, Y.; Kataoka, K. Spontaneous formation of nanosized unilamellar polyion complex vesicles with tunable size and properties. *J Am Chem Soc* **2010**, *132* 5, 1631-1636. DOI: 10.1021/ja908350e.

33. Aydinlioglu, E.; Abdelghani, M.; Le Fer, G.; Van Hest, J. C. M.; Sandre, O.; Lecommandoux, S. Robust Polyion Complex Vesicles (PICsomes) Based on PEO- b -poly(amino acid) Copolymers Combining Electrostatic and Hydrophobic Interactions: Formation, siRNA Loading and Intracellular Delivery. *Macromolecular Chemistry and Physics* **2022**, 2200306. DOI: 10.1002/macp.202200306.

34. Harada, A.; Kataoka, K. Selection between block- and homo-polyelectrolytes through polyion complex formation in aqueous medium. *Soft Matter* **2008**, *4* 1, 162-167. DOI: 10.1039/b713853a.

35. Harada, A.; Kataoka, K. Effect of Charged Segment Length on Physicochemical Properties of Core−Shell Type Polyion Complex Micelles from Block Ionomers. *Macromolecules* **2003**, *36* 13, 4995-5001. DOI: 10.1021/ma025737i.

36. Harada, A. K., Kazunori. Chain Length Recognition: Core-Shell Supramolecular Assembly from Oppositely Charged Block Copolymers. *Science* **1999**, *283* 5398, 65-67. DOI: 10.1126/science.283.5398.65.

37. Koide, A.; Kishimura, A.; Osada, K.; Jang, W.-D.; Yamasaki, Y.; Kataoka, K. Semipermeable polymer vesicle (PICsome) self-assembled in aqueous medium from a pair of oppositely charged block copolymers: physiologically stable micro-/nanocontainers of water-soluble macromolecules. *Journal of the American Chemical Society* **2006**, *128* 18, 5988-5989.

38. Krogstad, D. V.; Lynd, N. A.; Choi, S. H.; Spruell, J. M.; Hawker, C. J.; Kramer, E. J.; Tirrell, M. V. Effects of polymer and salt concentration on the structure and properties of triblock copolymer coacervate hydrogels. *Macromolecules* **2013**, *46* 4, 1512-1518. DOI: 10.1021/ma302299r.

39. Bos, I.; Timmerman, M.; Sprakel, J. FRET-Based Determination of the Exchange Dynamics of Complex Coacervate Core Micelles. *Macromolecules* **2021**, *54* 1, 398-411. DOI: 10.1021/acs.macromol.0c02387.

40. Amann, M.; Diget, J. S.; Lyngsø, J.; Pedersen, J. S.; Narayanan, T.; Lund, R. Kinetic Pathways for Polyelectrolyte Coacervate Micelle Formation Revealed by Time-Resolved Synchrotron SAXS. *Macromolecules* **2019**, *52* 21, 8227-8237.

41. Wu, H.; Ting, J. M.; Yu, B.; Jackson, N. E.; Meng, S.; de Pablo, J. J.; Tirrell, M. V. Spatiotemporal Formation and Growth Kinetics of Polyelectrolyte Complex Micelles with Millisecond Resolution. *ACS Macro Letters* **2020**, *9* 11, 1674-1680. DOI: 10.1021/acsmacrolett.0c00543.

42. Marras, A. E.; Vieregg, J. R.; Tirrell, M. V. Assembly and Characterization of Polyelectrolyte Complex Micelles. *J Vis Exp* **2020**, 157, e60894. DOI: 10.3791/60894.

43. Marras, A. E.; Campagna, T. R.; Vieregg, J. R.; Tirrell, M. V. Physical property scaling relationships for polyelectrolyte complex micelles. *Macromolecules* **2021**, *54* 13, 6585-6594.

44. Marras, A. E.; Ting, J. M.; Stevens, K. C.; Tirrell, M. V. Advances in the structural design of polyelectrolyte complex micelles. *The Journal of Physical Chemistry B* **2021**, *125* 26, 7076-7089.

45. Perry, S. L.; Leon, L.; Hoffmann, K. Q.; Kade, M. J.; Priftis, D.; Black, K. A.; Wong, D.; Klein, R. A.; Pierce, C. F., 3rd; Margossian, K. O.; et al. Chirality-selected phase behaviour in ionic polypeptide complexes. *Nat Commun* **2015**, *6*, 6052. DOI: 10.1038/ncomms7052.

46. Marras, A. E.; Vieregg, J. R.; Ting, J. M.; Rubien, J. D.; Tirrell, M. V. Polyelectrolyte Complexation of Oligonucleotides by Charged Hydrophobic-Neutral Hydrophilic Block Copolymers. *Polymers-Basel* **2019**, *11* 1, 83. DOI: 10.3390/polym11010083.

47. Ting, J. M.; Marras, A. E.; Mitchell, J. D.; Campagna, T. R.; Tirrell, M. V. Comparing Zwitterionic and PEG Exteriors of Polyelectrolyte Complex Micelles. *Molecules* **2020**, *25* 11. DOI: 10.3390/molecules25112553.

48. Ting, J. M.; Wu, H.; Herzog-Arbeitman, A.; Srivastava, S.; Tirrell, M. V. Synthesis and Assembly of Designer Styrenic Diblock Polyelectrolytes. *ACS Macro Letters* **2018**, *7* 6, 726-733. DOI: 10.1021/acsmacrolett.8b00346.

49. Blaiszik, B.; Chard, K.; Pruyne, J.; Ananthakrishnan, R.; Tuecke, S.; Foster, I. The materials data facility: data services to advance materials science research. *Jom-Us* **2016**, *68* 8, 2045-2052.

Chapter 3

Impact of Lightly Branched Star Polyelectrolyte Architecture on Polyelectrolyte Complexes

3.1 Introduction

Polyelectrolyte complexes (PECs) are dense, water-swollen, polymer rich phases spontaneously formed upon mixing oppositely charged polyelectrolytes.[1-3] Since polyelectrolyte complexation is an associative phase separation process based on charge-charge interactions, PECs can incorporate a variety of organic, inorganic and biologic charged molecules, making them attractive candidates for applications in nucleic acid delivery, underwater adhesives and nanoscale reactors.[4-9] However, rational design of PECs remains difficult, as their properties depend on a complex interplay between environmental factors such as solvent mixture, salinity, pH, and temperature in addition to the variety of supramolecular interactions between the oppositely charged polyelectrolytes.[10, 11] Recently, there has been a surge in interest toward using structural features of polyelectrolytes, such as length, charge density and charge blockiness to alter the stability, rheology and structure of PEC materials.[12, 13] Structure-property relationships centered around polyelectrolyte design are attractive because they can provide robust, chemically agnostic design principles for PECs and provide a path toward tailored PEC design within applications where environmental conditions are beyond control.[14] Polyelectrolyte charge density is one of the most promising parameters recently investigated, as it has been shown to consistently alter the rheology and stability of PECs.[14, 15]

By copolymerizing charged monomers with neutral monomers, one can reduce the charge density of the constituent polyelectrolytes within a PEC. Reducing charge density this way alters linear charge density, or charge density along the polymer backbone, and results in PECs with a

lower modulus and reduced salt resistance compared to their fully charged counterparts.[14] The modulus of PECs is highly sensitive to the number of ionic pairings between polymers, which act as stickers between oppositely charged polymer chains, increasing the viscosity of the PEC.[12, 13, 16, 17] Lowering charge density reduces sticker density, providing a straightforward path to weaken the mechanical properties of a PEC. PEC stability is also related to charge density, but that mechanism is generally rationalized through the influence of charge density on counterion dynamics, not electrostatic interactions.[18, 19]

Before complexation, the oppositely charged groups along a polyelectrolyte backbone experience significant electrostatic repulsion.[2] In solution, small molecule counterions and water molecules condense around charged groups along the polyelectrolyte backbone to reduce the effective charge density along the chain. Upon complexation, oppositely charged polyelectrolytes condense around each other to mediate electrostatic repulsion, releasing the small molecules and restoring their translational entropy. The entropic gain from counterion release is the majority of the thermodynamic driving force for polyelectrolyte complexation, and is directly related to the amount of salt a PEC can withstand before dissolution, otherwise known as the critical salt concentration (CSC).[19] The significant role of counter-ion release in the complexation process allows one to tune the stability of a PEC by altering the charge density of the constituent polyelectrolytes.

Reducing charge density through copolymerization with a neutral monomer weakens charge-charge interactions along a polyelectrolyte, reducing counterion condensation in solution and thus the translational entropy gain from complexation, leading to PECs with lower CSC.[2, 3, 19] Interestingly, CSC is not only sensitive to linear charge density but also spatial charge density, or the distribution of charged groups in space.[20] Chang et al. showed that increased blockiness raises

PEC salt resistance by creating PECs from sequence defined copolymers with identical charged fractions but increasingly blocky charged sequences.[19] They attributed this result to stronger interactions between counterions and charged groups in the blocky sequences, reasoning charged groups clustered closely together would experience more electrostatic repulsion relative to charged groups spaced apart more evenly. While this finding illustrates an important point, altering charge sequences can only vary the stability of copolyelectrolytes. Altering the CSC of PECs composed of linear, fully charged polyelectrolytes remains elusive. The CSC of fully charged polyelectrolytes show a pronounced dependence on degree of polymerization (DP) at low molecular weights which quickly plateaus to nearly constant values at higher DPs.[3] Since the salt resistance of a PEC determines the limits of the environments where it can be used, a reliable method to increase complex stability beyond the DP limited plateau value would be desirable.

While reducing charge density has been studied extensively in PEC literature, no studies have addressed methods to increase the charge density beyond linear, fully charged polyelectrolytes for use in bulk PECs. It is conceivable one could use chemical methods to increase the valency of each repeat unit of a polylectrolyte to increase the charge density past one charged group per repeat unit, but this approach would be synthetically challenging to apply to a variety of charged monomers. Instead, we were inspired to investigate branched polyelectrolytes by simulations that showed branched polyelectrolytes to have greater spatial charge density than linear counterparts, resulting in branched polyelectrolytes perturbing counterions more strongly relative to linear polyelectrolytes.[21] Here, we seek to increase spatial charge density of homopolyelectrolytes by altering their architecture from linear to lightly branched stars, in the hopes of precisely tuning PEC properties. We find spatial charge density to have a significant impact on the salt stability of our complexes while leaving the viscoelastic and structural properties

of our complexes essentially unaltered. This suggests harnessing the distinct structure-property relationships of linear and spatial charge density can be used to orthogonally control PEC stability, rheology and structure.

3.2 Results and Discussion

To investigate the effect of polyelectrolyte architecture on PECs, we chose to create homologous polyelectrolyte pairs via a combination of reactive polymers and click chemistry. This approach allows us to limit structural variation between the polyelectrolyte pairs within our PECs and has been used extensively in recent years.[14, 15, 22-25] However, many reactive polymer platforms suffer from inefficient functionalization, poor polymerization control, or unstable reactive groups.[14, 26] For this reason, we chose to investigate a new reactive polymer-click chemistry pairing to create homologous polyelectrolytes.

3.2.1 Polymer Synthesis and Functionalization

Poly(glycidyl methacrylate) (PGMA) stands out as an ideal reactive platform for a variety of reasons. PGMA is readily synthesized via both reversible addition fragmentation chain transfer (RAFT) and atom transfer radical polymerization (ATRP) and is stable upon storage in air and moisture for long periods of time.[27, 28] In addition, the pendant epoxy groups can serve as reactive handles which undergo rapid and quantitative thiol-epoxy functionalization in the presence of a small excess of thiol and a catalytic amount of base (Fig. 3.1).[27, 29] Finally, every thiol-epoxy reaction creates a thioether bond which can be oxidized to alter local polarity and a secondary hydroxyl group which can serve as a reactive handle for additional functionalization reactions.[27, 30, 31] For these reasons, we sought to optimize thiol-epoxy reactions of PGMA towards homologous polyelectrolytes for use in PEC studies.

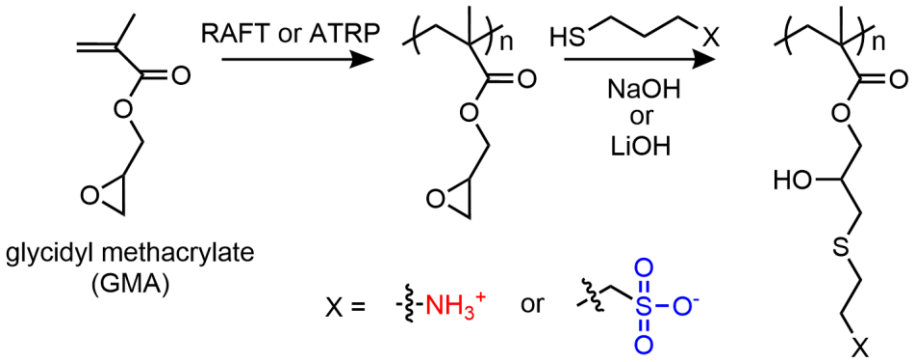

Figure 3.1 Generalized schematic of combining controlled polymerization of GMA with thiol-epoxy functionalization to achieve structurally homologous polyelectrolytes.

We synthesized PGMA via ATRP according to previously reported procedures.[30] To achieve cationic derivatives of PGMA, we react 2-(Boc-amino)ethanethiol in THF using LiOH as a base with a ratio of epoxy:thiol:base of 4:1:0.05. The Boc protected PGMA derivative was deprotected using a 1:1 mixture of dioxane:6M HCl, leading to a cationic derivative of PGMA bearing primary amines as cationic groups (Fig. 3.2). Typically, cationic derivatives of PGMA are achieved by deprotection using triflouroacetic acid (TFA).[32, 33] We chose to use HCl instead to avoid residual greasy TFA counterions. To create anionic PGMA derivatives, we reacted PGMA with sodium 3-mercapto-1-propanesulfonate at an epoxy:thiol ratio of 4:1 in a DMSO/H20 mixture, using the minimum amount of water necessary to dissolve the charged thiol. Slow addition of 0.1 equivalents of aqueous NaOH to epoxy drove quantitative sulfonate functionalization of PGMA (Fig. 3.2). To the best of our knowledge, this is the first report of anionic derivatization of PGMA through a thiol-epoxy mechanism.

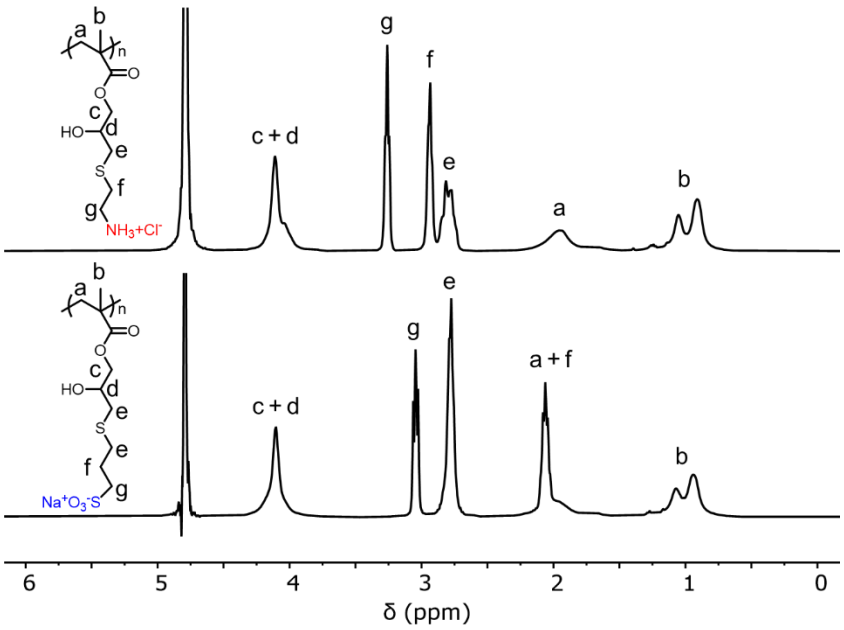

Figure 3.2 ^{1}H nuclear magnetic resonance (NMR) of cationic (top) and anionic (bottom) derivatives of linear PGMA produced via thiol-epoxy.

Next, we synthesized a series of well-defined linear, 4-armed, 6-armed and 8-armed PGMA with low dispersity <1.14 and roughly equal total DPs via ATRP (Fig. 3.2 and Table 3.1). We targeted 200 GMA units so small changes in DP would not result in significant changes in the CSC, since CSC generally follows the form $DP = \frac{1}{1-CSC}$.[34, 35] This size range also ensures the arm length of the higher branched stars would remain quite short, as simulations have shown more highly branched polyelectrolytes with shorter arms affect counterion dynamics most strongly relative to linear polyelectrolytes with the same DP.[21] These reactive precursors were then functionalized via thiol-epoxy click into the pairs of homologous polyelectrolytes used throughout the rest of this study. For brevity, coacervate samples are labeled according to the reactive polymer precursor their constituent polyelectrolyte pairs were derived from (i.e. L-GMA for linear PGMA, 4-GMA for 4-armed PGMA etc.).

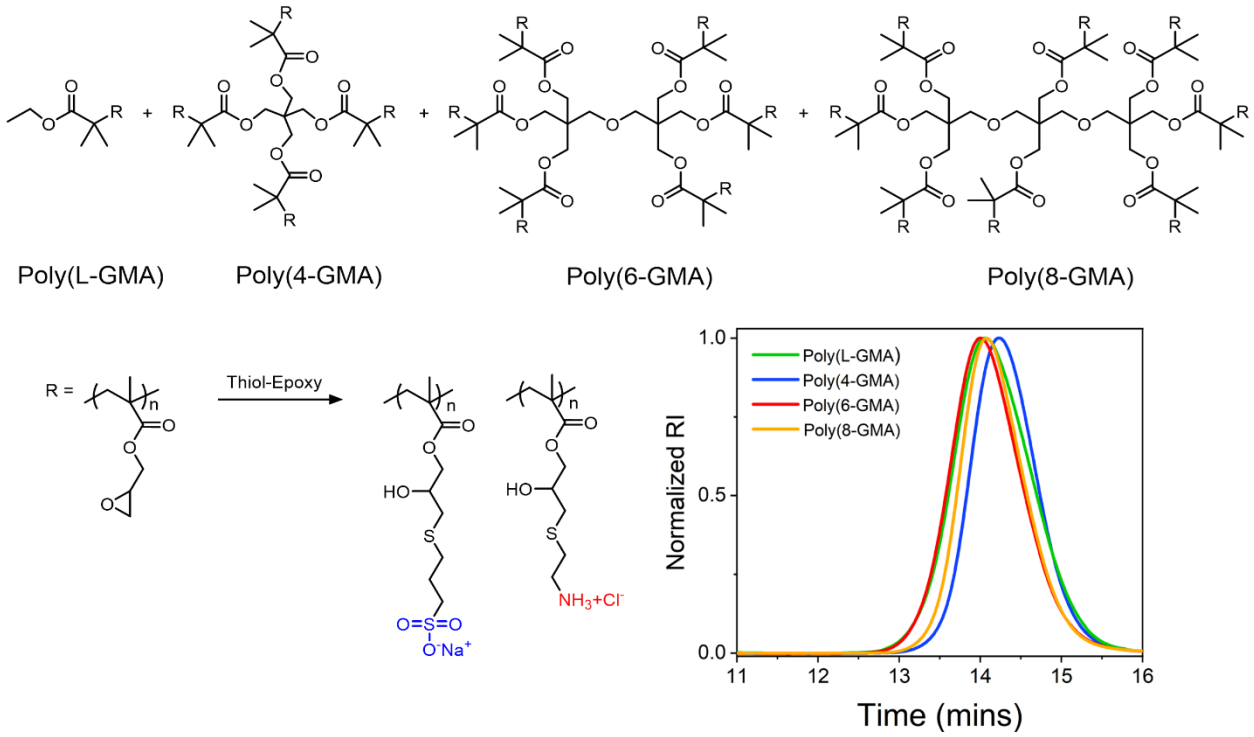

Figure 3.3 Synthetic scheme for linear and branched polyelectrolytes derived from PGMA. Overlaid GPC of neutral PGMA (bottom right).

Table 3.1 Molecular characteristics of PGMA precursors determined by SEC-MALS.

Precursor Polymer	$M_{n,MALS}$ (kg/mol)	$DP_{n,MALS}$	Đ
L-GMA	27.7	195	1.14
4-GMA	26.0	183	1.08
6-GMA	29.6	205	1.11
8-GMA	30.7	216	1.11

3.2.2 Optical Microscopy and Salt Resistance

Optical microscopy images allow us to straightforwardly assess the CSC and morphology of our PECs. In all cases, PECs are liquid-like coacervates (Fig. 3.4). At no added salt, the complexes form spherical droplets. Upon the addition of external salt, the PEC phase coalesces into large, macroscopic PEC phases containing water droplets, a morphology observed in previous examples of viscous liquid PECs.[11, 14, 36] Previous studies have shown that doubling the charge density of a constituent polyelectrolyte can drive a morphological transition from liquid to solid PECs.[37] Here, the PEC morphology is consistent across PEC architectures, indicating the lightly branch polyelectrolytes explored here do not increase charge density enough to alter PEC morphology.

To evaluate CSC, we examined PECs of all architectures at different salt concentrations. Optical microscopy shows 6-GMA and 8-GMA have higher CSCs than L-GMA and 4-GMA. L-GMA and 4-GMA pairings persist until approximately 750mM NaCl, whereas 6-GMA and 8-GMAs persist until 900 and 1050mM NaCl, respectively. The increase in CSC of ~50% from L-GMA to 8-GMA cannot be explained by the slight differences in molecular weight between the samples, as critical salt resistance scales slowly at higher molecular weights. This suggests architectural differences are the primary driving force for increased salt stability in these complexes, in line with previous observations of more compact charge distributions within a polyelectrolyte increasing the salt resistance of the resulting PEC.[19] However, if branched polyelectrolyte architectures increase CSC relative to linear PECs, why is there no significant difference in the CSC for L-GMA and 4-GMA?

There are a few potential reasons why CSC does not increase until 6-armed stars. First, charge density may simply not change enough when going from a linear to a 4-armed star

architecture. It is also possible the longer sidechains of 4-GMA relative to 6-GMA and 8-GMA decrease the average charge density felt by arms of 4-GMA, since the available space for each arm to occupy grows rapidly as chains extend radially from the polymer core. Similarly, the difference in CSC between 6 and 8-armed stars can be rationalized both by the increased number of arms radiating from the core and the shorter radial extension of 8-GMA increasing the steric congestion of charged groups relative to 6-GMA. As a consequence, it is possible 4-armed stars may begin to exhibit distinct salt resistances from equivalent linear counterparts at lower DPs and more compact radial chain distributions.

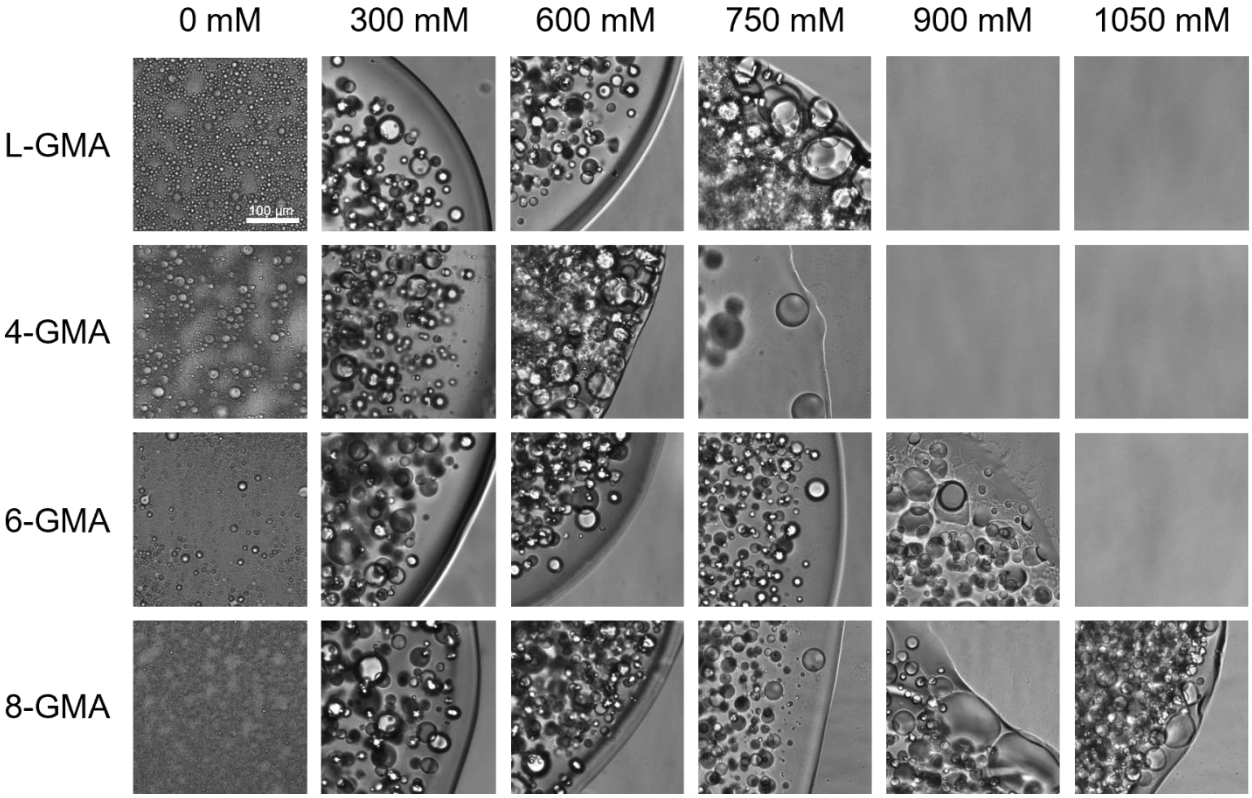

Figure 3.4 Optical micrographs of PECs composed of analogous polyelectrolytes derived from linear, 4-armed, 6-armed and 8-armed GMA precursors at various salt concentrations.

3.2.3 Rheology

Viscoelastic properties of each complex were analyzed using small amplitude oscillatory shear (SAOS) experiments across a range of temperatures (Fig. 3.5). The complexes displayed rheological behavior typical of "sticky rouse" viscoelastic liquids, with storage modulus (G') and loss modulus (G'') scaling as $\omega^{0.5}$ at moderate to high frequencies and G' and G'' scaling as ω^2 and ω at low frequencies.[17] However, there are a few interesting deviations from traditional Rouse-like behavior observed in the TTS data.

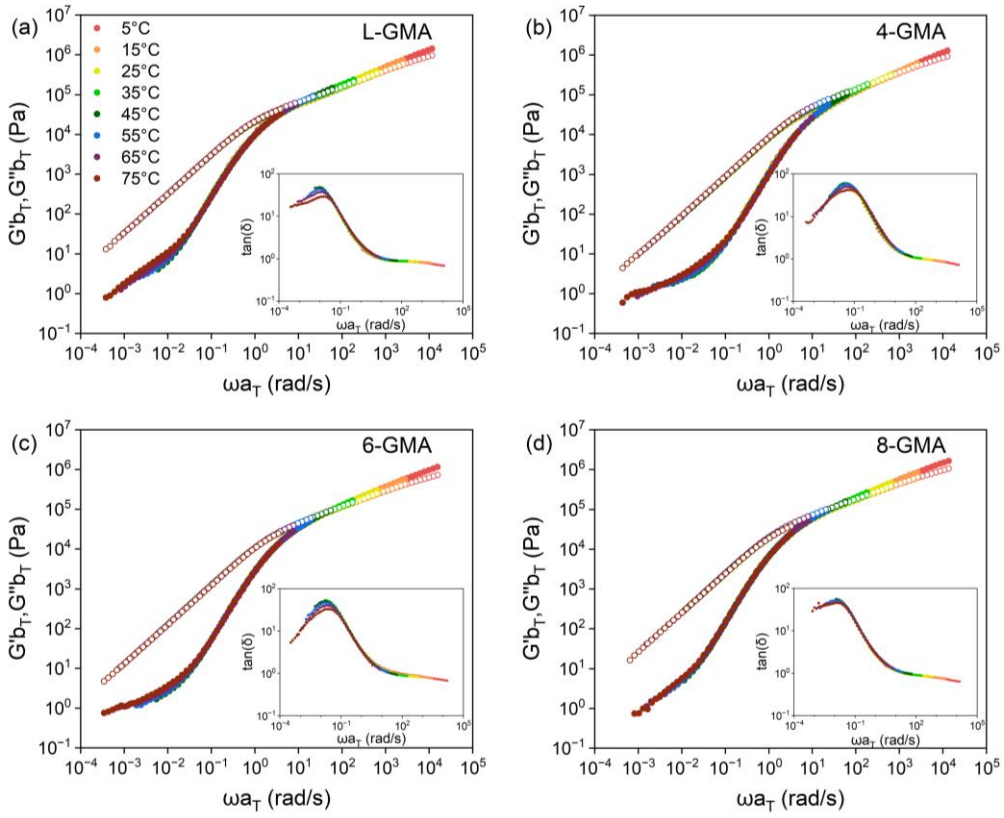

Figure 3.5 Time-temperature superposition (TTS) of frequency sweep data for 0 mM added NaCl PECs of (a) linear, (b) 4-armed, (c) 6-armed, and (d) 8-armed architectures (●,○ G',G''). Shift factors a_T and b_T and activation energies are tabulated in Table SX.

First, we observe a crossover of G' and G'' at intermediate frequencies which persists to the highest frequencies measured, reminiscent of entangled polymeric behavior. However, our materials are likely to be unentangled due to the relatively low molecular weight of our polymers,

their long side chains and the water content swelling the network (Table 2). We believe this crossover is not due to entanglement, but instead due to "sticky" interactions between segments of polymer chains enhancing the solid character of our PECs. The chemistry of our polyelectrolyte sidechains provides a variety of associative amphiphilic, hydrogen bonding and ionic intermolecular interactions which could contribute to this feature. Crossovers of this sort have been observed in other unentangled PEC systems capable of significant non-ionic supramolecular interactions.

Table 3.2 PEC solids content measured by TGA.[a]

PEC Architecture	L-GMA	4-GMA	6-GMA	8-GMA
Solids Content (%)	55.4 ± 1.4	54.8 ± 2.6	55.6 ± 1.3	55.8 ± 2.8

[a]Errors are standard deviations from 3 measurements.

Unentangled polymers G' and G'' are expected to scale as ω^2 and ω in the terminal regime.[38] However, there is an upturn in G' at low frequencies which deviates from the expected scaling of ω^2. This additional relaxation mode has been reported before in PEC literature and is often attributed to long range interactions or an artefact from instrumental limitations.[14, 35] Since the feature is not excessively noisy and is observed at torque values well above the sensitivity limit of our rheometer, we believe this upturn in storage modulus represents a secondary relaxation mode in our PECs. In other classes of materials such as associative protein hydrogels, low frequency upturns in storage modulus have been attributed to large sections of polymer chains with high valency interacting through long distances.[39] It is easy to envision fully charged homopolyelectrolytes sustaining intermolecular interactions between segments of multiple oppositely charged polyelectrolytes within a PEC, so it is not surprising a low frequency upturn in

storage modulus is observed here and in previous PEC studies. Future work tuning this additional long-range relaxation mode by altering supramolecular interactions such as hydrogen bonding, pi-pi stacking and amphiphilic associations in PECs will be necessary to fully explain the presence of this feature in some PEC systems but not others.

Lightly branched polyelectrolyte architectures do not systematically alter the shape of the SAOS data, shift factors or intrinsic viscosities of branched complexes relative to complexes (Figs. 3.6-8 and Tables 3.3-6). This was initially surprising, since changing from linear to branched polymers in uncharged systems is often accompanied by large differences in viscoelastic properties due to a shift in entanglement mechanism from reptation to arm-retraction.[38, 40] We attribute the absence of dramatic changes between the linear and branched polyelectrolytes to the high water content and consistent intermolecular interactions across our PECs (Table 2). Water swells PECs and increases entanglement molecular weights to much higher degrees of polymerization relative to uncharged materials. As a result, our materials are likely unentangled at this DP, which eliminates the primary difference in the diffusion of star and linear polymers. In addition, since all polymers are homopolyelectrolytes of approximately equal DP, the number and density of intrinsic ionic pairings known to dominate PEC dynamics should be approximately equal across all architectures. As a result, we see very consistent rheological profiles across all polyelectrolyte architectures.

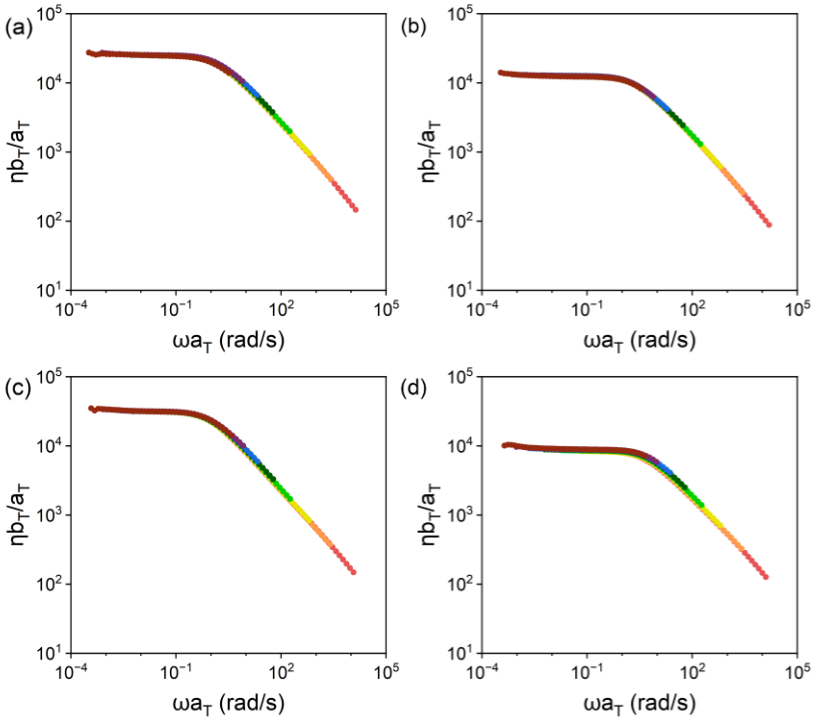

Figure 3.6 TTS of the complex viscosities of (a) L-GMA, (b) 4-GMA, (c) 6-GMA and (d) 8-GMA complexes at 0 mM added NaCl.

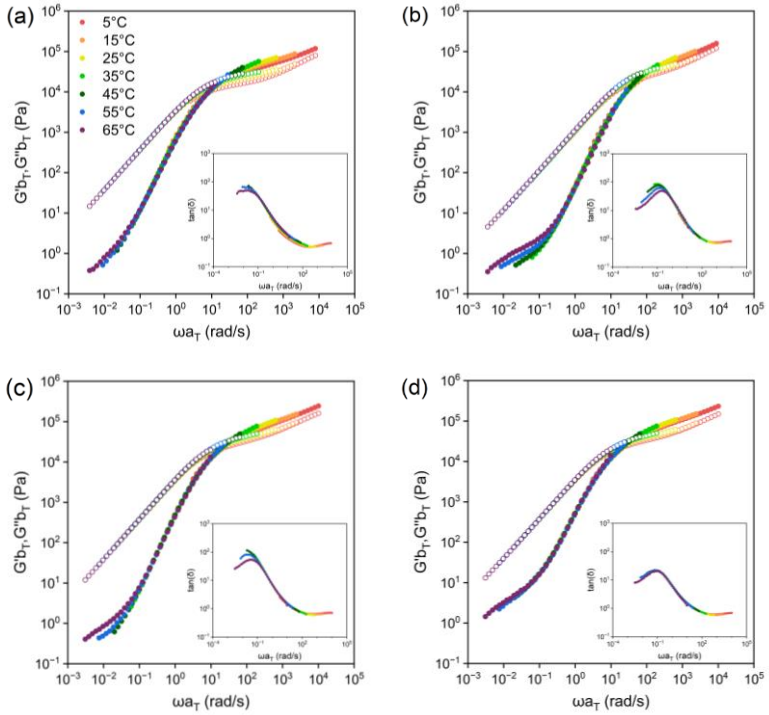

Figure 3.7 Time-temperature superposition of frequency sweep data for 500 mM added NaCl PECs of (a) linear, (b) 4-armed, (c) 6-armed, and (d) 8-armed architectures (●,○ G',G'') . Shift factors a_T and b_T are tabulated in Tables 3.5 and 3.6.

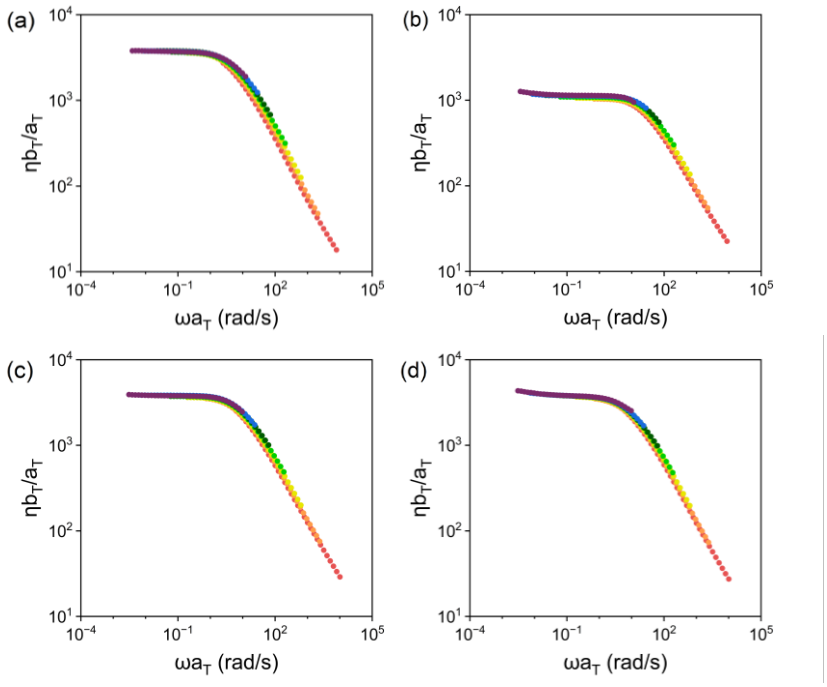

Figure 3.8 TTS of the complex viscosities of (a) L-GMA, (b) 4-GMA, (c) 6-GMA and (d) 8-GMA complexes at 500 mM added NaCl.

Table 3.3 Horizontal shift factors (a_T) for 0 mM added NaCl PECs.

Temperature	a_T			
	L-GMA	4-GMA	6-GMA	8-GMA
5	18.6	20.0	21.5	24.8
15	4.00	4.03	4.17	4.43
25	1	1	1	1
35	0.291	0.293	0.280	0.272
45	0.0948	0.0985	0.0906	0.0859
55	0.0339	0.0369	0.0324	0.0306
65	0.0131	0.0153	0.0125	0.0122
75	0.00602	0.00700	0.00518	0.00544

Table 3.4 Vertical shift factors (b_T) for 0 mM added NaCl PECs.

Temperature	b_T			
	L-GMA	4-GMA	6-GMA	8-GMA
5	1	1	1	1.07
15	1	1	1	1.03
25	1	1	1	1
35	1	1	1	0.968
45	1	1	1	0.937
55	1	1	1	0.909
65	1	1	1	0.882
75	1	1	1	0.856

Table 3.5 Horizontal shift factors (a_T) for 500 mM added NaCl PECs.

Temperature	a_T			
	L-GMA	4-GMA	6-GMA	8-GMA
5	12.6	14.0	16.1	16.2
15	3.32	3.53	3.81	3.81
25	1	1	1	1
35	0.326	0.317	0.298	0.298
45	0.115	0.111	0.100	0.100
55	0.0455	0.0437	0.0375	0.0375
65	0.0196	0.0183	0.0154	0.0154

Table 3.6 Vertical shift factors (b_T) for 500 mM added NaCl PECs.

Temperature	b_T shift factors			
	L-GMA	4-GMA	6-GMA	8-GMA
5	1	1.07	1.07	1.08
15	1	1.03	1.03	1.03
25	1	1	1	1
35	1	0.958	0.968	0.975
45	1	0.937	0.937	0.937
55	1	0.909	0.912	0.909
65	1	0.882	0.883	0.881

3.2.4 Small-angle X-ray Scattering

Small-angle X-ray scattering (SAXS) allows us to examine how altering molecular architecture influences the internal structures of our PECs. Figure 3.8 A-D shows vertically shifted overlays of complexes of each architecture arranged by salt concentration. The SAXS patterns obtained for each complex are nearly identical at every salt concentration, with prominent features closely matching each other.

In all cases, I(q) scales as q^{-4} at low q, suggesting smooth surfaces due to mesoscale concentration fluctuations with $R_g > 200$ nm (since $R_{g\,max} = 2\pi / q_{min}$). Concentration fluctuations of this nature have been observed previously in polyelectrolyte complexes. Perhaps the most consistent difference between the different architectures emerges in this feature, as the prominent -4 slope persists to q slightly higher q ranges as branching increases, suggesting the minimum size affected by these concentration fluctuations may be weakly influenced by architecture.

At high q, we see a correlation peak which at first seemed like a correlation peak indicating intermolecular spacing within the complex. However, upon closer inspection, the decay of $I(q) \sim q^{-4}$ at q ranges higher than the peak suggests this peak emerges as the result of small, smooth aggregates within the material, a feature more akin to small micellar associations than intermolecular spacings. Kratky plots demonstrate the collapsed, globular conformation of these structures (Fig. 3.9E). The absence of a gel-like rheological response suggests the clusters formed here are not permanent enough to form physical crosslinks, and are potentially dynamic associations of just a few monomers. The two aggregation mechanisms apparent via SAXS at low and high q might relate to the unexpected increases in G' observed in the crossover of G' at moderate frequencies and the uptick in G' at low frequencies, respectively. Significant future work will be needed to clarify the relationship between rheological features and aggregation in PECs.

As salt is added, the I(q) q upturn shifts to lower q values, and the correlation peak at high q shifts to lower q values and loses intensity. Cluster size, estimated using the onset of -2 slope in the Kratky plots, grows consistently as salt is increased from ~ 2.8 nm at 0 mM added salt to 4.2 nm at 900 mM added salt. The trends across salt concentrations are also consistent for each polyelectrolyte architecture, even at 900 mM, even though 6-GMA is near its CSC at this salt concentration and 8-GMA is much farther away from dissolution. This suggests similar structures are attainable in PECs regardless of their proximity to the CSC, assuming they have equivalent degrees of polymerization and linear charge density.

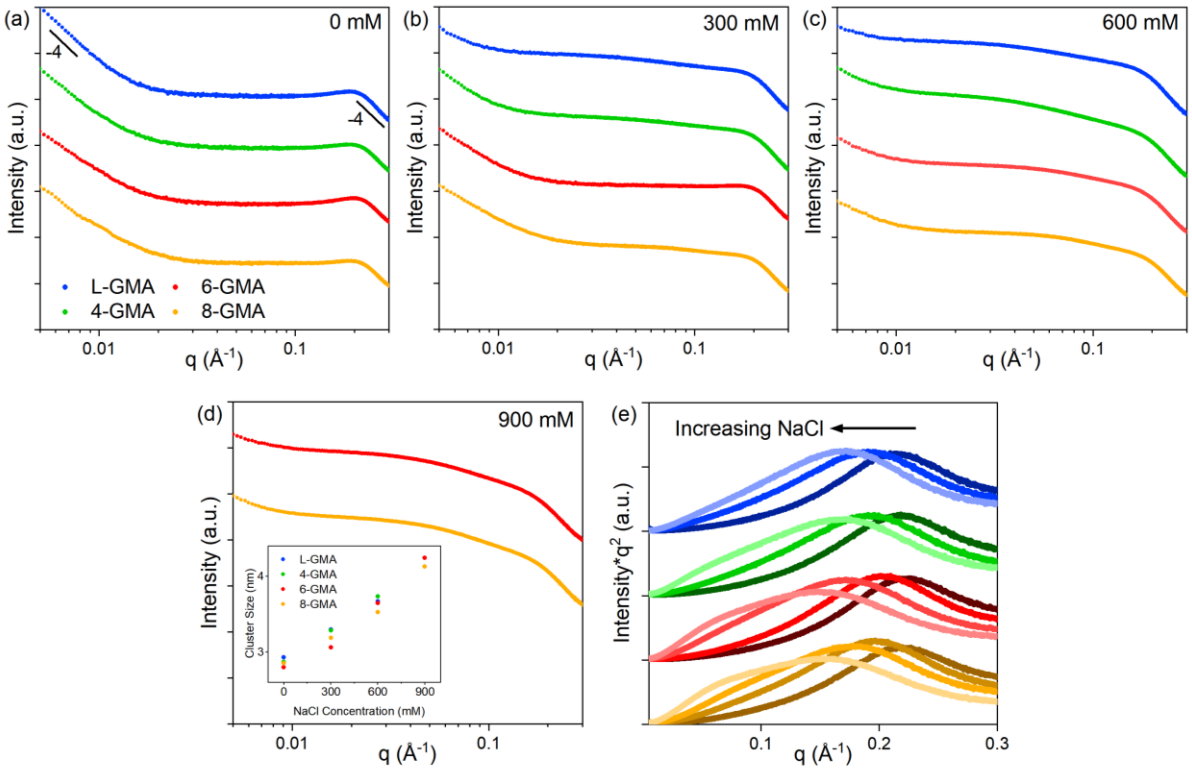

Figure 3.9 SAXS scattering patterns for polyelectrolyte pairs of every architecture at (a) 0mM, (b) 300mM (c) 600mM and (d) 900 mM added NaCl (inset figure shows the cluster size (R_g) corresponding to the onset of -4 slopes at high q.) (e) Kratky plots of linear (blue), 4-armed (green), 6-armed (red) and 8-armed (gold) PECs. Lighter shades correspond to higher salt concentrations, which go from 0-900 mM NaCl in 300 mM steps.

3.2.5 Discussion

Our results indicate polyelectrolyte architecture can significantly alter the thermodynamic stability of PECs while keeping their structures and mechanical properties nearly unchanged. The influence of architecture on thermodynamic stability is consistent with previous experimental results showing how increased spatial charge density can increase salt resistance of PECs and simulation results showing that branched polyelectrolytes drive charge density higher than linear counterparts. We hypothesize that the increased steric congestion allows branched polyelectrolytes to perturbing counter-ion dynamics more than linear analogues prior to complexation, leading to a greater degree of translational entropy gain during the complexation process. Fully understanding this mechanism and how chemically agnostic architecture-based CSC design principles are will require significant future work.

The negligible influence of branched polyelectrolyte architecture on structure and rheology is likely a result of our current materials being moderately long and lightly branched. As molecular weight increases, we would expect significant differences in the entanglement behavior for PECs composed of star polyelectrolytes and linear polyelectrolytes. However, since PECs are swollen by plasticizing water, the entanglement DP for star polyelectrolytes may be difficult to achieve synthetically. Similarly, one can imagine that introducing anisotropy through branched architectures such as bottlebrushes would lead to PECs with internal structures distinct from linear PECs. A more detailed understanding of the interplay between linear and spatial charge density could lead to increasingly precise PEC design, whereby the judicious incorporation of branched and statistical copolyelectrolytes enables rational design of PEC materials with orthogonal control over a range of CSCs and mechanical properties.

3.3 Conclusions

In this work, we evaluated the effect of polyelectrolyte architecture on PEC properties using homologous polyelectrolytes derived from the combination of thiol-epoxy and PGMA. The ease of PGMA synthesis and thiol-epoxy functionalization provides a straightforward pathway to homologous polyelectrolytes of various architectures. PECs from PGMA precursors produced viscous liquid complexes with architecture dependent CSC. In contrast, the rheology and structure of our PECs measured by SAOS and SAXS was consistent across architectures. Together, our results suggest salt resistance can be selectively altered by incorporating lightly branched polyelectrolytes in PECs, presenting a pathway for precise modification of PEC properties. Furthermore, our results suggest a fundamental difference between the structure-property relationships resulting from variations in linear charge density through copolymerization and those arising from altered spatial charge density through polyelectrolyte architecture, informing the design of PEC materials.

3.4 Experimental

3.4.1 Materials

All chemicals and solvents were purchased from Sigma Aldrich and used as received unless otherwise noted. 6 and 8-armed ATRP initiators were synthesized from according to literature proecures.[41]

3.4.2 Poly(glycidyl methacrylate) Synthesis

All polymers were synthesized via atom-transfer radical polymerization (ATRP) according to previous methods. In short, the desired amounts of monomer, initiator, dNbpy, and solvent would be added to a roundbottom flask and degassed with dry argon. After 20 minutes of sparging, CuBr would be added to the roundbottom. The mixture was then sparged at room temperature for an additional 5 minutes before being heated to 60 °C. The general reactant ratios were 1:2.5:1 of initiator:ligand:CuBr with monomer concentration set at 0.5 M. Reaction conversion was monitored by ^{1}H NMR and allowed to reach targeted theoretical molecular weights before being quenched with liquid nitrogen and exposed to air. Multi-armed reactions were designed with higher initiator to monomer ratios to combat the well-known tendency of branched macromolecules to couple at lower degrees of polymerization relative to linear polymers.[42]

3.4.3 Thiol-Epoxy Functionalization

To functionalize the PGMA precursors via thiol-epoxy, the following general procedure was used. To create anionic derivatives, PGMA, and 3-mercapto-1-propanesulfonate were dissolved in dimethyl sulfoxide (DMSO). Water was slowly added dropwise until all components were dissolved. Once homogenized, aqueous NaOH (2M) was added slowly. Occasionally, lightly functionalized PGMA would crash out and more DMSO or water would be added as

needed to solubilize the copolymer. This solution was allowed to stir at RT overnight and was then dialyzed against DI water for 3 days with the water changed twice daily.

To create cationic derivatives, we added slight alterations to previously reported methods. PGMA, THF and 2-(Boc-amino)ethanethiol were added to a scintillation vial at 1:4 ratio of epoxy:thiol. Aqueous LiOH solution (50 mg/mL) at 0.05 equivalents to epoxy groups was added to initiate thiol-epoxy. This solution was stirred overnight and then dried via vacuum. This crude mixture was then dissolved into dioxane and 6M HCl was slowly added such that the final composition was 1:1 dioxane:6M HCl. Upon addition of acid, the solution becomes cloudy over time. To address this, DI water would be added until the partially deprotected copolymer dissolved.

3.4.4 Polymer Characterization

To determine polymer molecular weight and dispersity, size exclusion chromatography-multi-angle light scattering (SEC-MALS) was performed on a Shimadzu Prominence LC system with a Wyatt Dawn Heleos MALS detector with a 658 nm laser and a SPD-M30A Photodiode Array detector. The eluent was chromatography grade tetrahydrofuran running at 1 mL/min at 25 °C. Wyatt Astra software was used to process the data. The dn/dc was estimated using 100% mass recovery. ^{1}H NMR spectra were obtained using either D_2O or CD_2Cl_2 on a Bruker 400 MHz NMR spectrometer at room tepmpertature.

3.4.5 Complex Formation

PECs were prepared at charge matched 1:1 conditions between polyanion and polycation repeating units with a total polymer solution during complexation was 10 mg/mL. All stock solutions were titrated to pH 3 to ensure full ionization of the primary amine groups for all polyelectrolyte architectures. Stock solutions of polyanions and polycations were added after stock solutions of water and NaCl stock solution and immediately vortexed to ensure rapid mixing.

3.4.6 Optical Microscopy

To visualize PECs, we used optical phase contrast microscopy. Then 200 µL of 10 mg/mL complex was mixed and immediately transferred to an ultralow attachment 96-well plate. The samples were allowed to equilibrate for a day before imaging and were carefully sealed to avoid evaporation. The plates were then imaged using a Leica DMI 6000B via the Leica Application Suite (LAS) software.

3.4.7 Rheology

Small angle oscillatory sweep experiments were performed on a stress-controlled DHR-3 rheometer (TA Instruments) using a 20 mm parallel plate geometry with the factory solvent trap attachments. Supernatant was placed around the edge of the sample to ensure the samples would not dry during measurements. PEC samples were prepared according to protocols described above and then centrifuged at 9000 g for 1h and aged for a day. Strain sweeps were performed to identify the linear viscoelastic regime for each sample. Frequency sweep experiments were performed on PECs of each architecture at 75-5 °C for 0 mM samples and 65-5 C for 500 mM samples, from high temperature to low temperature 5 minute equilibration times at each new temperature.

3.4.8 Thermogravimetric Analysis

To measure the solids content of our complexes, we placed 5-15 mg of complex into aluminum pans. The pans were placed in a OTF-1500X tube furnace (MTI), where they were heated to 110 °C

3.4.9 Small-Angle X-ray Scattering

Small-angle X-ray Scattering (SAXS) experiments were performed at the Advanced Photon Source (APS) line 12-ID-B at Argonne National Laboratory (ANL). Exposures were maintained at 0.1 s and taken at room temperature. Complexes were prepared in small ependorf tubes according to the procedures described above, centrifuged at 9000g for 1h and aged for 24 hours. These samples were carefully extracted and placed into holes drilled into an aluminum strip sealed by Kapton tape (Fisher Scientific Company) on both sides to minimize variations in sample thickness and reduce water loss. The SAXSLee package at beamline 12-ID-B was used to convert 2D images into one dimensional representations of q vs intensity, where q = 4pi/lambda sin(theta/2) and lambda. The Irena plugin package for Igor was used to process the SAXS data.

References

1. Srivastava, S.; Tirrell, M. V. Polyelectrolyte Complexation. In *Advances in Chemical Physics*, Rice, S. A., Dinner, A. R. Eds.; Advances in Chemical Physics, Vol. 161; John Wiley & Sons, Inc., **2016;** pp 499-544.

2. Muthukumar, M. 50th Anniversary Perspective: A Perspective on Polyelectrolyte Solutions. *Macromolecules* **2017**, *50* 24, 9528-9560. DOI: 10.1021/acs.macromol.7b01929.

3. Sing, C. E.; Perry, S. L. Recent progress in the science of complex coacervation. *Soft Matter* **2020**, *16* 12, 2885-2914, 10.1039/D0SM00001A. DOI: 10.1039/D0SM00001A.

4. Peters, D.; Kastantin, M.; Kotamraju, V. R.; Karmali, P. P.; Gujraty, K.; Tirrell, M.; Ruoslahti, E. Targeting atherosclerosis by using modular, multifunctional micelles. *Proceedings of the National Academy of Sciences* **2009**, *106* 24, 9815-9819.

5. Zhou, Z.; Yeh, C.-F.; Mellas, M.; Oh, M.-J.; Zhu, J.; Li, J.; Huang, R.-T.; Harrison, D. L.; Shentu, T.-P.; Wu, D. Targeted polyelectrolyte complex micelles treat vascular complications in vivo. *Proceedings of the National Academy of Sciences* **2021**, *118* 50, e2114842118.

6. Maggi, F.; Ciccarelli, S.; Diociaiuti, M.; Casciardi, S.; Masci, G. Chitosan nanogels by template chemical cross-linking in polyion complex micelle nanoreactors. *Biomacromolecules* **2011**, *12* 10, 3499-3507.

7. Lindhoud, S.; Norde, W.; Cohen Stuart, M. A. Effects of polyelectrolyte complex micelles and their components on the enzymatic activity of lipase. *Langmuir* **2010**, *26* 12, 9802-9808.

8. van Hees, I. A.; Hofman, A. H.; Dompé, M.; van der Gucht, J.; Kamperman, M. Temperature-responsive polyelectrolyte complexes for bio-inspired underwater adhesives. *European Polymer Journal* **2020**, *141*, 110034.

9. Zhao, Q.; Lee, D. W.; Ahn, B. K.; Seo, S.; Kaufman, Y.; Israelachvili, J. N.; Waite, J. H. Underwater contact adhesion and microarchitecture in polyelectrolyte complexes actuated by solvent exchange. *Nature materials* **2016**, *15* 4, 407-412.

10. Li, L.; Rumyantsev, A. M.; Srivastava, S.; Meng, S.; De Pablo, J. J.; Tirrell, M. V. Effect of Solvent Quality on the Phase Behavior of Polyelectrolyte Complexes. *Macromolecules* **2021**, *54* 1, 105-114. DOI: 10.1021/acs.macromol.0c01000.

11. Meng, S.; Liu, Y.; Yeo, J.; Ting, J. M.; Tirrell, M. V. Effect of mixed solvents on polyelectrolyte complexes with salt. *Colloid and Polymer Science* **2020**, *298* 7, 887-894. DOI: 10.1007/s00396-020-04637-0.

12. Akkaoui, K.; Yang, M.; Digby, Z. A.; Schlenoff, J. B. Ultraviscosity in Entangled Polyelectrolyte Complexes and Coacervates. *Macromolecules* **2020**, *53* 11, 4234-4246. DOI:10.1021/acs.macromol.0c00133.

13. Yang, M.; Shi, J.; Schlenoff, J. B. Control of Dynamics in Polyelectrolyte Complexes by Temperature and Salt. *Macromolecules* **2019**, *52* 5, 1930-1941. DOI: 10.1021/acs.macromol.8b02577.

14. Huang, J.; Morin, F. J.; Laaser, J. E. Charge-Density-Dominated Phase Behavior and Viscoelasticity of Polyelectrolyte Complex Coacervates. *Macromolecules* **2019**, *52* 13, 4957-4967. DOI: 10.1021/acs.macromol.9b00036.

15. Huang, J.; Laaser, J. E. Charge Density and Hydrophobicity-Dominated Regimes in the Phase Behavior of Complex Coacervates. *ACS Macro Letters* **2021**, *10* 8, 1029-1034. DOI: 10.1021/acsmacrolett.1c00382.

16. Liu, Y.; Santa Chalarca, C. F.; Carmean, R. N.; Olson, R. A.; Madinya, J.; Sumerlin, B. S.; Sing, C. E.; Emrick, T.; Perry, S. L. Effect of Polymer Chemistry on the Linear Viscoelasticity of Complex Coacervates. *Macromolecules* **2020**, *53* 18, 7851-7864. DOI: 10.1021/acs.macromol.0c00758.

17. Larson, R. G.; Liu, Y.; Li, H. Linear viscoelasticity and time-temperature-salt and other superpositions in polyelectrolyte coacervates. *Journal of Rheology* **2021**, *65* 1, 77-102.

18. Fu, J.; Schlenoff, J. B. Driving forces for oppositely charged polyion association in aqueous solutions: enthalpic, entropic, but not electrostatic. *Journal of the American Chemical Society* **2016**, *138* 3, 980-990.

19. Chang, L.-W.; Lytle, T. K.; Radhakrishna, M.; Madinya, J. J.; Vélez, J.; Sing, C. E.; Perry, S. L. Sequence and entropy-based control of complex coacervates. *Nature Communications* **2017**, *8* 1. DOI: 10.1038/s41467-017-01249-1.

20. Lytle, T. K.; Chang, L.-W.; Markiewicz, N.; Perry, S. L.; Sing, C. E. Designing electrostatic interactions via polyelectrolyte monomer sequence. *ACS central science* **2019**, *5* 4, 709-718.

21. Chremos, A.; Douglas, J. F. Counter-ion distribution around flexible polyelectrolytes having different molecular architecture. *Soft Matter* **2016**, *12* 11, 2932-2941.

22. Rahalkar, A.; Wei, G.; Nieuwendaal, R.; Prabhu, V. M.; Srivastava, S.; Levi, A. E.; De Pablo, J. J.; Tirrell, M. V. Effect of temperature on the structure and dynamics of triblock polyelectrolyte gels. *Journal of Chemical Physics* **2018**, *149* 16. DOI: 10.1063/1.5035083.

23. Krogstad, D. V.; Lynd, N. A.; Choi, S. H.; Spruell, J. M.; Hawker, C. J.; Kramer, E. J.; Tirrell, M. V. Effects of polymer and salt concentration on the structure and properties of triblock copolymer coacervate hydrogels. *Macromolecules* **2013**, *46* 4, 1512-1518. DOI: 10.1021/ma302299r.

24. Srivastava, S.; Andreev, M.; Levi, A. E.; Goldfeld, D. J.; Mao, J.; Heller, W. T.; Prabhu, V. M.; De Pablo, J. J.; Tirrell, M. V. Gel phase formation in dilute triblock copolyelectrolyte complexes. *Nature Communications* **2017**, *8*. DOI: 10.1038/ncomms14131.

25. Lou, J.; Friedowitz, S.; Qin, J.; Xia, Y. Tunable coacervation of well-defined homologous polyanions and polycations by local polarity. *ACS central science* **2019**, *5* 3, 549-557.

26. Neitzel, A. E.; Fang, Y. N.; Yu, B.; Rumyantsev, A. M.; de Pablo, J. J.; Tirrell, M. V. Polyelectrolyte complex coacervation across a broad range of charge densities. *Macromolecules* **2021**, *54* 14, 6878-6890.

27. Muzammil, E. M.; Khan, A.; Stuparu, M. C. Post-polymerization modification reactions of poly (glycidyl methacrylate) s. *RSC advances* **2017**, *7* 88, 55874-55884.

28. Hatton, F. L.; Derry, M. J.; Armes, S. P. Rational synthesis of epoxy-functional spheres, worms and vesicles by RAFT aqueous emulsion polymerisation of glycidyl methacrylate. *Polymer Chemistry* **2020**, *11* 39, 6343-6355.

29. Stuparu, M. C.; Khan, A. Thiol-epoxy "click" chemistry: Application in preparation and postpolymerization modification of polymers. *Journal of Polymer Science Part A: Polymer Chemistry* **2016**, *54* 19, 3057-3070.

30. Gadwal, I.; Stuparu, M. C.; Khan, A. Homopolymer bifunctionalization through sequential thiol–epoxy and esterification reactions: an optimization, quantification, and structural elucidation study. *Polymer Chemistry* **2015**, *6* 8, 1393-1404.

31. Kubo, T.; Easterling, C. P.; Olson, R. A.; Sumerlin, B. S. Synthesis of multifunctional homopolymers via sequential post-polymerization reactions. *Polymer Chemistry* **2018**, *9* 37, 4605-4610.

32. Buerkli, C.; Lee, S. H.; Moroz, E.; Stuparu, M. C.; Leroux, J.-C.; Khan, A. Amphipathic homopolymers for siRNA delivery: probing impact of bifunctional polymer composition on transfection. *Biomacromolecules* **2014**, *15* 5, 1707-1715.

33. Zhu, Z.; Jeong, G.; Kim, S. J.; Gadwal, I.; Choe, Y.; Bang, J.; Oh, M. K.; Khan, A.; Rao, J. Balancing antimicrobial performance with hemocompatibility in amphiphilic homopolymers. *Journal of Polymer Science Part A: Polymer Chemistry* **2018**, *56* 21, 2391-2396.

34. Wang, Q.; Schlenoff, J. B. The polyelectrolyte complex/coacervate continuum. *Macromolecules* **2014**, *47* 9, 3108-3116.

35. Li, L.; Srivastava, S.; Andreev, M.; Marciel, A. B.; de Pablo, J. J.; Tirrell, M. V. Phase behavior and salt partitioning in polyelectrolyte complex coacervates. *Macromolecules* **2018**, *51* 8, 2988-2995.

36. Meng, S.; Ting, J. M.; Wu, H.; Tirrell, M. V. Solid-to-Liquid Phase Transition in Polyelectrolyte Complexes. *Macromolecules* **2020**, *53* 18, 7944-7953. DOI: 10.1021/acs.macromol.0c00930.

37. Vieregg, J. R.; Lueckheide, M.; Marciel, A. B.; Leon, L.; Bologna, A. J.; Rivera, J. R.; Tirrell, M. V. Oligonucleotide-Peptide Complexes: Phase Control by Hybridization. *Journal of the American Chemical Society* **2018**, *140* 5, 1632-1638. DOI: 10.1021/jacs.7b03567.

38. Rubinstein, M.; Colby, R. H. *Polymer physics*; Oxford university press New York, 2003.

39. Tang, S.; Wang, M.; Olsen, B. D. Anomalous self-diffusion and sticky Rouse dynamics in associative protein hydrogels. *Journal of the American Chemical Society* **2015**, *137* 11, 3946-3957.

40. Fetters, L. J.; Kiss, A. D.; Pearson, D. S.; Quack, G. F.; Vitus, F. J. Rheological behavior of star-shaped polymers. *Macromolecules* **1993**, *26* 4, 647-654.

41. Aliakseyeu, A.; Hlushko, R.; Sukhishvili, S. A. Nonionic star polymers with upper critical solution temperature in aqueous solutions. *Polymer Chemistry* **2022**, *13* 18, 2637-2650. DOI: 10.1039/d2py00216g.

42. Matyjaszewski, K.; Miller, P. J.; Pyun, J.; Kickelbick, G.; Diamanti, S. Synthesis and Characterization of Star Polymers with Varying Arm Number, Length, and Composition from Organic and Hybrid

Inorganic/Organic Multifunctional Initiators. *Macromolecules* **1999**, *32* 20, 6526-6535. DOI: 10.1021/ma9904823.

Chapter 4

Structure and Properties of Bottlebrush Polyelectrolyte Complexes

4.1 Introduction

Mixing oppositely charged polyelectrolytes results in spontaneous associative phase separation, resulting in a polymer rich phase known as a polyelectrolyte complex (PEC) that is responsive to unique stimuli such as pH, ionic strength and temperature.[1-7] PECs have been used extensively in food products and cosmetics and are promising for applications in underwater adhesives, drug delivery and nanoreactors.[8-16] The ability of PECs to create hydrated materials with properties ranging from glassy solids to viscous liquids makes them especially attractive as a materials platform.[17, 18] However, it is still difficult to direct PEC properties through molecular design, limiting the adoption of this promising class of materials. This challenge was exacerbated by the fact that many of the natural polyelectrolytes studied early in PEC development were poorly characterized, making connections to PEC properties and molecular structure challenging. In recent years synthetic techniques for growing well-defined water-soluble polymers have matured a great deal, enabling the synthesis of increasingly precise synthesis of polyelectrolytes of various architectures.[19, 20]

Despite the increasing availability of structurally advanced polyelectrolytes, the majority of PEC studies still utilize linear blocky, statistical or homopolyelectrolytes.[21-26] This has left a gap in our understanding of how molecular-level details such as polymer architecture influence PEC stability, rheology and structure. Molecular structure-property relationships are attractive because they seem to be well-conserved across various polyelectrolyte pairings and they allow one to tune PEC properties without altering the surrounding environment.

Charge density is a fundamental parameter in PEC design that macromolecular architecture is well-poised to precisely tune. In statistical copolymers, increased charge density has been shown to raise PEC stability and strengthen PEC mechanical properties.[24, 27] Branched polyelectrolytes raise charge density relative to linear polyelectrolytes, making them attractive candidates for further enhancement of PEC properties. However, besides Chapter 3, there are no reports of altering charge density higher homopolyelectrolytes using branched polymers.

Bottlebrush polymers are comb polymers composed of linear mainchains with sidechain grafting dense enough to stretch mainchain and sidechain conformations relative to Gaussian coils. In uncharged bottlebrushes, dense sidechain packing can eliminate mainchain entanglement, reduce sidechain entanglement and drive unique self-assembly. Under the right circumstances, branched architectures like these can provide a path to study high charge density polyelectrolytes in PECs. However, the right molecular design is necessary.

The first published attempt at PECs from comb polyelectrolytes could not demonstrate comb-comb PECs due to insufficient charge density.[28] They attribute this result to their sparsely branched comb architecture with short side chains. Simulations showed these comb-like polyelectrolytes had lower charge density than comparable linear polymers, which reduced PEC stability. Here, we create charge dense bottlebrush polyelectrolytes by combining ring-opening metathesis polymerization (ROMP) and atom-transfer radical polymerization (ATRP) to understand the emergent properties of bottlebrush polyelectrolyte complexes (BPECs). We find that BPECs form solid gels, a feature we attribute to physical crosslinks arising from sidechain interdigitation. Using a combination of SAXS and Cryo-TEM, we investigate the internal structure of BPECs and generate a unified picture of the structure and properties of BPECs as a function of salt that will enable future exploration of branched polyelectrolytes in PECs.

4.2 Results and Discussion

4.2.1 Bottlebrush Polyelectrolyte Synthesis

To create highly branched bottlebrush polyelectrolytes with sizes on the order of MDa, we harnessed a synthetic approach combining ROMP, ATRP and post-polymerization modification reactions. Our approach, adapted from Yamauchi et al., utilizes a grafting-from approach centered around the monomer 2-endo,3-endo-Bis(2-bromoisobutyryloxymethyl)-5-norbornene (NB), which serves as a ROMP monomer due to the norbornene functionality and as an initiator for ATRP due to the two pendant 2-bromoisobutylate moieties (Fig. 4.1).[29] ROMP of NB proceeds rapidly to produce Poly(NB) (PNB) with narrow dispersity and molecular weights in line with theoretical values (300:1 NB:G3). From PNB, we graft neutral sidechains of poly(tert-butyl methacrylate) (PtBMA) and poly(dimethylamino ethyl methcacrylate) (PDMAEMA) via ATRP (Fig. 4.1). Sidechains are converted into polyelectrolytes through quantitative de-tertbutylation and quaternization reactions to form PNB-*g*-MANa and PNB-*g*-TMEAMA, respectively (Fig. 4.2). For brevity, we will refer to the graft polymers PNB-*g*-MANa as PMANa and PNB-*g*-TMAEMA as $TMAEMA_X$ where X can be S or L for short or long sidechain TMAEMA. Two sidechain lengths of TMAEMA were made to evaluate the effect of chain length matching/mismatching, with the longer TMAEMA sidechains more closely match the DP of the PMANa sidechains and the short TMAEMA sidechains having approximately approximately half the DP of the longer TMAEMA sidechains (Fig. 4.1).

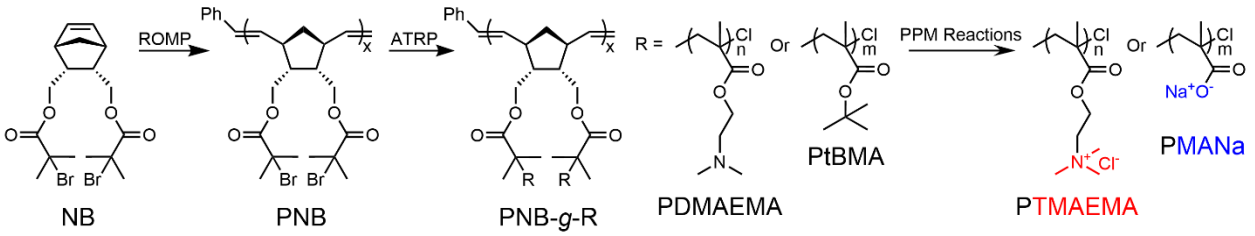

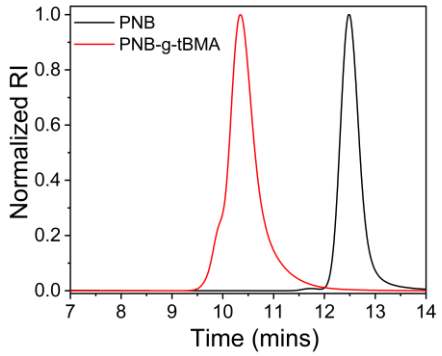

Polymer Name	Main Chain DP_n	Side Chain DP_n	$Đ$
PNB	**287**	**N/A**	**1.01**
PNB-*g*-tBMA	**287**	**82**	**1.06**
PNB-*g*-TMAEMA$_S$	**287**	**37***	**N/A**
PNB-*g*-TMAEMA$_L$	**287**	**89***	**N/A**

Figure 4.1 (top) Scheme for bottlebrush polyelectrolyte synthesis. (bottom left) GPC demonstrating conversion of macromonomer PNB into bottlebrush PNB-*g*-tBMA. (bottom right) Table with molecular characterization of bottlebrushes. *Estimated via ^{1}H NMR.

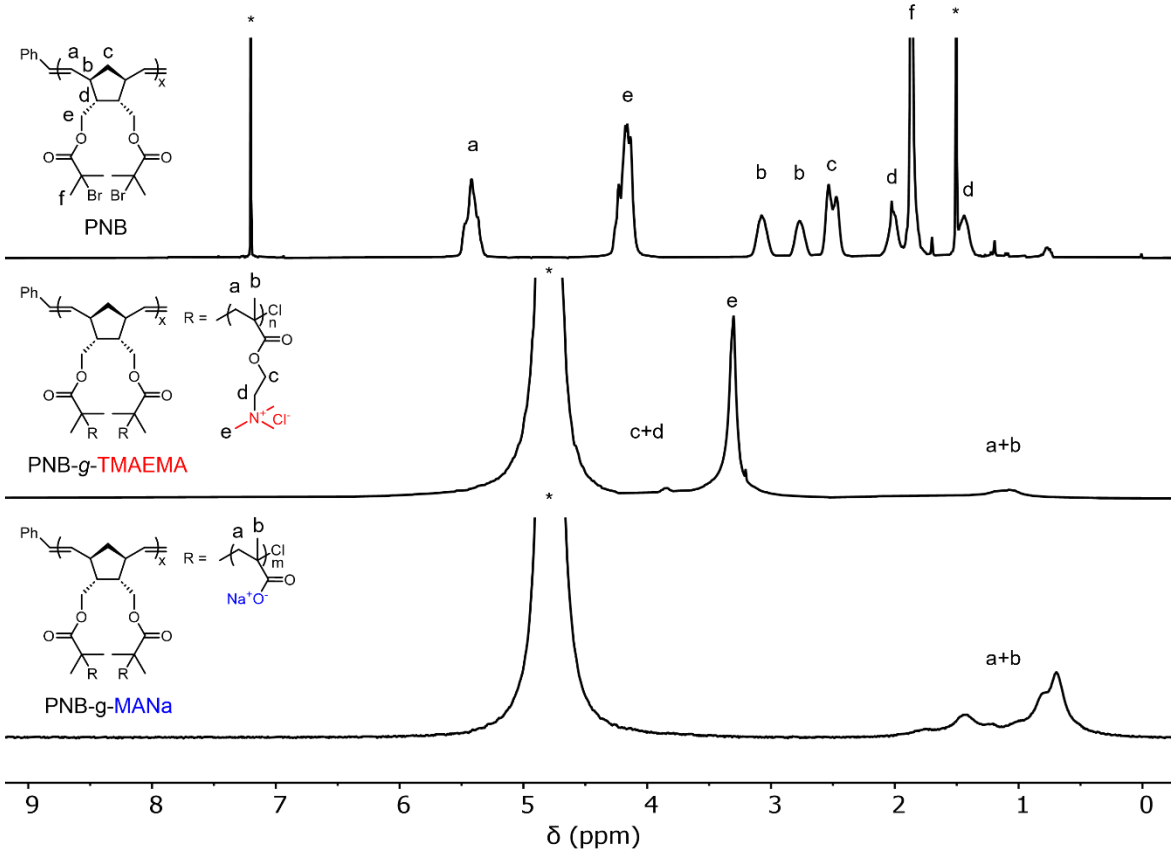

Figure 4.2 ^{1}H NMR of (top) PNB macroinitiator in CD_2Cl_2 (middle) PNB-*g*-TMAEMA in D_2O and (bottom) PNB-*g*-MANa in D_2O.

4.2.2 BPEC Morphology and Optical Microscopy

BPEC samples were prepared by sequentially mixing water, NaCl stock solutions and polymers followed by rapid mixing. The turbid samples were then centrifuged to coalesce the BPEC phase for further study. All BPECs were created using stock solutions of water, polymer and salt titrated to pH 10, to account for the tendency of PMANa's pKa to shift upward at higher branching densities.[30, 31] Since previous reports show the pKa of carboxylic acid containing polyelectrolytes decreases when complexed with quaternary-amine containing polyelectrolytes, we reasoned pH 10 should be sufficiently basic to ensure the PMANa groups are charged during complexation.[25]

Upon centrifugation, the complex is a white solid (Fig. 4.3). The complex swells with added salt, remaining white untili around 400 mM added salt, where the BPEC becomes hazy. At 500 mM salt, the complex is nearly clear. No complex forms at higher salt concentrations. The macroscopic appearance of BPECs was identical for matched and mismatched sidechains.

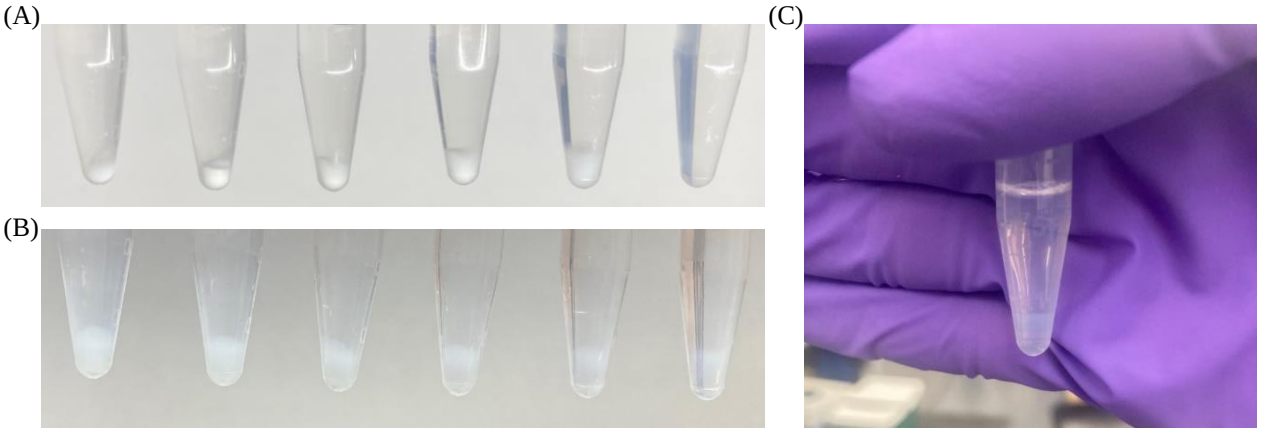

Figure 4.3 Photographs of BPECs of PMANa and PTMAEMA$_L$ with matched sidechains as a function going from (A) 0-500 mM NaCl from left to right in 100 mM increments (B) 400-500 mM NaCl from left to right in 20 mM incriments. (C) Photograph of BPECs with 500 mM added salt with with a colored background to make the faint complex more visually apparent.

We use optical microscopy to visualize BPECs at the microscale as a function of salt (Fig. 4.4). Microscopy images showed the BPECs to be cloudy aggregates at all salt concentrations with a critical salt concentration (CSC) of 500 mM added NaCl. This microscale morphology indicates BPECs form solid-like precipitates or gels. Interestingly, there is no transition from precipitate to coacervate before the CSC. In general, PECs transition from solid like precipitates through liquid-like coacervates before dissolution. Here, however, the complex dissolves somewhere between 500-525 mM added NaCl, so the transition from solid to liquid complex must occupy an extremely narrow phase space if it exists at all. The microscale morphologies and CSC of BPECs at matched and mismatched sidechain lengths are indistinguishable. At all salt concentrations, all BPECs studied here appear as solid precipitates under optical microscopy.

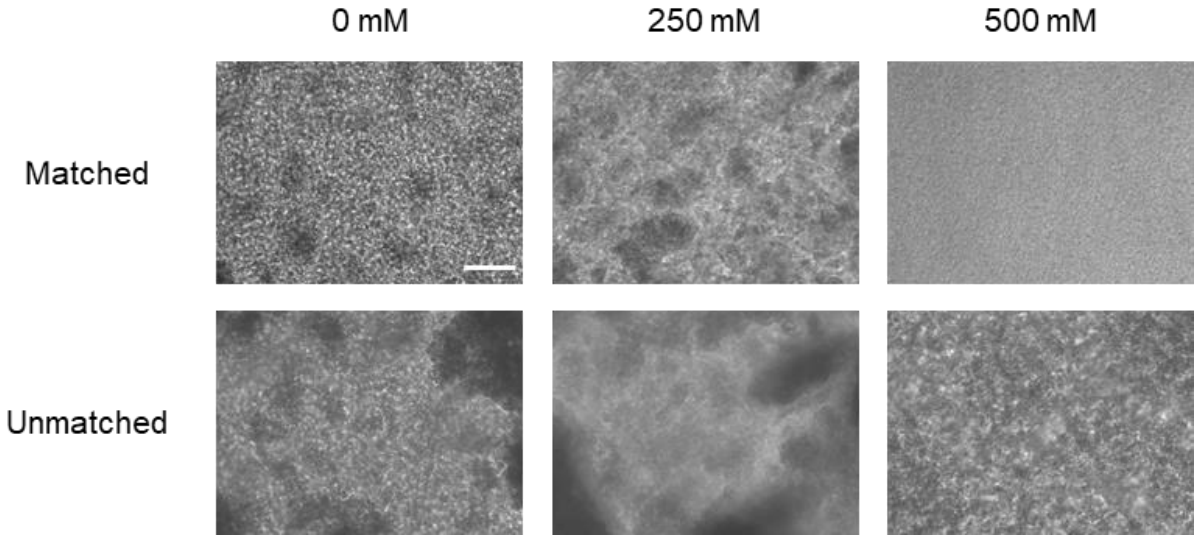

Figure 4.4 Optical microscopy of BPECs of PMANa and PTMAEMA with matched and unmatched sidechains as a function of added NaCl. Scale bar is 100 μm.

4.2.3 Rheology

Small angle oscillatory shear (SAOS) experiments allowed us to further quantify the physical state and determine the stimuli-responsiveness of our materials. The BPECs show gel-like response with storage modulus (G') above loss modulus (G'') at all frequencies, temperatures and salt concentrations measured. With no added salt, our materials begin as soft gels which further

soften as salt is added, temperature is increased or sidechain length mismatch is increased (Fig. 4.5). Super-soft water-swollen mechanical responses could make BPECs attractive as wound healing materials for application in soft tissues. It was initially unclear why these materials are behaving as gels, as gel-like mechanical properties are normally attributed to some type of physical or chemical crosslink.

Previous reports from have observed gel-like rheological responses in PECs. However, this feature is often attributed to aggregation at various length scales, usually driven by hydrophobic interactions between polyelectrolytes.[18, 32] Here, we have no obvious source of hydrophobic interactions capable of inducing physical crosslinks, suggesting the gel-like behavior observed here is not caused by amphiphilic interactions within the system. We hypothesize that intermolecular associations between interdigitated bottlebrush sidechains restrict motion and act as physical crosslinks, a novel mechanism for PEC gel formation. To fully understand the internal structure of PECs, we turn to Cryo-TEM and SAXS.

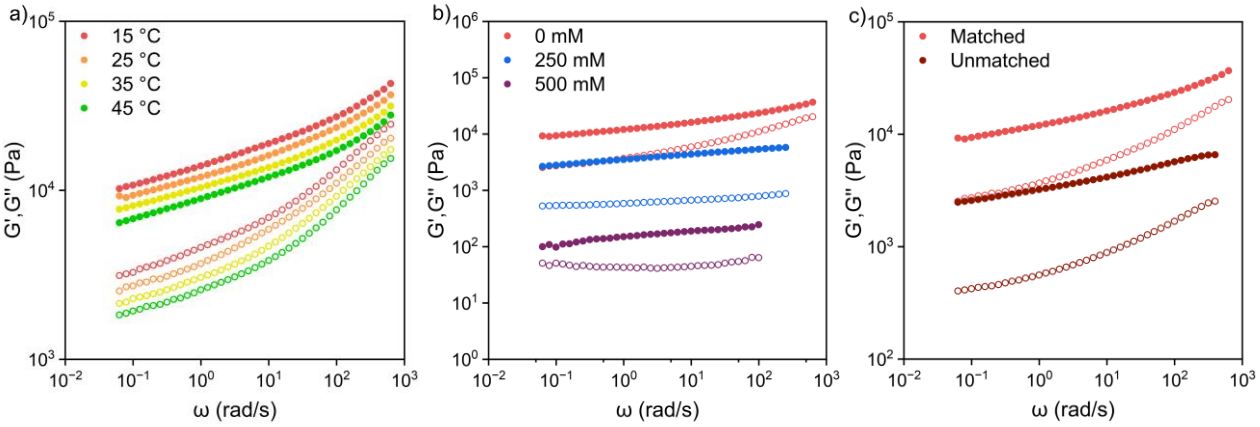

Figure 4.5 Frequency sweeps for BPECs with (a) 0 mM added NaCl at different temperatures (b) 0, 250 and 500 mM added NaCl at 25°C and (c) matched or mismatched sidechain lengths.

4.2.4 Internal Structure Observation via Cryo-TEM

To better understand the underlying structure of our gel-like BPEC, we performed Cryo-TEM experiments, reasoning that our bottlebrushes are long and densely branched enough to be imaged directly. To obtain clear images of PMANa, $PTMAEMA_L$, and BPECs, we diluted the polymer concentration to 0.5 mg/mL. Representative Cryo-TEM images of PMANa, $PTMAEMA_L$ and BPECs are shown in Figure 4.6.

Cryo-TEM images of the individual polyelectrolytes reveals densely branched polyelectrolytes with lengths on the order of 100 nm and widths of approximately 10-15 nm. The bottlebrushes are highly extended which is expected due to the steric congestion and electrostatic repulsion between the densely grafted sidechains. These samples were flash frozen to better preserve the solution-state conformations of the bottlebrushes, giving us reasonable confidence the chain conformations observed here are representative of the bottlebrushes in solution. The contrast is sufficient in the low salt case to allow us to estimate the bottlebrush thickness using imageJ analysis (Fig. 4.6B). To the best of our knowledge, these are the first images of bottlebrush polyelectrolytes without external contrast agent.

With no added salt, the BPECs form densely packed structures with smooth surfaces. At this salt concentration the PECs exhibit dense inter-chain packing, with no discernible features attributable to individual polyelectrolytes. Additionally, the surface of the BPEC is highly curved, which is surprising given the rigidity of the uncomplexed bottlebrush polyelectrolytes. The smooth, curved surfaces and densely packed structure of the low salt BPECs shows polyelectrolyte complexation provides a strong driving force for sidechain association of oppositely charged bottlebrushes in the absence of added salt, significantly perturbing the mainchain conformation of the constituent bottlebrushes within a BPEC.

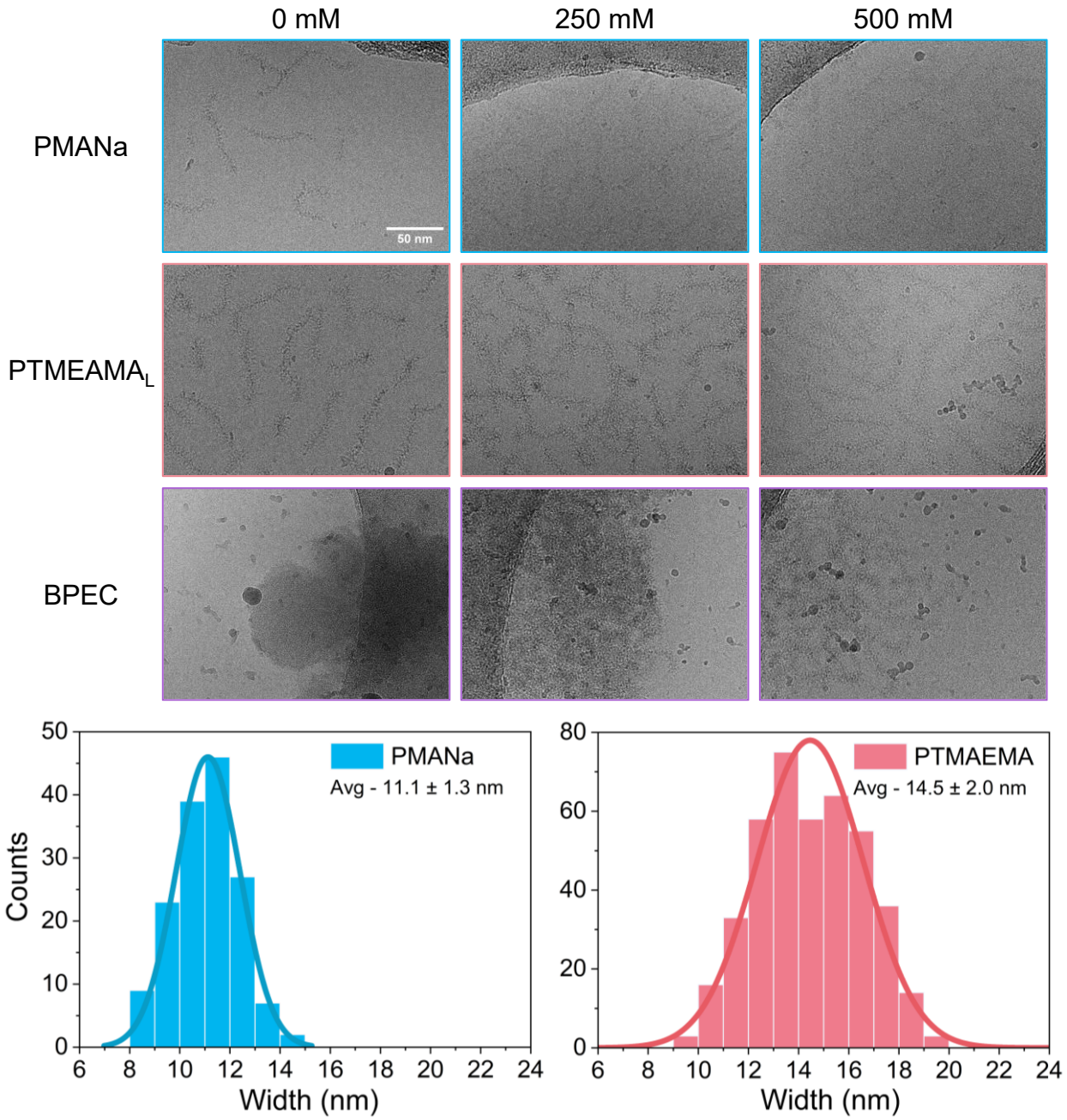

Figure 4.6 (Top) Cryo-TEM microscopy of bottlebrushes of PMANa and PTMAEMA$_L$ and BPECs with matched sidechains as a function of added NaCl. Scale bar is 50 nm. (Bottom) Histograms of bottlebrush width acquired via ImageJ analysis of 0 mM added salt bottlebrushes.

At 250 mM added salt, the BPEC swells, adopting a more expanded network architecture with rougher surfaces (Fig. 4.6). At first it was unclear if the lighter spaces in the complex are voids within the BPEC or thinner regions within the BPEC composed of PMANa, which has much less contrast than PTMAEMA$_L$. However, examining this material under higher magnification

suggests most of the lighter regions are still filled (Fig. 4.7). The surfaces of the BPEC are rougher and less curved than in the low salt case. This makes sense, as introducing salt reduces the amount of intrinsic bonds between oppositely charged sidechains, lowering the driving force for mainchain contortion.

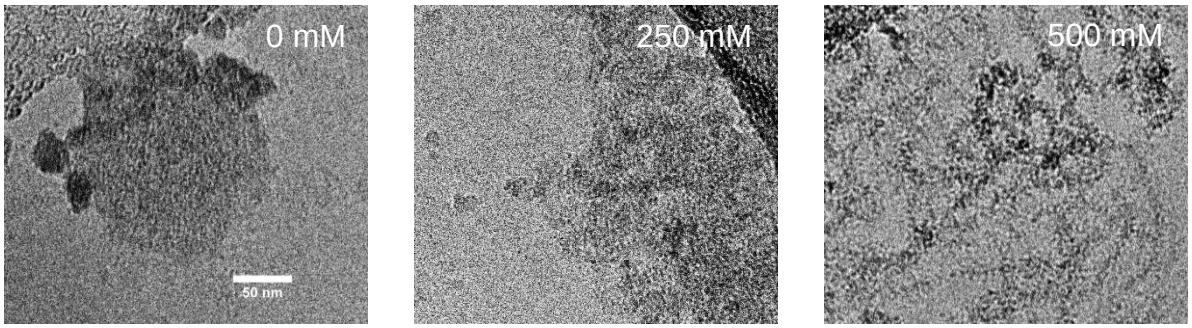

Figure 4.7 Cryo-TEM microscopy of bottlebrushes of BPECs with matched sidechains at 0, 250 and 500 added NaCl from left to right. These images more clearly demonstrate the difference between lightly filled spaces in the 250 mM added salt samples and the empty spaces outside the complex. These images were acquired at 120,000 x magnification. Scale bar is 50 nm.

At 500 mM added salt the BPEC swells, becoming a swollen disordered network with no obvious surfaces (Figs. 6 and 7). The bottlebrushes in this case are much more elongated than at other salt concentrations and connect at joints akin to crosslinks. These large, multivalent joints could be the physical crosslinks leading to gel-like rheological behavior in BPECs. If so, one can imagine how lowering salt would increase the joint density within the network and raise the modulus of the material in a manner analogous to crosslink density in traditional crosslinked polymer networks.

Mismatched complexes look very similar to the matched complexes in Cryo-TEM, progressing as salt is added from a densely packed network to slightly swollen network before finally expanding into an expanded filamentous architecture (Fig. 4.8). It is difficult to detect differences in the mismatched and matched BPECs structures using Cryo-TEM alone.

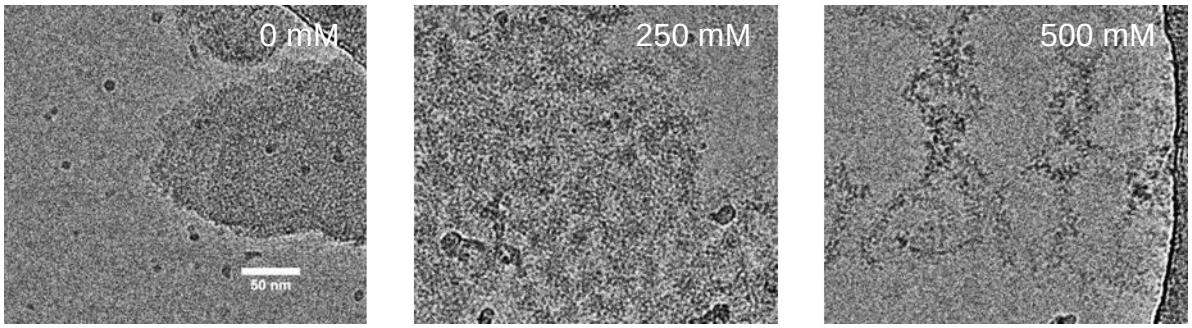

Figure 4.8 Cryo-TEM microscopy of BPECs with mismatched sidechains at 0, 250 and 500 mM added NaCl from left to right. These images were acquired at 120,000 x magnification. Scale bar is 50 nm.

To the best of our knowledge, these images provide the first look inside the structure of a polyelectrolyte complex with molecular resolution. By growing tens of thousands of charged repeat units from a single mainchain, we created polyelectrolytes significantly larger and more compact than most studied in the literature. This novel arrangement of charged groups allows us to directly observe the individual polyelectrolytes and the network structure adopted bottlebrush polyelectrolytes upon complexation via Cryo-TEM. However, these images may not be representative of the BPEC structure upon centrifugation and only allow us to observe small sections of BPEC at a time. To fully understand the structure of BPECs, a combination of Cryo-TEM and a more statistically powerful structural determination method like small angle x-ray scattering (SAXS) is appropriate.

4.2.5 Internal Structure Analysis via SAXS

To investigate the structure of our BPEC materials in the bulk, we performed small angle x-ray scattering (SAXS) (Fig. 4.9). First, we will discuss the SAXS results from the length matched pair in detail and then compare them to the structural trends for the mismatched case. All samples show an upturn at low q, suggesting large clusterings with R_g > 300 nm (since the maximum observable $R_g = 2pi/q_{min}$). At high q, I(q) as $\sim q^{-1}$, which we attribute to extended bottlebrush sidechains. Mid q features evolve as a function of added salt but can broadly be described as an R_g

describing aspects of the bottlebrushes in every case except 0 mM added salt. At no added salt, the data are best described qualitatively, whereas the data for 100-500 mM added salt were amenable to model fitting via a shape-independent two-level Beaucage model fit.

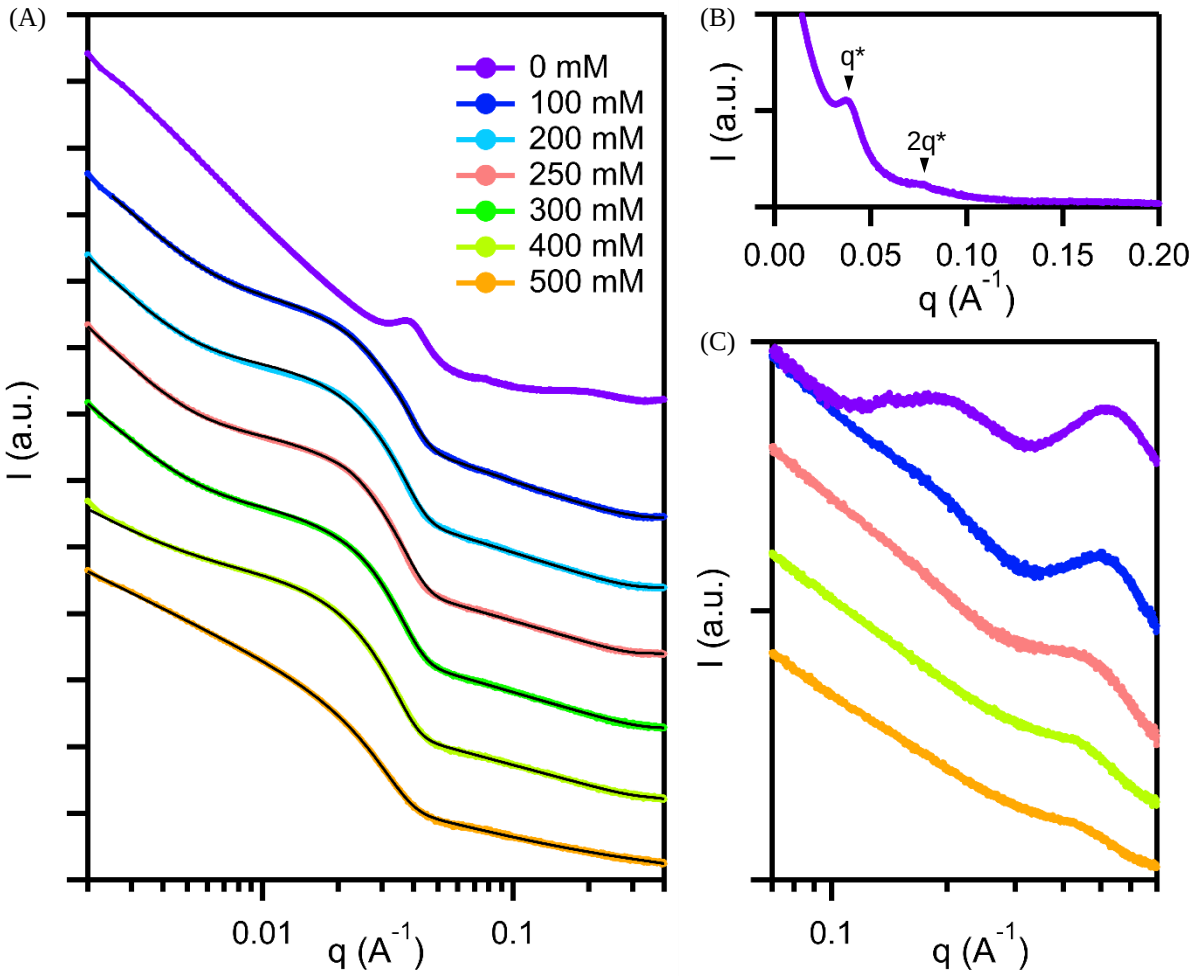

Figure 4.9 (A) SAXS patterns of BPECs taken with 0-500 mM NaCl added salt taken at 4 m detector distance. (B) log q vs I of a BPEC with 0 mM NaCl and arrows indicating q* and 2q (C) High q SAXS data for BPECs taken at 2.4 m detector distance. of BPECs of PMANa and PTMAEMA with matched and unmatched sidechains as a function of added NaCl. Scale bar is 100 µm.

At no added salt, I(q) scales with $q^{-3.8}$ at low q, which indicates a mass fractal network with smooth surfaces in good agreement with Cryo-TEM images taken at similar ionic strength. At mid q, a correlation peak appears at q* ~ 0.0375, corresponding to an average distance of 16.8 nm. At first, we believed this to be the average distance between PMANa and PTMAEMA bottlebrushes,

as correlation peaks arising from bottlebrush-bottlebrush spacings have been reported for solutions of bottlebrush polyelectrolytes and uncharged bottlebrush melts.[33-35] However, this interpretation is inconsistent with observations from the Cryo-TEM images. The average width of a bottlebrush estimated via Cryo-TEM is approximately 13 nm, which means there would need to be around 4 nm of empty space between bottlebrushes to accommodate a nearly 17 nm inter-bottlebrush distance. We observe densely packed BPEC structures at 0 mM added salt via Cryo-TEM with no evidence of such 4 nm gaps (Figs. 6 and 7). Furthermore, we observe a higher order reflection at $2q^*$ in the SAXS pattern consistent with lamellar ordering (Fig. 4.9B). Taken together, these results suggest portions of the complex adopt a lamellae-like structures with domain spacing of approximately 17 nm, albeit weakly (Fig. 4.10A). The spacing suggests significant but incomplete sidechain interpenetration. As the 0 mM salt case presents the strongest driving force for sidechain association, incomplete interpenetration under these conditions suggests sidechain interdigitation is hindered beyond a certain point, likely due to steric congestion near the bottlebrush core. It is possible improved matching of side-chain lengths and the development of appropriate annealing procedures could drive BPECs towards more finely ordered structures and greater sidechain interpenetration.

At high q, we observe scattering from the bottlebrush sidechains as well as two correlation peaks in the no added salt BPEC. Scattering from the two prominent correlation peaks obscures the slope at high q in this region, making it difficult to estimate sidechain conformations for this salt concentration. The first wide correlation peak at $q \sim 0.22$ we attribute to inter-sidechain distances that are reinforced by steric and electrostatic repulsion in the uncomplexed portions of sidechains. This correlation peak diminishes quickly upon the addition of salt. We attribute the second correlation peak at $q \sim 0.53$ to the intermolecular spacing of interdigitated bottlebrush

sidechains (Fig. 4.10B). The intensity of this peak diminishes upon the addition of salt and moves to lower q, with sidechain interdigitation distance moving from 1.2-1.4 nm as salt is added.

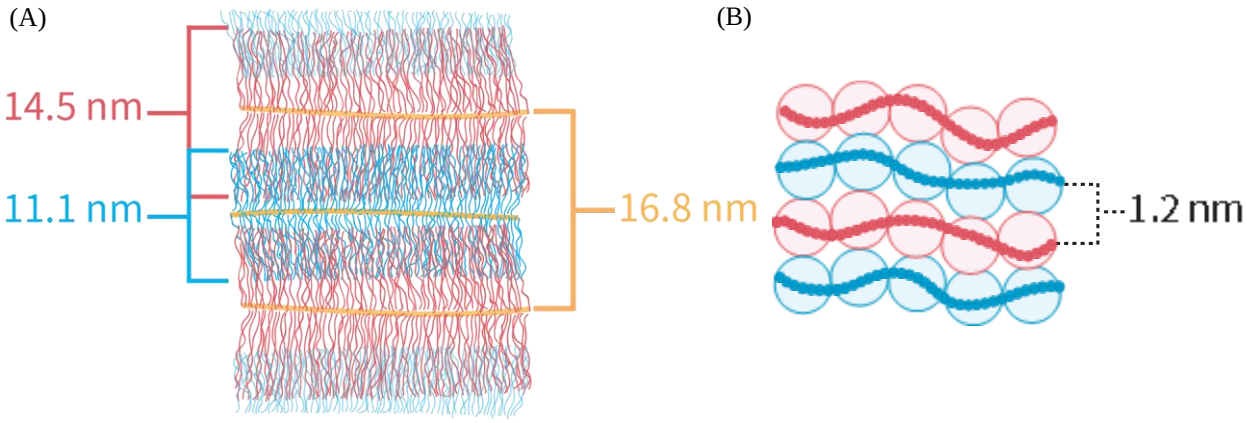

Figure 4.10 Schematic illustration of (A) a portion of 0 mM added salt BPEC aligned in a lamellar fashion in 2D and (B) illustration of sidechain interdigitation and correlation lengths. Bottlebrush widths are estimated via Cryo-TEM whereas mainchain lamellar spacing and sidechain correlation lengths are estimated via q* peak positions at mid q and low q in SAXS, respectively.

Upon the addition of salt, the scattering pattern of BPECs are significantly altered. The most prominent difference is the feature at mid q. At first, we attempted to model this feature as a flexible cylinder, but efforts to fit the data with this form factor failed to capture the highly negative slope at mid q. The sharp decreases in intensity where I(q) scales more negatively than q^{-4} can arise from diffuse electron density boundaries or polydispersity. As these are mixtures of two structurally distinct bottlebrushes with varying levels of sidechain interpenetration and poorly defined boundaries between species, both factors could be leading to the extremely negative slopes of this feature. To model our data, we applied a shape-independent Beaucage model fit with two levels set to describe the low-q ($q < 0.01$) and high q ($q > 0.01$) regimes.

The Beaucage model is frequently used to fit SAXS data with a Guinier regime and power law tail, especially when applying an exact scattering model is challenging or impossible.[36, 37] The model fits R_g and a Porod exponent P. Here, Porod exponents are available for both levels of the fit, whereas R_g is only visible for level one within the q range available here. Porod exponents,

allow one to understand how matter is distributed within a material, which we use here to understand both sidechain conformation and network architecture.

For fractal objects such as polymers and polymer networks, mass is distributed with respect to distance r as $M(r) \sim r^d$ and can be described in SAXS via the value of P in regions where $I(q) \sim q^{-P}$.[38, 39] There are two primary types of fractals, which can be easily distinguished via SAXS. Surface fractals are characterized by filled structures where only the surface of the structure is fractal. In SAXS, surface fractals are indicated by regions where I(q) decays with Porod exponents of 3-4 and provide the fractal dimension of the surface D_s through the relationship $P = 6 - D_s$. Within a mass fractal both the structures that compose the network and the surfaces of those structures are fractal. Mass fractals are characterized by Porod exponents of of 1-3, where Porod exponents closer to 3 represent more collapsed structures and values approaching 1 represent extended structures. In the appropriate q regime, Porod exponents from scattering data can be related to the Flory exponent (v) though the relation $q^{1/v} \sim q^{-P}$ to provide a straightforward relationship between scattering data and polymer conformation.[38] For reference, a P of -2 corresponds to melt behavior. The two-level Beaucage model applied here allows us to examine the Porod exponents at low q, corresponding to the network architecture adopted within the BPEC as well as the Porod exponents at high q, which correspond to the sidechain conformation of the bottlebrushes.

Our model fits allow us to establish structural trends emerging in BPECs upon the addition of salt. First, the Porod exponent from Level 1 fits for 100-300 mM added salt suggests that the network behaves as a surface fractal with a surface slightly rougher than the 0 mM added salt case. Between 300 and 400 mM, a transition from surface fractal to mass fractal occurs, as indicated by a Porod exponent below 3 for the 400 mM sample. At 500 mM, the network adopts an even more

expanded conformation with a Porod exponent of 1.84, indicating the overall network adopts an average conformation between that of a polymer in a melt (P = 2) and in a good solvent (P = 1.7). This network evolution is consistent with the traditional understanding of complex structural evolution where the addition of salt breaks intrinsic ion pairs, introducing water and swelling the network and agrees well with the network development observed in the Cryo-TEM images.

Table 4.1 Beaucage Model Fitting Results for Matched BPECs

mM added NaCl	Level 1 (q < 0.01)		Level 2 (q > 0.01)			
	B	P	G	Rg	B	P
100	1.14 e-07	3.48	0.68	9.56	4.81 e -05	1.32
200	2.36 e-08	3.58	0.703	9.93	5.52 e-05	1.18
250	2.13 e-08	3.58	0.59	9.90	6.42 e -05	1.08
300	8.21 e-08	3.30	0.47	10.0	5.25 e-05	1.09
400	2.49 e-05	2.15	0.43	10.8	5.17 e-05	1.01
500	2.16 e-04	1.84	0.04	9.74	3.66 e-05	1.00

Level 2 allows us to examine radius of gyration of the bottlebrushes and their sidechain conformations. In general, the Rg observed here seems to grow slightly with the addition of salt. The sidechains of the bottlebrushes extend as salt is added, evidenced by the decreasing Porod slope at level two as salt is increased. This is counterintuitive, as one would expect the sidechains to adopt a more collapsed conformation upon the addition of salt. Extension upon the addition of salt suggests a greater thermodynamic penalty for chain collapse in the uncomplexed regions relative to complexed sidechain regions, despite the significant steric congestion in complexed areas.

For the mismatched case, the trends are largely the same with a few significant differences. First, at no added salt there is little to no evidence of lamellar ordering, possibly due to the poorly matched sidechain length hindering the development of ordered structures. There is a weak correlation peak at q ~ 0.045 indicating an average domain spacing of approximately 14.0 nm. Interestingly, the first correlation peak at q ~ 0.22 is still present, but much weaker in this sample. This could be due to the shorter PTMAEMA sidechains being more complexed on average, as

PTMAEMA solutions scatter more strongly in this regime than PMANa (Fig. 4.12). Since these samples have much shorter PTMAEMA sidechains, a larger fraction of those sidechains could be available for complexation, leaving fewer uncomplexed sidechains to scatter and contribute to this correlation peak. The peak attributed to intramolecular scattering of bottlebrush sidechains at high q follows identical trends to the peak found in the matched case, losing intensity and shifting to lower q 1.2 to 1.4 nm as salt is added.

The fits from the Beaucage model indicate very similar trends to the matched case for 100-400 mM samples. As salt is added, the Porod exponent from level one shifts from a surface fractal at 100-300 mM to a mass fractal at 400 mM. Level 2 shows Rg increases as salt is added and the sidechains become more extended. The Rg's in this case are slightly smaller, which is to be expected as this bottlebrushes with smaller sidechains should also exhibit a smaller radius of gyration, whether that be the mainchain or sidechain R_g. Interestingly, the porod exponent of this level is slightly larger than that of the matched case, suggesting that that sidechains in this conformation can adopt a more compact conformation relative to those in the matched BPECs. This could be due to a higher relative degree of sidechain interpenetration of $TMAEMA_S$ in this case. Mismatched BPEC samples at 500 mM were too soft to handle without disrupting their internal structure, making SAXS measurements infeasible.

Table 4.2 Beaucage-model Fitting Results for Mismatched BPECs.

	Level 1		**Level 2**			
	B	**P**	**G**	**Rg**	**B**	**P**
100	**1.59 e-07**	**3.38**	**0.413**	**8.61**	**1.61 e-05**	**1.6487**
200	**2.40 e-08**	**3.61**	**0.382**	**8.60**	**4.40 e-05**	**1.33**
300	**3.21 e-7**	**3.04**	**0.297**	**9.08**	**3.84 e-05**	**1.26**
400	**4.00 e-4**	**1.73**	**0.188**	**9.77**	**3.18 e-05**	**1.15**

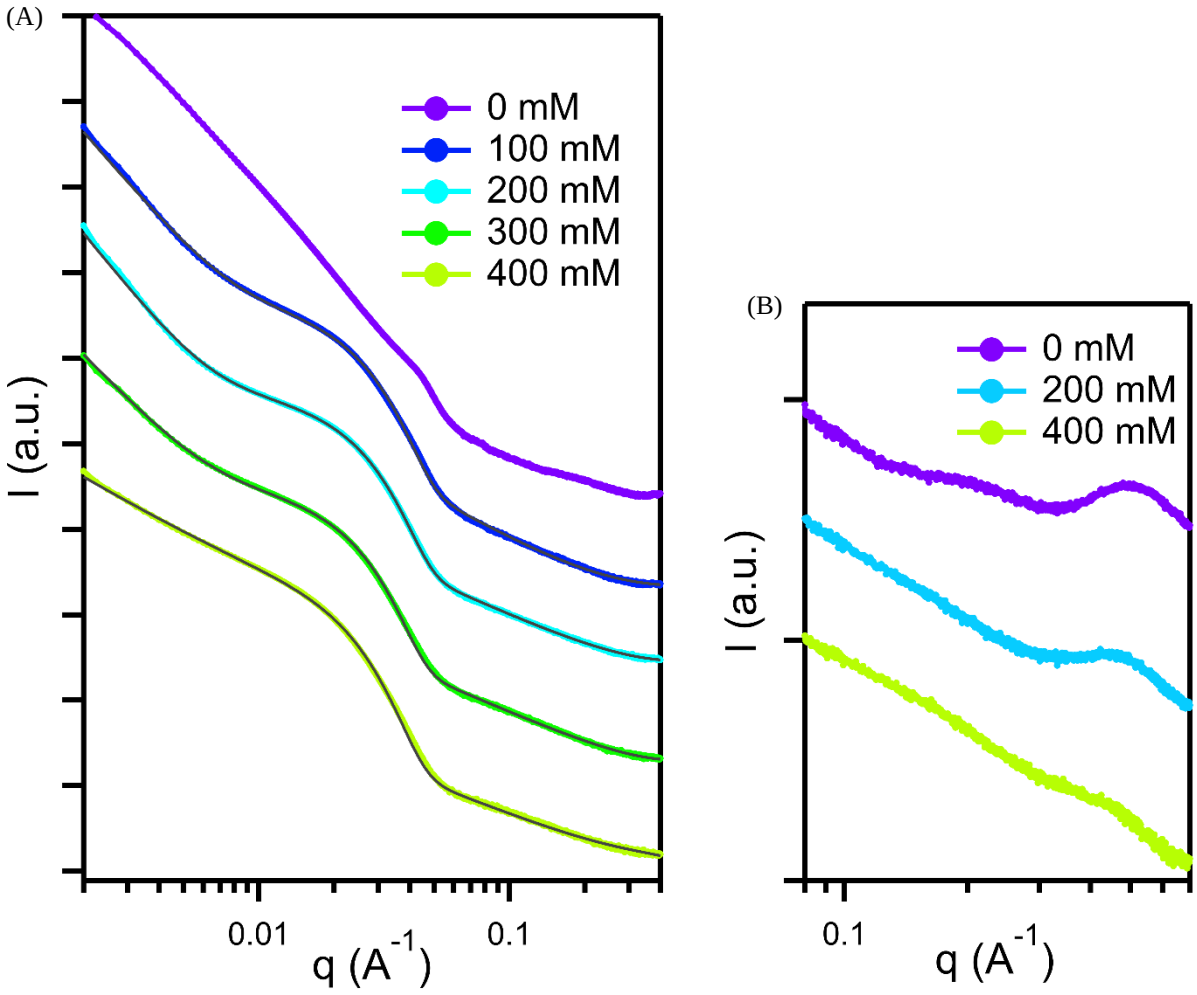

Figure 4.11 (A) SAXS patterns of BPECs taken with 0-500 mM NaCl added salt taken at 4 m detector distance. (B) log q vs I of a BPEC with 0 mM NaCl and arrows indicating q* and 2q (C) High q SAXS data for BPECs taken at 2.4 m detector distance.

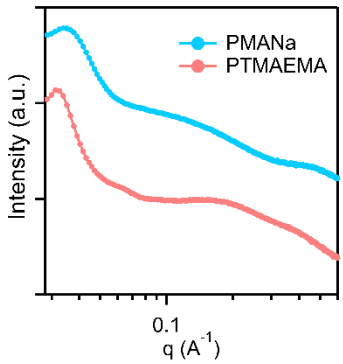

Figure 4.12 SAXS of bottlebrushes at 20 wt%. Correlation peaks at low q correspond to average inter-bottlebrush distances of 17.7 nm and 19.3 nm for PMANa and PTMAEMA$_L$, respectively.

4.3 Conclusion

Taken together, our data provide a descriptive picture of the internal structure and material properties of polyelectrolyte complexes composed of oppositely charged bottlebrush polyelectrolytes. We synthesized long and densley branched bottlebrush polymers using a combination of ROMP and ATRP, which we converted into polyelectrolytes using quantitative post-polymerization modification. BPECs of PMANa and PTMAEMA bottlebrushes form white solids that behave mechanically as gels that soften with added salt, increased heat and greater sidechain mismatching. Cryo-TEM reveals the presence of crossover points between bottlebrushes that could act as joints in the network. We hypothesize that these joints act as physical crosslinks that restrict polymer motion, leading to gel-like mechanical response. As salt or temperature is lowered, the density of crosslinks increases, giving rise to higher moduli gels. Cryo-TEM images and SAXS data reinforce each other to provide a cohesive model of the BPEC structural development upon the addition of salt. BPEC at low salt are densely packed surface fractal networks with internal domain spacings of ~ 17 nm and smooth surfaces that expand upon the addition of salt. Between 300 and 400 mM added NaCl, the network to become a mass fractal which expands upon the addition of salt until dissolving above 500 mM. Sidechains expand as salt is added, suggesting steric congestion in interdigitated complexed regions of the BPECs favor chain extension less than electrostatic repulsion in uncomplexed regions of the chain. Our results develop a fundamental understanding of the structure and properties of polyelectrolyte complexes composed of bottlebrush polyelectrolytes, enabling future investigation into the mechanical and structural variation attainable by incorporating branched polyelectrolytes into PEC design.

4.4 Experimental

4.4.1 Materials

All solvents and chemicals were purchased from Sigma-Aldrich and used without any further purification unless otherwise noted. Gen 3 Grubbs Catalyst was prepared from reacting pyridine and Gen 2 Grubbs obtained from Sigma-Aldrich through standard literature procedure.[40]

4.4.2 Monomer Synthesis

To prepare ROMP monomer NB we utilized previously described methods.[29] 250 mL of anhydrous THF was cannula transferred into a flame dried 500 mL glass round bottom flask. Dry TEA was added. Next, an addition funnel was attached to the apparatus and filled with 25mL of dry THF and 10.5 mL of α-bromoisobutyryl bromide (BIB). The round bottom was placed in an ice bath and BIB solution was added dropwise over the course of 30 minutes. White TEA salts precipitated out of solution as the reaction proceeded. The solution was left to stir at room temperature overnight. The crude product was filtered, concentrated, redissolved in diethyl ether and washed once with water (200 mL) twice with saturated sodium bicarbonate (200 mL) and once again with water before the magnesium sulfate was added to the organic phase. Once dry, the solution was concentrated via vacuum overnight, resulting in a yellow beige powder. The crude product was purified via column chromatography using 20:1 hexane:ethyl acetate. Fractions containing product were identified via TLC with iodine staining and subsequently concentrated via rotary evaporation, dissolved in ethyl acteate, filtered through 0.2 um PTFE filters and allowed to crystallize in a 70x55mm crystallization dish overnight, resulting in white crystals of NB.

4.4.3 PolyNB Synthesis

ROMP polymerizations of the Poly(NB) macroinitiator were carried out in an inert glovebox. A 1 M stock of NB in CHCl2 and 5mM Stock of G3 in CH2Cl2 were used to add the appropriate amounts of NB and G3 to the reaction vessel. The reaction was allowed to proceed for 15 minutes and then quenched with an excess of ethyl vinyl ether and stirred for an additional 30 minutes before removal from the glovebox. The mixture was diluted with CH_2Cl_2 and precipitated into MeOH via dropwise addition. The precipitate was filtered and dried via vacuum to give Poly(NB).

4.4.4 Bottlebrush Synthesis

Bottlebrush polymers were grown via a grafting from approach using ATRP off our polyNB macroinitiator. We aimed for low conversion to avoid the well-known tendency of multifunctional initiators to couple at low polymerization conversions.[41]

To grow polyNB-g-DMAEMA, we dissolved PNB, PMDETA and DMAEMA in anisole such that DMAEMA was at 0.5 M. The solution was degassed using ultrapure Argon for 30 minutes. CuCl and $CuCl_2$ were added at a ratio of 1:0.25:1 of CuCl:$CuCl_2$:initiating sites. The polymers were precipitated into hexanes, dissolved into $CHCl_3$, filtered through a silica plug and reprecipitated into hexanes before being dried via vacuum. PolyNB-g-DMAEMA was then dissolved in dioxane and introduced to iodomethane at a 4-6x excess of iodomethane to amine. The resulting yellow mixture was filtered and the solid collected was dissolved in water in the presence of a counterion exchange resin at 1:10:100 mass ratio of polymer:resin:water. This mixture was stirred for 24 hours and then filtered. The filtered solution was then dialyzed against four liters of 3 M NaCl for three days, with the solution changed once per day before being dialyzed against DI H_2O. The solution was filtered and lyophilized to provide a white powder.

PolyNB-g-tBMA was synthesized using the same procedures as polyNB-g-DMAEMA except the solvent was ethyl acetate. The polymer was precipitated in methanol, redissolved in $CHCl_3$, filtered through a silica plug and precipitated in methanol again before being dried via vacuum. The resulting polymer was dissolved in hexafluoro-2-propanol (HFIP) at 50 mg/mL before concentrated HCl was added slowly at 2x excess of tert-butyl groups. Upon the addition of acid, the polymer crashed out of solution as a waxy white solid. The minimum amount of water to dissolve the polymer was added to allow the reaction to proceed for 8 hours at room temperature. The resulting mixture was dialyzed against four liters of DI water for 5 days with the water changed twice a day. De-tert butylation efficiency was checked via 1H NMR. If necessary, this procedure was repeated to achieve full de-tert butylation.

4.4.5 Polymer Characteriztaion

To determine polymer molecular weight and dispersity, size exclusion chromatography-multi-angle light scattering (SEC-MALS) was performed on a Shimadzu Prominence LC system with a Wyatt Dawn Heleos MALS detector with a 658 nm laser and a SPD-M30A Photodiode Array detector. The eluent was chromatography grade tetrahydrofuran running at 1 mL/min at 25 °C. Wyatt Astra software was used to process the data. The polymers dn/dc was measured. ^1H NMR spectra were obtained using either D_2O or CD_2Cl_2 on a Bruker Avance 400 MHz NMR spectrometer at room tepmpertature (25C).

4.4.6 Complex Preparation

Complexes were prepared at 1:1 charge stoichiometric conditions between anionic and cationic repeat units. The complexes were formed by sequential addition of water, NaCl stock solution, polycation and polyanion and immediately vortexed. All solutions were titrated to a pH of 10 to ensure all polyelectrolytes were fully charged. The total polymer concentration for each sample was fixed at 10 mg/mL.

4.4.7 Optical Microscopy

To directly image BPEC morphology at the microscale, we used optical phase contrast microscopy on a Leica DMI 6000B. Images were acquired using Leica Application Suite software. PEC samples were prepared at 100 μL total volume and transferred into ultralow attachment 96-well plates immediately after having been vortexed. These plates were sealed to minimize evaporation. Microscopy samples were allowed to age overnight to ensure the phase separation process was largely completed.

4.4.8 Rheology

Rheology experiments were performed on a stress-controlled Discovery HR-3 rheometer from TA Instruments. A 20 mm parallel plate geometry was used. During measurements, supernatant was added to a solvent trap attachment and around the complex to ensure the BPEC stayed hydrated throughout. Frequency sweeps were performed at 45 to 15°C.

4.4.9 Transmission Electron Microscopy

Cryo-TEM images were obtained using a Thermo Titan Krios G3i at 300kV at 81,000x with a Gatan 3 direct detector. Bottlebrush and BPEC Samples were prepared at 0.5 mg/mL total polymer concentration. Then, 3.5 μL of sample was blotted onto a plasma cleaned Quantifoil copper grid 200 mesh 1.2/1.3, blotted for 1 second, and rapidly plunged into liquid ethane.

4.4.10 Small Angle X-ray Scattering

SAXS was collected at beamline 12-ID-B at the Advanced Photon Source at Argonne National Laboratory. Samples were loaded into holes drilled in an aluminum strip and sealed with Kapton tape to minimize evaporation and irradiated with 14 keV photon energy at 4 and 2.4 meter detector distance. Data reduction, background subtraction and data fitting were performed using the Irena plugin package within Igor.

4.5 References

1. Li, L.; Rumyantsev, A. M.; Srivastava, S.; Meng, S.; de Pablo, J. J.; Tirrell, M. V. Effect of solvent quality on the phase behavior of polyelectrolyte complexes. *Macromolecules* **2020**, *54* 1, 105-114.

2. Li, L.; Rumyantsev, A. M.; Srivastava, S.; Meng, S.; De Pablo, J. J.; Tirrell, M. V. Effect of Solvent Quality on the Phase Behavior of Polyelectrolyte Complexes. *Macromolecules* **2021**, *54* 1, 105-114. DOI: 10.1021/acs.macromol.0c01000.

3. Li, L.; Srivastava, S.; Andreev, M.; Marciel, A. B.; de Pablo, J. J.; Tirrell, M. V. Phase Behavior and Salt Partitioning in Polyelectrolyte Complex Coacervates. *Macromolecules* **2018**, *51* 8, 2988-2995. DOI: 10.1021/acs.macromol.8b00238.

4. Muthukumar, M. 50th Anniversary Perspective: A Perspective on Polyelectrolyte Solutions. *Macromolecules* **2017**, *50* 24, 9528-9560. DOI: 10.1021/acs.macromol.7b01929.

5. Sing, C. E.; Perry, S. L. Recent progress in the science of complex coacervation. *Soft Matter* **2020**, *16* 12, 2885-2914, 10.1039/D0SM00001A. DOI: 10.1039/D0SM00001A.

6. Srivastava, S.; Tirrell, M. V. Polyelectrolyte Complexation. In *Advances in Chemical Physics*, Rice, S. A., Dinner, A. R. Eds.; Advances in Chemical Physics, Vol. 161; John Wiley & Sons, Inc., 2016; pp 499-544.

7. Van der Gucht, J.; Spruijt, E.; Lemmers, M.; Stuart, M. A. C. Polyelectrolyte complexes: Bulk phases and colloidal systems. *Journal of colloid and interface science* **2011**, *361* 2, 407-422.

8. Lueckheide, M.; Vieregg, J. R.; Bologna, A. J.; Leon, L.; Tirrell, M. V. Structure-Property Relationships of Oligonucleotide Polyelectrolyte Complex Micelles. *Nano Letters* **2018**, *18* 11, 7111-7117. DOI: 10.1021/acs.nanolett.8b03132.

9. Blocher, W. C.; Perry, S. L. Complex coacervate-based materials for biomedicine. *WIREs Nanomedicine and Nanobiotechnology* **2017**, *9* 4, e1442. DOI: 10.1002/wnan.1442.

10. Voets, I. K.; de Keizer, A.; Cohen Stuart, M. A. Complex coacervate core micelles. *Advances in Colloid and Interface Science* **2009**, *147-148*, 300-318. DOI: 10.1016/j.cis.2008.09.012.

11. Peters, D.; Kastantin, M.; Kotamraju, V. R.; Karmali, P. P.; Gujraty, K.; Tirrell, M.; Ruoslahti, E. Targeting atherosclerosis by using modular, multifunctional micelles. *Proceedings of the National Academy of Sciences* **2009**, *106* 24, 9815-9819.

12. Lindhoud, S.; Norde, W.; Cohen Stuart, M. A. Effects of polyelectrolyte complex micelles and their components on the enzymatic activity of lipase. *Langmuir* **2010**, *26* 12, 9802-9808.

13. Maggi, F.; Ciccarelli, S.; Diociaiuti, M.; Casciardi, S.; Masci, G. Chitosan nanogels by template chemical cross-linking in polyion complex micelle nanoreactors. *Biomacromolecules* **2011**, *12* 10, 3499-3507.

14. Zhao, Q.; Lee, D. W.; Ahn, B. K.; Seo, S.; Kaufman, Y.; Israelachvili, J. N.; Waite, J. H. Underwater contact adhesion and microarchitecture in polyelectrolyte complexes actuated by solvent exchange. *Nature materials* **2016**, *15* 4, 407-412.

15. van Hees, I. A.; Hofman, A. H.; Dompé, M.; van der Gucht, J.; Kamperman, M. Temperature-responsive polyelectrolyte complexes for bio-inspired underwater adhesives. *European Polymer Journal* **2020**, *141*, 110034.

16. Zhou, Z.; Yeh, C.-F.; Mellas, M.; Oh, M.-J.; Zhu, J.; Li, J.; Huang, R.-T.; Harrison, D. L.; Shentu, T.-P.; Wu, D. Targeted polyelectrolyte complex micelles treat vascular complications in vivo. *Proceedings of the National Academy of Sciences* **2021**, *118* 50, e2114842118.

17. Wang, Q.; Schlenoff, J. B. The polyelectrolyte complex/coacervate continuum. *Macromolecules* **2014**, *47* 9, 3108-3116.

18. Meng, S.; Ting, J. M.; Wu, H.; Tirrell, M. V. Solid-to-Liquid Phase Transition in Polyelectrolyte Complexes. *Macromolecules* **2020**, *53* 18, 7944-7953. DOI: 10.1021/acs.macromol.0c00930.

19. Smith, A. E.; Xu, X.; McCormick, C. L. Stimuli-responsive amphiphilic (co) polymers via RAFT polymerization. *Progress in polymer science* **2010**, *35* 1-2, 45-93.

20. York, A. W.; Kirkland, S. E.; McCormick, C. L. Advances in the synthesis of amphiphilic block copolymers via RAFT polymerization: stimuli-responsive drug and gene delivery. *Adv Drug Deliver Rev* **2008**, *60* 9, 1018-1036.

21. Marras, A. E.; Ting, J. M.; Stevens, K. C.; Tirrell, M. V. Advances in the structural design of polyelectrolyte complex micelles. *The Journal of Physical Chemistry B* **2021**, *125* 26, 7076-7089.

22. Krogstad, D. V.; Lynd, N. A.; Choi, S. H.; Spruell, J. M.; Hawker, C. J.; Kramer, E. J.; Tirrell, M. V. Effects of polymer and salt concentration on the structure and properties of triblock copolymer coacervate hydrogels. *Macromolecules* **2013**, *46* 4, 1512-1518. DOI: 10.1021/ma302299r.

23. Krogstad, D. V.; Lynd, N. A.; Miyajima, D.; Gopez, J.; Hawker, C. J.; Kramer, E. J.; Tirrell, M. V. Structural evolution of polyelectrolyte complex core micelles and ordered-phase bulk materials. *Macromolecules* **2014**, *47* 22, 8026-8032. DOI: 10.1021/ma5017852.

24. Huang, J.; Morin, F. J.; Laaser, J. E. Charge-Density-Dominated Phase Behavior and Viscoelasticity of Polyelectrolyte Complex Coacervates. *Macromolecules* **2019**, *52* 13, 4957-4967. DOI: 10.1021/acs.macromol.9b00036.

25. Yang, M.; Shi, J.; Schlenoff, J. B. Control of Dynamics in Polyelectrolyte Complexes by Temperature and Salt. *Macromolecules* **2019**, *52* 5, 1930-1941. DOI: 10.1021/acs.macromol.8b02577.

26. Akkaoui, K.; Yang, M.; Digby, Z. A.; Schlenoff, J. B. Ultraviscosity in Entangled Polyelectrolyte Complexes and Coacervates. *Macromolecules* **2020**, *53* 11, 4234-4246. DOI: 10.1021/acs.macromol.0c00133.

27. Huang, J.; Laaser, J. E. Charge Density and Hydrophobicity-Dominated Regimes in the Phase Behavior of Complex Coacervates. *ACS Macro Letters* **2021**, *10* 8, 1029-1034. DOI: 10.1021/acsmacrolett.1c00382.

28. Johnston, B. M.; Johnston, C. W.; Letteri, R. A.; Lytle, T. K.; Sing, C. E.; Emrick, T.; Perry, S. L. The effect of comb architecture on complex coacervation. *Organic & biomolecular chemistry* **2017**, *15* 36, 7630-7642.

29. Yamauchi, Y.; Horimoto, N. N.; Yamada, K.; Matsushita, Y.; Takeuchi, M.; Ishida, Y. Two-Step Divergent Synthesis of Monodisperse and Ultra-Long Bottlebrush Polymers from an Easily Purifiable ROMP Monomer. *Angewandte Chemie* **2021**, *133* 3, 1552-1558. DOI: 10.1002/ange.202009759.

30. Plamper, F. A.; Ruppel, M.; Schmalz, A.; Borisov, O.; Ballauff, M.; Müller, A. H. E. Tuning the Thermoresponsive Properties of Weak Polyelectrolytes: Aqueous Solutions of Star-Shaped and Linear Poly(N,N-dimethylaminoethyl Methacrylate). *Macromolecules* **2007**, *40* 23, 8361-8366. DOI: 10.1021/ma071203b.

31. Plamper, F. A.; Becker, H.; Lanzendörfer, M.; Patel, M.; Wittemann, A.; Ballauff, M.; Müller, A. H. E. Synthesis, Characterization and Behavior in Aqueous Solution of Star-Shaped Poly(acrylic acid). *Macromolecular Chemistry and Physics* **2005**, *206* 18, 1813-1825. DOI: 10.1002/macp.200500238.

32. Yang, M.; Sonawane, S. L.; Digby, Z. A.; Park, J. G.; Schlenoff, J. B. Influence of "Hydrophobicity" on the Composition and Dynamics of Polyelectrolyte Complex Coacervates. *Macromolecules* **2022**, *55* 17, 7594-7604. DOI: 10.1021/acs.macromol.2c00267.

33. Sarapas, J. M.; Martin, T. B.; Chremos, A.; Douglas, J. F.; Beers, K. L. Bottlebrush polymers in the melt and polyelectrolytes in solution share common structural features. *Proceedings of the National Academy of Sciences* **2020**, *117* 10, 5168-5175.

34. Horkay, F.; Chremos, A.; Douglas, J. F.; L Jones, R.; Lou, J.; Xia, Y. Systematic investigation of synthetic polyelectrolyte bottlebrush solutions by neutron and dynamic light scattering, osmometry, and molecular dynamics simulation. *The Journal of Chemical Physics* **2020**, *152* 19.

35. Horkay, F.; Chremos, A.; Douglas, J. F.; Jones, R.; Lou, J.; Xia, Y. Comparative experimental and computational study of synthetic and natural bottlebrush polyelectrolyte solutions. *The Journal of Chemical Physics* **2021**, *155* 7, 074901.

36. Wu, H.; Ting, J. M.; Werba, O.; Meng, S.; Tirrell, M. V. Non-equilibrium phenomena and kinetic pathways in self-assembled polyelectrolyte complexes. *J Chem Phys* **2018**, *149* 16, 163330. DOI: 10.1063/1.5039621.

37. Beaucage, G. Approximations leading to a unified exponential/power-law approach to small-angle scattering. *Journal of applied crystallography* **1995**, *28* 6, 717-728.

38. Anitas, E. M. Small-angle scattering from mass and surface fractals. *Complexity in biological and physical systems* **2018**, 169-191.

39. Rubinstein, M.; Colby, R. H. *Polymer physics*; Oxford university press New York, 2003.

40. Love, J. A.; Morgan, J. P.; Trnka, T. M.; Grubbs, R. H. A practical and highly active ruthenium-based catalyst that effects the cross metathesis of acrylonitrile. *Angewandte Chemie* **2002**, *114* 21, 4207-4209.

41. Matyjaszewski, K.; Miller, P. J.; Pyun, J.; Kickelbick, G.; Diamanti, S. Synthesis and Characterization of Star Polymers with Varying Arm Number, Length, and Composition from Organic and Hybrid Inorganic/Organic Multifunctional Initiators. *Macromolecules* **1999**, *32* 20, 6526-6535. DOI: 10.1021/ma9904823.

Chapter 5. Summary and Outlook

5.1 Summary

Polyelectrolyte complexes represent a novel class of polymer assemblies with the potential to impact a wide variety of technologies. However, tuning the properties of PECs presents a significant challenge due to the wide variety of variables involved in PEC formation. Structure-property relationships based on altering molecular-level details of the constituent polyelectrolytes within a PEC have shown promise in recent years, as they generally apply to a wide range of polyelectrolyte pairings and allow one to alter PEC properties when control of environmental variables is difficult or impossible. However, there is still a lack of understanding of how different polymer architectures influence the properties of PECs. In the preceding chapters, we addressed fundamental questions around the role of polyelectrolyte architecture in the development of PEC materials.

In Chapter 2 we examine the effect of charged block length mismatch in D-PCM cores. Previously, equal charged block lengths were considered essential for D-PCM formation. In this chapter, we use salt annealing to create a library of micelles from a suite of diblock polyelectrolytes with vastly different charged block lengths. Through a combination of salt annealing, Cryo-TEM, DLS and SAXS, we demonstrated D-PCM formation from mismatched diblocks for the first time and showed how their core size, ion pair aggregation number and ion pair density do not scale consistently with changing block length. Instead, D-PCM core features grow via a unique interdependent mechanism whereby the block length of one polyelectrolyte modulates the ability of the block length of the other polyelectrolyte to contribute to the physical attributes of the core. This result broadens the design space for charged assemblies and could be significant in the design

of structured PEC gels and PEC polymersomes where the size and density of the complex domain is crucial to their function.

In Chapter 3 we show how lightly branched polyelectrolytes can be used to selectively alter PEC stability while leaving other physical properties unchanged. Charge density has shown promise as a means to predictably tune the properties of PECs in recent years, a difficult feat due to the vast array of variables involved in the complexation process. Inspired by simulations showing how branched polyelectrolytes increase charge density relative to linear counterparts, we set out to investigate the role of lightly branched polyelectrolytes on polyelectrolyte complexes. In this chapter, we use reactive polymers and click chemistry to create structurally analogous polyelectrolytes of linear, 4-armed, 6-armed and 8-armed architectures to investigate the effect of non-linear architecture on PECs. We demonstrated a new, facile route to homologous polyelectrolytes through thiol-epoxy click reactions of small molecules onto poly(glycidyl methacrylate) precursors of various architectures. Using optical microscopy, rheology and SAXS, we show the salt resistance of the complexes depend on polyelectrolyte architecture while the mechanical properties and structure remain essentially unaltered. We attribute the ability to precisely tune the properties of PECs using architecture to the distinct roles of spatial charge density in governing thermodynamic stability and the linear charge density in dictating the mechanical and structural properties of PECs. Our findings are a step towards architecturally determined, chemically agnostic design principles allowing precise, orthogonal property modification of PECs.

In Chapter 4 we explore the structure and properties of bottlebrush polyelectrolyte complexes. Numerous examples within the polymer literature demonstrate the wide range of properties attainable through altering polymer architecture from a linear to bottlebrush

configuration. However, there are no previous reports detailing how PEC properties change when the constituent polyelectrolytes are bottlebrushes. To address this knowledge gap, we synthesized high molecular weight, densely grafted bottlebrush polyelectrolytes through a grafting from approach that combines ATRP, ROMP and quantitative post-polymerization modifications. The resulting BPECs morphology, mechanical properties and internal structure were then characterized with optical microscopy, rheology, cryo-TEM and SAXS. BPECs are mechanically frozen opaque gels which swell and weaken with salt. We hypothesize that the gel-like rheological behavior is due to physical crosslinks formed by the interdigitation of oppositely charged bottlebrush sidechains. Cryo-TEM allowed us to directly observe the molecular conformations of polyelectrolytes within a PEC for the first time, which when combined with SAXS allowed us to develop a structural model for BPECs that spans the network architecture, sidechain conformation and sidechain spacing. Our results provide a foundational understanding of the structure and properties of BPECs and will be critical towards understanding the incorporation of densely branched, anisotropic materials within BPECs in the future.

We believe the findings outline clear paths for future study into the role of polymer architecture in the stability, structure and self-assembly of PEC materials. However, there are underdeveloped research areas we hope our work encourages renewed interest in. Specifically, we believe using polyelectrolyte complexation to mix polymers with distinct architectures and association mechanisms provides a pathway to use polyelectrolyte architecture to direct polymer assembly in ways unavailable within uncharged polymer systems.

5.2 Outlook - Branched Polymers to Direct PEC Structure

As the field of polymer science celebrates its centennial anniversary, many researchers have recognized the current disparity between the chemical and structural sophistication attainable in biological and synthetic polymers. In particular, there is a growing need for advances in polymer chemistry and characterization to access advanced structures capable of performing specific functions over multiple time and length scales.[1] Modern polyelectrolyte complexation research seeks to understand the thermodynamic forces driving aspects of intricate self-assembly and hierarchy found in biomacromolecules, such as nucleic acids, proteins, or membraneless organelles.[2] However, it is challenging to incorporate hydrogen bonding motifs and hydrophobic interactions ubiquitous in natural polyelectrolytes into synthetic analogs. Throughout the introduction, we highlighted model PEC examples emphasizing how controlled polymer architecture, enhanced by complementary non-covalent driving forces, can create new directions in charge-driven assembly. In the research chapters, we demonstrated how polyelectrolyte architecture can be harnessed to tune PEC properties. In this final section, we discuss experimental barriers and opportunities for expanding the range of accessible polyelectrolyte materials and architectures. We anticipate an interdisciplinary approach combining principles in polymer science, molecular engineering, and supramolecular chemistry will be key to designing next-generation PEC platforms which exhibit controlled self-assembly and reassembly, more diverse morphologies folding, and multi-phase compartmentalization.

In terms of functional polyelectrolyte materials development, solubility remains one of the main challenges in creating more heterogeneous PECs so parameters like amphiphilicity can be investigated. The problem can be thought of in two parts: chemical synthesis and materials processing. First, synthesizing blocky polyelectrolytes with blocks of such disparate solubilities in

organic/water solutions can be challenging, and often motivates the use of post-polymerization functionalization reactions to circumvent this issue.[3, 4] Weakly ionizable and/or protected (meth)acrylates are common candidates, as the monomer precursors can be solubilized in polar organic solvents (e.g., dimethylformamide or tetrahydrofuran) before polymerization and, if needed, converted into polyelectrolytes via quaternization, hydrolysis, or similar deprotection reactions.[5, 6] However, this limits the scope of ionic groups which can be explored to a handful of systems. More recent PEC reports from the Qin/Xia[7] and Laaser[8] groups have demonstrated the functionalization of poly(N-acryloxy succinimide) systems, expanding systematic polyelectrolyte libraries with fundamental structure-property relationships. Another route to organic-soluble polyelectrolytes involves the use of greasy counterions to impart organic solubility to polyelectrolytes, which has been performed for alkaline anion exchange membrane fuel cell applications. For example, Tsai et al. synthesized controlled polystyrene-*block*-poly(vinylbenzyltrimethylammonium tetrafluoroborate) (PS-*b*-[PVBTMA][BF_4]), imparted with organic solubility by first ion exchanging the chloride counterions of the monomer with sodium tetrafluoroborate.[9] The authors then used potassium hydroxide to exchange BF_4 into a more traditional hydroxyl counterion, PS-*b*-[PVBTMA][OH]. This strategy can be employed to prepare more exotic polymer candidates as PEC materials. However, mutual solubility alone does not ensure a chemically customized PEC system will arrive at an equilibrium state upon mixing.

For advanced PEC networks associating by not only electrostatic but also hydrophobic or other stabilizing interactions, it is unclear how to drive kinetically trapped states into thermodynamic products. The PEO/PAGE system in Figure 1.6 is thought to be facilitated by the liquid nature of PEC domains, which allows chain rearrangement to a near-equilibrium structure.[10, 11] Meanwhile, polyelectrolyte pairs which form solid PEC domains might require external stimuli

to overcome kinetic aggregation in water and achieve such structured phases.[12, 13] The expansion of rigorous annealing protocols for PEC materials based on temperature, salt, cosolvents, or other additives are needed to fully explore these intermediate states. Previously described salt annealing methods have enabled reproducible micelles,[12, 14, 15] and we anticipate analogous methods can be incorporated into PECs overall. Inspiration for amphiphilic annealing protocols may arise from micelleplexes, which are micelles with hydrophobic cores and charged coronas which form PEC nanoparticles when complexed with oppositely charged polymers, and therefore must balance electrostatic and hydrophobic interactions to avoid kinetic products.[16-18] In amphiphilic networks, strong hydrophobic interactions could introduce separate kinetic barriers and require additional annealing steps to reassemble and selectively order phase separated domains. Figure 6(A-B) depicts this idea for oppositely charged triblock polymer gels. While the capability of charged-neutral-charged systems to form ordered morphologies has been established, to the extent of our knowledge, only one previous report has shown networks of chemically distinct domains from combinations of mixed architectures in hydrophobic-hydrophilic-charged polymers.[19] Creating structured materials in this manner may necessitate multi-step, directed assembly annealing processes to navigate and overcome the presence of orthogonal driving forces for association.[19]

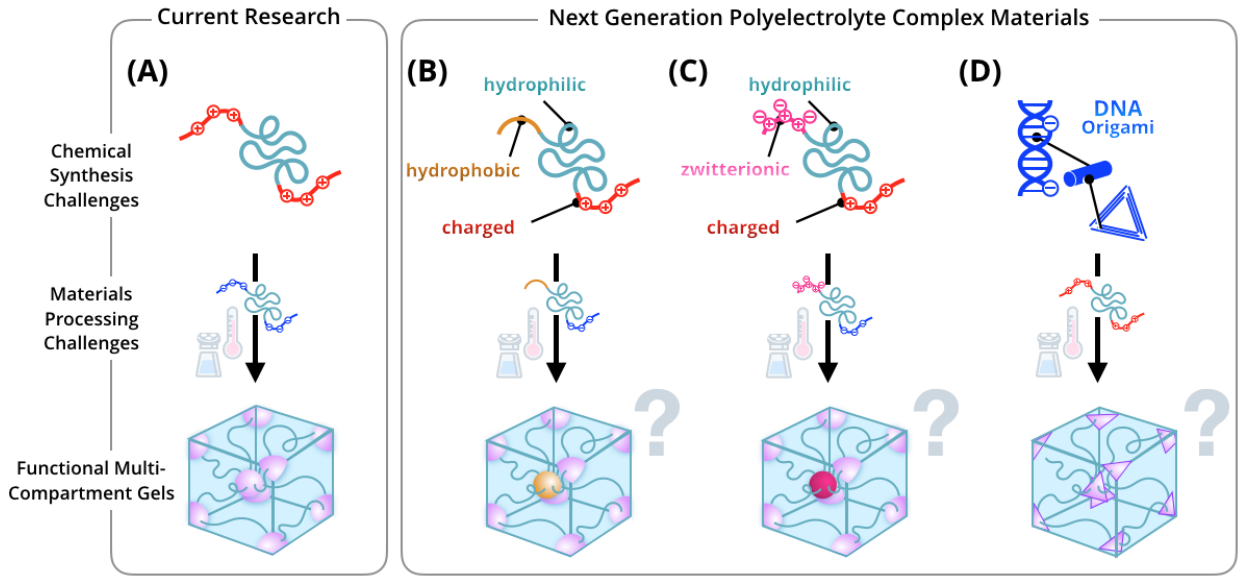

Figure 5.1. Molecular engineering opportunities for the development of functional, multicompartment polyelectrolyte complex gels, driven by ongoing innovations and advances in chemical synthesis and materials processing. (A) Combinations of oppositely charged triblocks can give rise to classical structures and morphologies. (B) Mixed architectures, such as hydrophobic-hydrophilic-charged ABC triblock polymers, may conceivably lead to ordered hydrophobic and polyelectrolyte complex domains. (C) Mixed architectures, such as completely water-soluble zwitterionic-hydrophilic-charged ABC triblock polymers, may also drive selective phase separation and assembly. (D) Hybrid materials like DNA origami may be templated into regular complex domains, thereby increasing the hierarchical framework of 3D geometries toward future materials design paradigms.

In contrast to our discussion on developing new synthesis and processing methods, there are also readily available strategies not yet utilized in PECs. For example, polyelectrolyte complexation provides a unique opportunity to readily blend oppositely charged polymers with different architectures.[20] While there are many examples of polyelectrolyte complexation comprising linear homopolymers, diblock, and triblock polymers, far fewer focus on branched polyelectrolytes, despite the vast potential of nonlinear macromolecular architectures to drive novel assembly in charge-driven materials. Recent polymer chemistry advances have highlighted facile routes to a variety of advanced architectures, e.g., janus bottlebrush,[21-24] cyclic,[25-27] multiblock,[28-30] miktoarm,[31-35] and bottlebrush multiblock polymers,[32, 36] but many of these systems are either uncharged or utilize a limited selection of polyelectrolytes. Can blending

oppositely charged star and bottlebrush polyelectrolytes lead to uniquely ordered gels with internal structures rivaling triblock/triblock PEC gels? Greater synthetic development of facile routes to well-controlled branched polyelectrolytes would accelerate the study of advanced architectures in polyelectrolyte complexes.

Zwitterionic blocks could provide an additional associating segment for highly ordered PEC structures from purely hydrophilic multiblock polymers. For example, double hydrophilic zwitterionic-neutral block polymers like poly(ethylene oxide)-*block*-poly(2-(methacryloyloxy)ethyl phosphorylcholine)) (PEO-*b*-PMPC) can de-mix based on hydration mechanisms and phase separate to form well-defined structures in concentrated aqueous conditions.[37, 38] Similarly, zwitterionic-charged block polymers have been utilized to form core-shell PCM nanoparticles.[39, 40] Can complexation of oppositely charged zwitterionic-hydrophilic-charged ABC block polymers lead to new types of multicompartmental assemblies with separate hydrophilic, zwitterionic, and PEC domains, as illustrated for gels in Figure 5.1C? The unique capability of PEC systems to easily blend oppositely charged block polyelectrolytes with disparate sequences and block numbers may expand the design space for PEC based multiblock systems far beyond the expansive design-space of uncharged self-assembled materials. Towards this end, we envision incorporating increasingly sophisticated polyelectrolytes and charged materials with immense structural control, such as DNA nanostructures.

Structural DNA nanotechnology boasts the highest structural resolution of designable soft materials. While frequently employed as the final product of self-assembly, the dense negative charges along the DNA backbone present opportunities to utilize DNA nanotechnology as a component within PEC assembly as illustrated in Figure 5.1D. Most reports of complexation with DNA origami are intended to prevent degradation of the nanostructures and do not explore the

structural role DNA could have in emergent self-assembly of network- or nanoparticle-based materials facilitated by polyelectrolyte complexation. The specific programmability and sub-nanometer precision open new doors for programmed orientation of patterning within polyelectrolyte complexes and enable dynamic control over material properties including stiffness, surface area, and charge density. DNA hybridization has already shown to drastically change PEC phase and PCM architecture. Expanding this design space beyond single-stranded and double-stranded DNA may provide equally facile routes to increasingly complex soft materials.

In conclusion, controlled polyelectrolyte architecture has proven to be a crucial parameter determining self-assembly pathways in polyelectrolyte complexation and provides ample opportunities for advanced materials development. In this perspective, we have discussed how within PEC gels, precise control over macromolecular design and experimental variables like ionic strength and polymer concentration allow easy access to a wide range of structural and mechanical properties. Branched polyelectrolytes with increasingly exotic architectures display novel assembly mechanisms and have proved useful for achieving unique PEC nanostructures with novel functionality. Moving forward, we have forecasted potential obstacles to realizing the full potential of PEC materials, as well as areas amenable to future advancement. We propose expanding the field to include amphiphilic polyelectrolytes, zwitterionic-neutral-charged polyelectrolytes and DNA nanostructures to enable access to next-generation PEC materials with increasingly complex internal structures for advanced applications in numerous interdisciplinary fields.

5.3 References

1. Perry, S. L.; Sing, C. E. 100th Anniversary of Macromolecular Science Viewpoint: Opportunities in the Physics of Sequence-Defined Polymers. *ACS Macro Letters* **2020**, *9* 2, 216-225. DOI: 10.1021/acsmacrolett.0c00002.

2. Sing, C. E.; Perry, S. L. Recent progress in the science of complex coacervation. *Soft Matter* **2020**, *16* 12, 2885-2914. DOI: 10.1039/d0sm00001a.

3. Karanam, S.; Goossens, H.; Klumperman, B.; Lemstra, P. "Controlled" Synthesis and Characterization of Model Methyl Methacrylate/tert-Butyl Methacrylate Triblock Copolymers via ATRP. *Macromolecules* **2003**, *36* 9, 3051-3060. DOI: 10.1021/ma021399+.

4. Blasco, E.; Sims, M. B.; Goldmann, A. S.; Sumerlin, B. S.; Barner-Kowollik, C. 50th Anniversary Perspective: Polymer Functionalization. *Macromolecules* **2017**, *50* 14, 5215-5252. DOI: 10.1021/acs.macromol.7b00465.

5. Steinschulte, A. A.; Gelissen, A. P. H.; Jung, A.; Brugnoni, M.; Caumanns, T.; Lotze, G.; Mayer, J.; Pergushov, D. V.; Plamper, F. A. Facile Screening of Various Micellar Morphologies by Blending Miktoarm Stars and Diblock Copolymers. *ACS Macro Letters* **2017**, *6* 7, 711-715. DOI: 10.1021/acsmacrolett.7b00328.

6. Choi, I.; Suntivich, R.; Plamper, F. A.; Synatschke, C. V.; Müller, A. H. E.; Tsukruk, V. V. pH-Controlled Exponential and Linear Growing Modes of Layer-by-Layer Assemblies of Star Polyelectrolytes. *Journal of the American Chemical Society* **2011**, *133* 24, 9592-9606. DOI: 10.1021/ja203106c.

7. Lou, J.; Friedowitz, S.; Qin, J.; Xia, Y. Tunable Coacervation of Well-Defined Homologous Polyanions and Polycations by Local Polarity. *ACS Cent Sci* **2019**, *5* 3, 549-557. DOI: 10.1021/acscentsci.8b00964.

8. Huang, J.; Morin, F. J.; Laaser, J. E. Charge-Density-Dominated Phase Behavior and Viscoelasticity of Polyelectrolyte Complex Coacervates. *Macromolecules* **2019**, *52* 13, 4957-4967. DOI: 10.1021/acs.macromol.9b00036.

9. Tsai, T.-H.; Versek, C.; Thorn, M.; Tuominen, M.; Coughlin, E. B. Block Copolymers Containing Quaternary Benzyl Ammonium Cations for Alkaline Anion Exchange Membrane Fuel Cells (AAEMFC). In *Polymers for Energy Storage and Delivery: Polyelectrolytes for Batteries and Fuel Cells*, ACS Symposium Series, Vol. 1096; American Chemical Society, 2012; pp 253-265.

10. Ortony, J. H.; Choi, S. H.; Spruell, J. M.; Hunt, J. N.; Lynd, N. A.; Krogstad, D. V.; Urban, V. S.; Hawker, C. J.; Kramer, E. J.; Han, S. Fluidity and water in nanoscale domains define coacervate hydrogels. *Chemical Science* **2014**, *5* 1, 58-67. DOI: 10.1039/c3sc52368c.

11. Krogstad, D. V.; Lynd, N. A.; Miyajima, D.; Gopez, J.; Hawker, C. J.; Kramer, E. J.; Tirrell, M. V. Structural evolution of polyelectrolyte complex core micelles and ordered-phase bulk materials. *Macromolecules* **2014**, *47* 22, 8026-8032. DOI: 10.1021/ma5017852.

12. Marras, A. E.; Vieregg, J. R.; Ting, J. M.; Rubien, J. D.; Tirrell, M. V. Polyelectrolyte Complexation of Oligonucleotides by Charged Hydrophobic-Neutral Hydrophilic Block Copolymers. *Polymers-Basel* **2019**, *11* 1, 83. DOI: 10.3390/polym11010083.

13. Wu, H.; Ting, J. M.; Werba, O.; Meng, S.; Tirrell, M. V. Non-equilibrium phenomena and kinetic pathways in self-assembled polyelectrolyte complexes. *J Chem Phys* **2018**, *149* 16, 163330. DOI: 10.1063/1.5039621.

14. Lueckheide, M.; Vieregg, J. R.; Bologna, A. J.; Leon, L.; Tirrell, M. V. Structure-Property Relationships of Oligonucleotide Polyelectrolyte Complex Micelles. *Nano Letters* **2018**, *18* 11, 7111-7117. DOI: 10.1021/acs.nanolett.8b03132.

15. Marras, A. E.; Vieregg, J. R.; Tirrell, M. V. Assembly and Characterization of Polyelectrolyte Complex Micelles. *J Vis Exp* **2020**, 157, e60894. DOI: 10.3791/60894.

16. Laaser, J. E.; McGovern, M.; Jiang, Y.; Lohmann, E.; Reineke, T. M.; Morse, D. C.; Dorfman, K. D.; Lodge, T. P. Equilibration of Micelle-Polyelectrolyte Complexes: Mechanistic Differences between Static and Annealed Charge Distributions. *J Phys Chem B* **2017**, *121* 17, 4631-4641. DOI: 10.1021/acs.jpcb.7b01953.

17. Jiang, Y.; Sprouse, D.; Laaser, J. E.; Dhande, Y.; Reineke, T. M.; Lodge, T. P. Complexation of Linear DNA and Poly(styrenesulfonate) with Cationic Copolymer Micelles: Effect of Polyanion Flexibility. *J Phys Chem B* **2017**, *121* 27, 6708-6720. DOI: 10.1021/acs.jpcb.7b03732.

18. Laaser, J. E.; Lohmann, E.; Jiang, Y.; Reineke, T. M.; Lodge, T. P. Architecture-Dependent Stabilization of Polyelectrolyte Complexes between Polyanions and Cationic Triblock Terpolymer Micelles. *Macromolecules* **2016**, *49* 17, 6644-6654. DOI: 10.1021/acs.macromol.6b01408.

19. Pham, T. T. H.; Wang, J.; Werten, M. W. T.; Snijkers, F.; de Wolf, F. A.; Cohen Stuart, M. A.; van der Gucht, J. Multi-responsive physical gels formed by a biosynthetic asymmetric triblock protein polymer and a polyanion. *Soft Matter* **2013**, *9* 37, 8923-8930, 10.1039/C3SM51751A. DOI: 10.1039/C3SM51751A.

20. Störkle, D.; Duschner, S.; Heimann, N.; Maskos, M.; Schmidt, M. Complex formation of DNA with oppositely charged polyelectrolytes of different chain topology: Cylindrical brushes and dendrimers. *Macromolecules* **2007**, *40* 22, 7998-8006. DOI: 10.1021/ma0711689.

21. Kawamoto, K.; Zhong, M.; Gadelrab, K. R.; Cheng, L.-C.; Ross, C. A.; Alexander-Katz, A.; Johnson, J. A. Graft-through Synthesis and Assembly of Janus Bottlebrush Polymers from A-Branch-B Diblock Macromonomers. *Journal of the American Chemical Society* **2016**, *138* 36, 11501-11504. DOI: 10.1021/jacs.6b07670.

22. Wang, Q.; Xiao, A.; Shen, Z.; Fan, X.-H. Janus particles with tunable shapes prepared by asymmetric bottlebrush block copolymers. *Polymer Chemistry* **2019**, *10* 3, 372-378. DOI: 10.1039/c8py01467a.

23. Nguyen, H. V.; Gallagher, N. M.; Vohidov, F.; Jiang, Y.; Kawamoto, K.; Zhang, H.; Park, J. V.; Huang, Z.; Ottaviani, M. F.; Rajca, A.; et al. Scalable Synthesis of Multivalent Macromonomers for ROMP. *ACS Macro Lett* **2018**, *7* 4, 472-476. DOI: 10.1021/acsmacrolett.8b00201.

24. Li, Y.; Themistou, E.; Zou, J.; Das, B. P.; Tsianou, M.; Cheng, C. Facile Synthesis and Visualization of Janus Double-Brush Copolymers. *ACS Macro Letters* **2011**, *1* 1, 52-56. DOI: 10.1021/mz200013e.

25. Haque, F. M.; Grayson, S. M. The synthesis, properties and potential applications of cyclic polymers. *Nature Chemistry* **2020**, *12* 5, 433-444. DOI: 10.1038/s41557-020-0440-5.

26. Wei, H.; Chu, D. S. H.; Zhao, J.; Pahang, J. A.; Pun, S. H. Synthesis and Evaluation of Cyclic Cationic Polymers for Nucleic Acid Delivery. *ACS Macro Letters* **2013**, *2* 12, 1047-1050. DOI: 10.1021/mz400560y.

27. Danial, M.; Tran, C. M.; Jolliffe, K. A.; Perrier, S. Thermal gating in lipid membranes using thermoresponsive cyclic peptide-polymer conjugates. *J Am Chem Soc* **2014**, *136* 22, 8018-8026. DOI: 10.1021/ja5024699.

28. Bates, F. S.; Hillmyer, M. A.; Lodge, T. P.; Bates, C. M.; Delaney, K. T.; Fredrickson, G. H. Multiblock Polymers : Panacea or Pandora's Box? *Science* **2012**, *336* April, 434-440. DOI: 10.1126/science.1215368.

29. Gody, G.; Barbey, R.; Danial, M.; Perrier, S. Ultrafast RAFT polymerization: multiblock copolymers within minutes. *Polymer Chemistry* **2015**, *6* 9, 1502-1511. DOI: 10.1039/c4py01251h.

30. Beyer, V. P.; Kim, J.; Becer, C. R. Synthetic approaches for multiblock copolymers. *Polymer Chemistry* **2020**, *11* 7, 1271-1291. DOI: 10.1039/c9py01571j.

31. Bates, M. W.; Barbon, S. M.; Levi, A. E.; Lewis, R. M.; Beech, H. K.; Vonk, K. M.; Zhang, C.; Fredrickson, G. H.; Hawker, C. J.; Bates, C. M. Synthesis and Self-Assembly of ABn Miktoarm Star Polymers. *ACS Macro Letters* **2020**, *9* 3, 396-403. DOI: 10.1021/acsmacrolett.0c00061.

32. Levi, A. E.; Lequieu, J.; Horne, J. D.; Bates, M. W.; Ren, J. M.; Delaney, K. T.; Fredrickson, G. H.; Bates, C. M. Miktoarm Stars via Grafting-Through Copolymerization: Self-Assembly and the Star-to-Bottlebrush Transition. *Macromolecules* **2019**, *52* 4, 1794-1802. DOI: 10.1021/acs.macromol.8b02321.

33. Khanna, K.; Varshney, S.; Kakkar, A. Miktoarm star polymers: advances in synthesis, self-assembly, and applications. *Polymer Chemistry* **2010**, *1* 8. DOI: 10.1039/c0py00082e.

34. Li, Z.; Kesselman, E.; Talmon, Y.; Hillmyer, M. A.; Lodge, T. P. Multicompartment Micelles from ABC Miktoarm Stars in Water. *Science* **2004**, *306*, 98-101.

35. Lodge, T. P.; Rasdal, A.; Li, Z.; Hillmyer, M. A. Simultaneous, Segregated Storage of Two Agents in a Multicompartment Micelle. *Journal of the American Chemical Society* **2005**, *127*, 17608-17609.

36. Kerr, A.; Hartlieb, M.; Sanchis, J.; Smith, T.; Perrier, S. Complex multiblock bottle-brush architectures by RAFT polymerization. *Chem Commun (Camb)* **2017**, *53* 87, 11901-11904. DOI: 10.1039/c7cc07241d.

37. Blanazs, A.; Warren, N. J.; Lewis, A. L.; Armes, S. P.; Ryan, A. J. Self-assembly of double hydrophilic block copolymers in concentrated aqueous solution. *Soft Matter* **2011**, *7* 14. DOI: 10.1039/c1sm05771e.

38. Wu, J.; Wang, Z.; Yin, Y.; Jiang, R.; Li, B.; Shi, A.-C. A Simulation Study of Phase Behavior of Double-Hydrophilic Block Copolymers in Aqueous Solutions. *Macromolecules* **2015**, *48* 24, 8897-8906. DOI: 10.1021/acs.macromol.5b01993.

39. Ting, J. M.; Marras, A. E.; Mitchell, J. D.; Campagna, T. R.; Tirrell, M. V. Comparing Zwitterionic and PEG Exteriors of Polyelectrolyte Complex Micelles. *Molecules* **2020**, *25* 11. DOI: 10.3390/molecules25112553.

40. Ishihara, K. Revolutionary advances in 2-methacryloyloxyethyl phosphorylcholine polymers as biomaterials. *J Biomed Mater Res A* **2019**, *107* 5, 933-943. DOI: 10.1002/jbm.a.36635.